Acta Pharmaceutica Sinica B 2026;16(7):4491−4523

Chinese Pharmaceutical Association
Institute of Materia Medica, Chinese Academy of Medical Sciences

Acta Pharmaceutica Sinica B

www.elsevier.com/locate/apsb
www.sciencedirect.com

ORIGINAL ARTICLE

Discovery of novel tumor-targeting peptide-oncolytic peptide based conjugates (PPCs): A new paradigm for targeted oncolytic-immunotherapy

Qianyao Yu[a,†], Jingfang Yao[a,†], Ming Meng[a], Zixuan Zhang[b,c], Chengjian Pang[d], Zhihao Zhang[d], Qing Liu[e], Xinqi Chen[e], Rilei Yu[b,c], Kewei Wang[a], Yunkun Qi[a,*]

[a]*School of Pharmacy, Qingdao University Medical College, Qingdao University, Qingdao 266071, China*
[b]*Key Laboratory of Marine Drugs, Chinese Ministry of Education, School of Medicine and Pharmacy, Ocean University of China, Qingdao 266003, China*
[c]*Laboratory for Marine Drugs and Bioproducts, Qingdao Marine Science and Technology Center, Qingdao 266237, China*
[d]*The Affiliated Hospital of Qingdao University, Qingdao 266003, China*
[e]*State Key Laboratory Base for Eco-Chemical Engineering in College of Chemical Engineering, Qingdao University of Science and Technology, Qingdao 266042, China*

Received 21 August 2025; received in revised form 22 November 2025; accepted 11 December 2025

KEY WORDS

Mirror-image peptides;
Oncolytic peptides;
Oncolytic-immunotherapy;
Peptide−drug conjugate;
Targeted cancer therapy;
Tyr[3]-octreotate;
Tumor-targeting peptide-oncolytic peptide based

Abstract Oncolytic peptides, which possess synergistic oncolytic-immunotherapy effects, have exhibited advantages including unique anticancer mechanism, overcoming drug resistance and broad anticancer spectrum in clinic. Nevertheless, conventional oncolytic peptides often suffer from poor stability, limited efficacy, and moderate anticancer selectivity. In this study, the stability-, potency-, and selectivity-guided optimizations were conducted on the first-in-class oncolytic peptide Clip-71. The robust synthetic strategy, *in vitro* and *in vivo* anticancer activity, and anticancer mechanism especially immune activation ability were systematically investigated for obtained peptides. The first round of stability-guided optimization identified the mirror-image peptides represented by QY-8, which possessed strikingly high stability, as well as outstanding *in vitro* and *in vivo* anticancer activities. Subsequently, to address the limited selectivity and nonspecific distribution of oncolytic peptides, the second round of

*Corresponding author.
E-mail addresses: qiyunkun@163.com, qiyunkun@qdu.edu.cn (Yunkun Qi).
†These authors made equal contributions to this work.

Peer review under the responsibility of Chinese Pharmaceutical Association and Institute of Materia Medica, Chinese Academy of Medical Sciences.

https://doi.org/10.1016/j.apsb.2026.01.006

conjugates (PPC_S); Clip-71

selectivity-guided and PPCs-strategy based optimization was conducted on QY-8. Strikingly, the novel PPC QY-13, which was obtained through conjugation of the SSTR2-targeting peptide Tyr^3-octreotate to QY-8, exhibited most potent anticancer activities both *in vitro* and *in vivo*, enhanced immunostimulatory activity, and superior biosafety as well as tumor targeting potency. Collectively, this study not only established promising strategies to significantly improve the anticancer potential of cytotoxic peptides, but also provided the new paradigm for targeted oncolytic-immunotherapy.

1. Introduction

Cancer, especially drug-resistant malignancies, is a global health challenge and remains one of the major barriers to improving life expectancy worldwide[1]. Although tremendous efforts have been devoted to developing novel anticancer therapeutics, global cancer incidence and mortality are still rapidly increasing[1-4]. Moreover, high degrees of heterogeneity among cancer cells constitute an increasing obstacle to traditional anticancer therapy[5-9]. Modern biotechnologies have driven the development of a variety of novel anticancer peptides (ACPs)[6], which possess unique skeleton and mechanism of anticancer action[10-12]. Over the past two decades, peptides have emerged as promising anticancer agents and exhibited multiple anticancer activities[6,12-15], such as peptide–drug conjugates (PDCs) which facilitate the cell-penetrating and tumor-targeting of small molecule drugs[16-20], cytotoxic peptides which possess the membrane disruption/permeation potency[6,21,22], and peptide based antagonists for cancer immunotherapy[23-27].

Recently, oncolytic peptides, which possess synergistic oncolytic-immunotherapy effects, offer a new therapeutic modality to overcome cancer heterogeneity[7,28-32]. The cationic amphiphilic oncolytic peptides could locate and bind to negatively charged cytomembranes that are uniquely and homogeneously displayed by cancer cells[7,9]. Upon binding to the membrane of cancer cells, oncolytic peptides could disrupt cancer cell membrane or induce membrane destabilization, followed by the release of danger associated molecular patterns (DAMPs) and tumor antigens from cancer cells, resulting in systemic anticancer immune responses[33-35]. Promisingly, because of their simple structures, superior membrane lytic mechanism, and unique immunostimulatory activity, oncolytic peptides have emerged as striking anticancer candidates and multiple oncolytic peptides have entered clinical evaluation (*e.g.*, CyPep-1, LTX-315, LL-37, and, EP-100, etc.) (Table 1)[34,36-39].

Oncolytic peptides are generally composed of cationic amino acid residues (*e.g.*, Lys, Arg) and hydrophobic amino acid residues (*e.g.*, Trp, Leu, Phe, Ile), which confer the amphiphilicity and high cell permeability[7,9,40-42]. Of note, the peptide sequence $(KFAKFAK)_n$, which affords the derived peptides Phor 14, Phor18 (also known as Clip-71), and Phor 21, was found to exhibit potent and broad-spectrum anticancer effects in both *in vitro* and *in vivo* anticancer studies[43-46]. Moreover, the hybrid peptide EP-100, which is an oncolytic peptide composed of LHRH ligand and Clip-71, has entered clinical trials and exhibited positive anticancer responses in Phase I/II oncology trials (Clinical Trials.gov Identifier: NCT00949559 and NCT01485848)[36,47]. Nevertheless, most oncolytic peptides and their derivatives are rich in lysine (K) and arginine (R) residues, which tend to be easily degraded by proteases[48-50]. Recently, numerous studies have reported that the poor proteolytic stability, moderate anticancer durability, as well as limited selectivity and nonspecific distribution may hinder the widespread applications of oncolytic peptides[51,52]. To circumvent the stability issues and mitigate the off-target toxicity of oncolytic peptides, their administration is predominantly conducted *via* intratumoral or peritumoral injection.

To improve the stability and anticancer durability of anticancer peptides, several strategies have been applied, represented by the amino acid sequence-based modification, N- and/or C-terminal modification and drug delivery systems (DDSs)[53-60]. Besides, the stapling strategy has been widely applied on various anticancer peptides[49,61-67]. Nevertheless, to the best of our knowledge, except natural-source peptide LTX-315, little effort has been devoted to the systemic optimizations, aiming to simultaneously address the key limitations of oncolytic peptides including poor stability, limited efficacy, and moderate anticancer selectivity. Therefore, it is desirable to develop systematic strategies which could comprehensively improve the proteolytic stability, anticancer efficacy, and anticancer selectivity of artificially designed oncolytic peptides.

In our efforts to improve both the proteolytic stability and anticancer durability of oncolytic peptides, the first round of stability- and potency-guided optimization was conducted on the first-in-class oncolytic peptide Clip-71. To reduce the manufacture cost and facilitate the accelerated synthesis of oncolytic peptides,

Table 1 Oncolytic peptides in clinical evaluations.

Oncolytic peptides	Amino acid sequences[a]	Indication	Phase
LL-37	H-LLGDFFRKSKEKIGKEFKRIVQRIKDFLRNLVPRTES–OH	Melanoma	I/II
LTX-315	H-KKWWKKW-Dip-K-NH_2	Carcinomas	I/II
CyPep-1	Ac-yGrkkrrqrrrGktlrvakaiykryie-NH_2	Advanced solid tumors	I/II
EP-100	H-KFAKFAKKFAKFAKKFAKQHWSYGLRPG–OH	Advanced solid tumors	I/II

[a]The capital first letters and small first letters represent L-type and D-type amino acid residues.

the economic and robust manual synthetic strategy was established. Then, the canonical N- and/or C-terminal modifications were conducted on Clip-71. Mirror-image peptides, which are composed of D-amino acid residues, are gaining increasing interest as potential therapeutic candidates due to their significantly enhanced stability and reduced immunogenicity compared with their L-type counterparts[26,68-70]. Inspired by the mirror-image phage display strategy developed by Liu et al.[23,69,71-73] and D-type peptides based therapeutics, L- to D-amino acid residue substitutions were performed on Clip-71.

Through the first round of stability- and potency-guided optimization, the Clip-71-derived peptides were rationally designed and efficiently synthesized. In particular, the *in vivo* and *in vitro* anticancer activity, time-kill kinetics, serum stability, anti-migration activity, hemolysis effects, and anticancer mechanism were explored for synthetic peptides. Compared with the parent peptide Clip-71 and N-/C-terminal modified peptides, mirror-image peptides represented by QY-8 possessed strikingly high proteolytic stability, sustained anticancer durability and significantly improved *in vivo* anticancer potency. Besides, mechanism explorations indicated that QY-8 possessed potent cell membrane disrupting effects, which induced the rapid death of cancer cells. Specifically, compared with the lead peptide Clip-71, QY-8 exhibited significantly increased anticancer activity in the mice model.

Subsequently, to address the limited selectivity and nonspecific distribution of oncolytic peptides[16,17,74], the second round of selectivity-guided and PPCs strategy-based optimization was conducted on QY-8. Inspired by the peptide−drug conjugates (PDCs) strategy[36,42,46], it is anticipated that conjugating oncolytic peptide with tumor targeting peptide (termed as PPCs strategy) will address the drawbacks of inadequate selectivity, and meanwhile improve the *in vivo* anticancer potency of oncolytic peptide. Somatostatin Receptor 2 (SSTR2) mediated drug targeting is considered as a highly promising strategy to deliver anticancer agents into SSTR2-expressing tumors[17,74]. Therefore, to further enhance the anticancer potency and selectivity of oncolytic peptides, we strategically fused oncolytic peptides with tumor specific SSTR2-targeting 'homing' peptide, affording the novel tumor-targeting peptide and oncolytic peptide based conjugates (PPCs).

The novel PPCs were cost-effectively synthesized *via* the DIC/Oxyma based accelerated manual solid phase peptide synthesis (SPPS). The systematic *in vitro* and *in vivo* activity, proteolytic stability, subcellular distribution, and anticancer mechanism especially immunostimulatory activity were investigated for the obtained PPCs. It was found that the PPCs strategy could address the key limitations of oncolytic peptide, including poor stability, limited efficacy, and moderate anticancer selectivity. The novel PPC QY-13 exhibits remarkable stability and sustained anticancer durability, which endows it with long-term anticancer potential. In particular, QY-13 exhibits selective localization and toxicity towards cancer cells with high expression of SSTR2 proteins. Furthermore, QY-13 exhibited significantly enhanced immunostimulatory activity compared to QY-8, effectively activating anticancer immune responses through the dual pathways of inducing ICD production and promoting $CD8^+$ T cell infiltration. This robust and specific immune response contributes significantly to its long-term anticancer efficacy and may help in preventing cancer recurrence. Of note, QY-13 exhibited the most potent anticancer potentials in both *in vitro* and *in vivo* experiments, as well as promising biosafety and tumor targeting potency.

Collectively, the stability-, potency-, and selectivity-guided optimizations were conducted on the first-in-class oncolytic peptide Clip-71. Nineteen Clip-71-derived peptides and hybrid peptides were rationally designed, efficiently synthesized, and systematically evaluated for their anticancer potentials. The novel tumor-targeting peptide and D-type oncolytic peptide-based conjugates (PPCs) were developed. Strikingly, the novel PPC QY-13 exhibited the most promising anticancer potentials in both *in vitro* and *in vivo* experiments, establishing QY-13 a particularly promising candidate for oncolytic-immunotherapy. In summary, it is anticipated that this study will not only pave the way for the optimization of other oncolytic peptides, but also provide reliable references for the development of novel tumor-targeting peptide-oncolytic peptide based conjugates (PPCs).

2. Results and discussion

2.1. The design and synthesis of oncolytic peptides

As a typical oncolytic peptide, Clip-71 possesses a linear amphiphilic α-helical structure, consisting of eighteen amino acid residues (KFAKFAKKFAKFAKKFAK) (Fig. 1A). This composition contains eight hydrophilic lysine residues and ten hydrophobic amino acids, including five phenylalanines and five alanines (Fig. 1B and C). Previous studies reported that C-terminal hydrazidation and N-terminal acetylation could improve the stability of anticancer peptides[51,75,76]. Therefore, C-terminal hydrazidation and N-terminal acetylation were conducted on Clip-71, affording derived peptides QY-1 and QY-2 (Table 2). Meanwhile, as N-terminal PEG modification may improve the proteolytic stability of peptides[16,19,77,78], PEG chains of different lengths were attached to the N-terminal of Clip-71, yielding the derived peptides QY-3, QY-4, QY-5, and QY-6. Among them, QY-3 contains both N-terminal PEG modification and C-terminal hydrazide modification.

6-Aminoacetic acid (Acp) is a non-natural amino acid frequently used as a linker in peptide conjugation, which can also improve the stability of peptides[79,80]. Thus, the Acp moiety was attached to the N-terminal of Clip-71, affording the derived peptide QY-7. Recently, compared with their L-amino acid counterparts, the mirror-image peptides, which are composed of D-type amino acid residues, have gained increasing interest as potential therapeutic candidates due to their significantly enhanced proteolytic stability and reduced immunogenicity[26,69,73]. The mirror

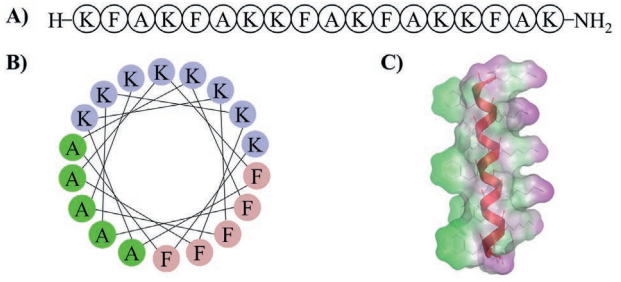

Figure 1 Structure of oncolytic peptide Clip-71. (A) The amino acid sequence of Clip-71. (B) The idealized helical wheel projection of Clip-71 (generated using HeliQuest software, https://heliquest.ipmc.cnrs.fr/cgi-bin/ComputParams.py). (C) The calculated secondary structure model of Clip-71 (generated by the MOE 2014. 0901).

Table 2 The synthetic results for Clip-71 derived peptides and TATE-Oncolytic peptides based PPCs.

Peptides	Amino acid sequence[a]	R_t[c] (min)	ESI-MS (Da)[b]	
			Calculated mass	Observed mass
Clip-71	H-KFAKFAKKFAKFAKKFAK-NH_2	15.13	2133.71	2133.34
QY-1	H-KFAKFAKKFAKFAKKFAK-$NHNH_2$	15.08	2148.73	2148.37
QY-2	Ac-KFAKFAKKFAKFAKKFAK-$NHNH_2$	16.83	2190.76	2190.39
QY-3	H-AEEA-KFAKFAKKFAKFAKKFAK-$NHNH_2$	18.19	2293.88	2293.44
QY-4	[NH_2-PEG_1-CH_2]-KFAKFAKKFAKFAKKFAK-NH_2	16.78[d]	2234.82	2234.65
QY-5	MOEOEA-KFAKFAKKFAKFAKKFAK-NH_2	18.70[d]	2249.83	2249.65
QY-6	MOEOEOEA-KFAKFAKKFAKFAKKFAK-NH_2	18.84[d]	2293.88	2293.73
QY-7	H-Acp-KFAKFAKKFAKFAKKFAK-NH_2	17.27[d]	2246.87	2246.84
QY-8	H-kfakfakkfakfakkfak-NH_2	15.17	2133.71	2133.66
QY-9	7-DCCA-AEEA-KFAKFAKKFAKFAKKFAK-NH_2	22.65[d]	2522.13	2523.47
QY-10	7-DCCA-AEEA-kfakfakkfakfakkfak -NH_2	17.11[e]	2522.13	2521.50
QY-11	H-fCYwKTCT-OH	14.94[d]	1049.23	1048.42
QY-12	H-KFAKFAKKFAKFAKKFAK-AEEA-fCYwKTCT-OH	18.12	3311.07	3311.59
QY-13	H-kfakfakkfakfakkfak-AEEA-fCYwKTCT-OH	18.04	3311.07	3311.31
QY-14	Ac-K(Biotin)-AEEA-fCYwKTCT-OH	16.79[f]	1590.89	1590.22
QY-15	Ac-K(Biotin)-AEEA-kfakfakkfakfakkfak-NH_2	18.00[d]	2675.38	2675.06
QY-16	Ac-K(Biotin)-AEEA-kfakfakkfakfakkfak-AEEA-fCYwKTCT-OH	20.09[d]	3852.73	3852.37
QY-17	7-DCCA-AEEA-kfakfakkfakfakkfak-AEEA-fCYwKTCT-OH	19.04[e]	3699.49	3700.65
QY-18	RhB-AEEA-kfakfakkfakfakkfak-NH_2	18.68[e]	2705.43	2703.66
QY-19	RhB-AEEA-kfakfakkfakfakkfak-AEEA-fCYwKTCT-OH	20.46[e]	3882.79	3881.00

[a]The capital first letters and small first letters represent L-type and D-type amino acid residues, respectively. [b]Calculated and observed ESI-MS, average isotopes. [c]R_t, retention time in analytical RP-HPLC. Condition: a linear gradient of 20%–60% buffer B [0.1% TFA (trifluoroacetic acid) in CH_3CN] in buffer A (0.1% TFA in water) over 30 min (10%–20% for 2 min, then 20%–60% for 30 min) on an Agilent C18 column, λ =214 nm. [d]RP-HPLC condition: 20%–60% buffer B in buffer A over 30 min (20% for 2 min, then 20%–60% for 30 min) on an Agilent C18 column, λ =214 nm. [e]RP-HPLC condition: 30%–60% buffer B in buffer A over 30 min (20%–30% for 2 min, then 30%–60% for 30 min) on an Agilent C18 column, λ =214 nm. [f]RP-HPLC condition: 20%–70% buffer B in buffer A over 30 min (20% for 2 min, then 20%–70% for 30 min) on an Agilent C18 column, λ =214 nm.

image of Clip-71 was designed through D-type amino acid substitutions, generating the D-type peptide QY-8. To monitor differences in cellular uptake and subcellular localization between L-type and D-type oncolytic peptides, the typical fluorophore 7-DCCA was attached to Clip-71 and QY-8, affording peptides QY-9 and QY-10, respectively. Besides, to further improve the anticancer efficiency and selectivity of oncolytic peptides, tumor-targeting peptide and oncolytic peptide based hybrid peptides were designed and systematically evaluated, which will be discussed below.

The efficient synthetic method was established for the accelerated manual synthesis of Clip-71-derived peptides (Fig. 2A). The *N*,*N*′-diisopropylcarbodiimide (DIC)/[ethyl 2-cyano-2-(hydroxyimino)-acetate] (Oxyma)-based condensation system has the advantages of high coupling efficiency and low explosion risk[81,82], and can reduce the side reactions represented by racemization[83-86]. The DIC/Oxyma-based coupling procedures were generally conducted at high temperature (above 70 °C), which may cause burns to the operators and limit the application of DIC/Oxyma-based manual SPPS[84,85,87]. Qi et al.[88-91] reported the DIC/Oxyma-based peptide synthesis under moderate reaction conditions (*e.g.*, 50 °C), which facilitates the efficient manual synthesis of various peptides. Using our previously established DIC/Oxyma-based coupling strategy, the robust manual synthesis of Clip-71-derived peptides was achieved in the normal constant-temperature shaker at 50 °C (Fig. 2). Of note, compared with traditional HCTU/DIEA method (Fmoc-amino acids:HCTU:DIEA = 3 eq:2.8 eq:6 eq), the overall time required for a single SPPS cycle was shortened by about 50% through utilization the DIC/Oxyma-based condensation system (Fmoc-amino acids:DIC:Oxyma = 3 eq: 6 eq: 3 eq).

The Rink Amide MBHA resin was applied for the synthesis of derived peptides with C-terminal amide[67,92,93]. Additionally, the 2-chlorotrityl-$NHNH_2$ resin, which was prepared from the commercially available 2-Cl-(Trt)-Cl resin, was applied for the synthesis of derived peptides with C-terminal hydrazidation[69,81,86]. The Wang resin was applied for the synthesis of peptides with C-terminal carboxyl[94-96]. The DIC/Oxyma-based manual SPPS was utilized for the coupling of natural amino acid residues at 50 °C. Meanwhile, the HATU/HOAt/DIEA system was utilized for the condensation of N-terminal of AEEA, 7-DCCA, MOEOEA, MOEOEOEA, Acp, and NH_2-PEG_1-CH_2 (Supporting Information Fig. S2). Through the combined utilization of DIC/Oxyma and HATU/HOAt/DIEA-based condensation systems, peptide cleavage, peptide purification, and lyophilization, the Clip-71-derived peptides (QY-1 to QY-10) were obtained.

Notably, each of the synthetic peptides could be obtained on more than ten milligrams scale with the purity above 95% determined by analytical RP-HPLC.

The synthetic peptides were characterized by RP-HPLC, ESI-MS, and CD analysis (Table 2, Figs. 2 and 3 and Supporting Information Fig. S3−S23). Of note, the analytical RP-HPLC spectra for each crude and purified peptide, the isolated yields, and the ESI-MS spectra for each synthetic peptide were provided in Fig. S3−S23. As expected, the L-type peptide Clip-71 and corresponding D-type peptide QY-8 exhibited basically the same retention time in analytical RP-HPLC analysis (Table 2). Moreover, to further verify the correctness and potential racemization of the DIC/Oxyma based condensation system, the peptide QY-8 synthesized by the HCTU/DIEA based condensation system at 28 °C or the DIC/Oxyma based condensation system at 50 °C was analyzed by the analytical RP-HPLC. For the coinjections of QY-8 synthesized by different strategies, only one main peak was detected by the analytical RP-HPLC and ESI-MS analysis (Fig. 2B−D). These data proved the robustness of DIC/Oxyma condensation system, which features with low rate of racemization during peptide synthesis at 50 °C. Collectively, utilizing DIC/Oxyma based condensation system, the efficient and robust synthetic strategy was established, which could achieve cost-effective manual synthesis of Clip-71 derived peptides.

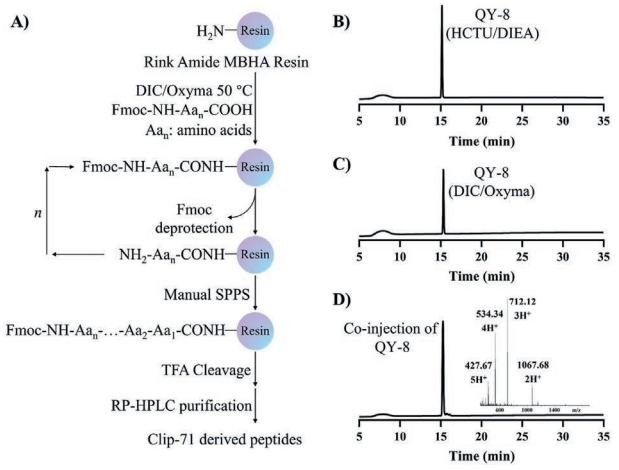

Figure 2 Synthesis and identification of Clip-71 derived peptides. (A) The synthetic route of Clip-71 derived peptides. (B) The RP-HPLC spectrum of QY-8 synthesized by the HCTU/DIEA condensation system at 28 °C. (C) The RP-HPLC spectrum of QY-8 synthesized by the DIC/Oxyma condensation system at 50 °C. (D) RP-HPLC and ESI-MS spectra of coinjections of QY-8 prepared by two condensation systems. RP-HPLC condition: a linear gradient of 20%−60% buffer B in buffer A over 30 min (10%−20% for 2 min, then 20%−60% for 30 min) on an Agilent C18 column. The ESI-MS of QY-8 gave the observed mass of 2133.36 (calculated 2133.71 Da, average isotopes).

As one of the promising oncolytic peptides, Clip-71, which is an amphipathic helical peptide, has been in phase I/II clinical trials (Clinical Trials.gov Identifier: NCT00949559 and NCT01485848)[97]. The previous studies indicated that the amphiphilic structure is vital for the oncolytic peptides to achieve membrane disruption and anticancer effects. Thus, to study the potential influence of structural modifications on the secondary structure of Clip-71, the CD spectra were conducted on Clip-71-derived peptides (Fig. 3A). The CD spectra of QY-1 and QY-2, which contain C-terminal hydrazidation, basically resembled the spectrum of Clip-71. Besides, QY-3, QY-4, QY-5, and QY-6, which contain different lengths of PEG at the N-terminal of peptides, or QY-7 containing N-terminal Acp modification, all exhibited similar CD trends as that of Clip-71. Moreover, there was no significant difference in CD spectra between Clip-71 and QY-3, which contains both C-terminal hydrazidation and N-terminal AEEA. Collectively, the CD spectra indicated that modifications such as N-terminal alkylation, N-terminal PEGylation or C-terminal hydrazidation did not significantly impair the secondary structure of prototype Clip-71.

Recently, D-type peptides, which are composed of D-type amino acid residues and possess high proteolytic stability, are considered as striking skeletons as promising diagnostic tools and therapeutic agents[23,69,71]. Previous studies have shown that L-type to D-type amino acid substitutions can improve proteolytic stability without compromising the anticancer activity of oncolytic peptides[30,98]. Therefore, D-type amino acid substitutions were conducted on Clip-71, affording the D-type peptide QY-8. Generally, the D-type peptide should be the mirror image form of its L-amino acid counterpart[23,24]. As expected, the CD spectrum of QY-8 was basically the mirror image form of Clip-71. Moreover, the structural prediction based on MOE software also showed that Clip-71 and QY-8 maintain mirror symmetry (Fig. 3B). Besides, for the coinjection of purified Clip-71 and QY-8, only one peak was detected by the analytical RP-HPLC analysis

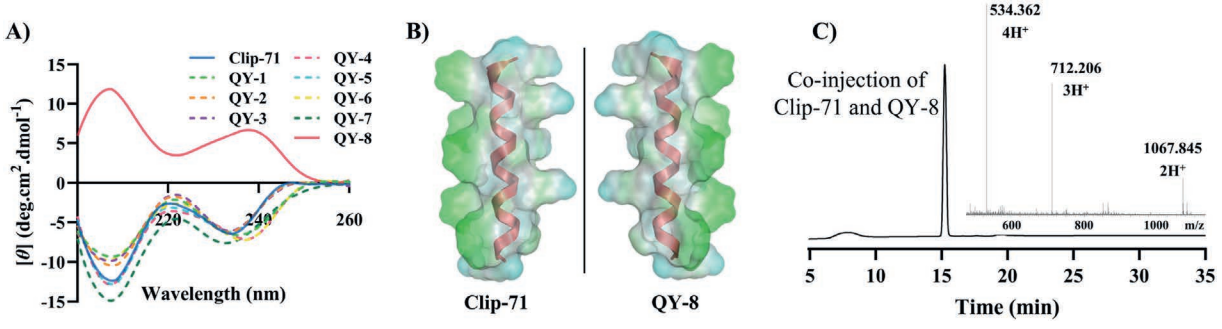

Figure 3 Characterization of Clip-71 derived peptides. (A) The CD spectra of Clip-71 and its derived peptides. (B) Calculated secondary structure models of Clip-71 and QY-8 (generated by the MOE 2014. 0901). (C) RP-HPLC and ESI-MS spectra of coinjections of Clip-71 and QY-8. RP-HPLC condition: a linear gradient of 20%−60% buffer B in buffer A over 30 min (10%−20% for 2 min, then 20%−60% for 30 min) on an Agilent C18 column. The ESI-MS of Clip-71 and QY-8 gave the observed mass of 2133.585 (calculated 2133.711 Da, average isotopes).

(Fig. 3C). Combined with analytical RP-HPLC and ESI-MS, these data further verified the correctness of the synthetic peptides and the robustness of the DIC/Oxyma condensation system (Figs. S3 and S11). In general, the CD data suggested that N-terminal (*e.g.*, acetylation, PEGylation) and/or C-terminal (*e.g.*, hydrazidation) modifications, as well as the D-amino acid substitutions, did not impair the amphipathic structure of prototype Clip-71.

2.2. *In vitro cytostatic effects of Clip-71 and its derived peptides*

To assess the *in vitro* anticancer activity of Clip-71 and its derived peptides, the cytotoxicity assay was conducted against two suspended cancer cell lines (A20 and Daudi) and two adherent cancer cell lines (4T1 and A549). The cytostatic effects were quantified as IC_{50} value, which represents the mean of three separate assays (Table 3). As expected, the Clip-71 and its derived peptides exhibited a dose-dependent inhibitory effect on the proliferation of cancer cells (Supporting Information Fig. S24). As shown in Table 3, the IC_{50} values of Clip-71 against A20, Daudi, 4T1, and A549 cells were 34.2, 57.2, 74.6, and 36.3 μmol/L, respectively, indicating that the four cancer cell lines were not sensitive to Clip-71, with IC_{50} remaining above 30 μmol/L even after 24 h of treatment.

The derivatives (QY-1, QY-2, QY-3, QY-5, and QY-6) containing N-terminal acylation, AEEA, MOEOEOEA, MOEOEA, and/or C-terminal hydrazidation exhibited similar cytotoxicity to Clip-71. Compared with the prototype Clip-71, the derived peptide QY-4 exhibited slightly improved cytotoxicity against the four cancer cell lines. Specifically, the attachment of N-terminal alkylation (QY-7) may improve the cytotoxicity against all four cancer cell lines, with about 2−4-fold increase compared with that of Clip-71. Remarkably, the D-type peptide QY-8 showed the highest activity against A20, Daudi, 4T1, and A549 cells, with IC_{50} values of 3.4, 21.2, 11.8 and 11.4 μmol/L, respectively, which were about 2−10 times better than those of Clip-71. Collectively, the IC_{50} data indicated that the N-terminal acetylation and PEGylation, as well as C-terminal hydrazidation maintain the inherent activity of Clip-71. Of note, the D-amino acid substitutions (QY-8) could significantly enhance the cytotoxicity effects of Clip-71.

2.3. *The time-kill curve assay for Clip-71 and its derived peptides*

Except for the *in vitro* anticancer activity quantified as the IC_{50} value, the durability of anticancer effects is also the key index to evaluate the anticancer potential of oncolytic peptides[30,75]. Since Clip-71 and its derived peptides may be degraded at the cellular level and gradually lose their anticancer effects, the anticancer durability of Clip-71 derived peptides was measured by the time-killing curve assay. Thus, to investigate the influence of anticancer durability of Clip-71 and its derived peptides over time, the time-killing curve assay was performed on A20 suspended cancer cells and 4T1 adherent cancer cells. *In vitro* cytotoxicity test data showed that the IC_{50} values of QY-8 against A20 cells and 4T1 cells were about 5 and 15 μmol/L respectively (Table 3). Therefore, 5 or 15 μmol/L of Clip-71 and its derived peptides were incubated with A20 cells or 4T1 cells respectively, over a time-course at 4, 12, 24, 36, 48, and 72 h.

Table 3 IC_{50} values (μmol/L) of Clip-71 and its derived peptides.

Peptides	A20	Daudi	4T1	A549
Clip-71	34.2 ± 1.3	57.2 ± 1.7	74.6 ± 5.6	36.3 ± 6.1
QY-1	38.6 ± 1.7	38.9 ± 3.8	61.0 ± 7.3	72.1 ± 4.3
QY-2	27.6 ± 4.3	35.5 ± 5.9	47.8 ± 5.1	71.2 ± 8.4
QY-3	28.6 ± 1.3	30.6 ± 4.2	42.3 ± 0.8	52.9 ± 7.3
QY-4	22.2 ± 3.4	28.9 ± 3.4	25.3 ± 2.7	35.6 ± 3.2
QY-5	32.1 ± 5.3	44.1 ± 8.3	46.9 ± 1.1	59.9 ± 6.6
QY-6	39.2 ± 6.4	36.1 ± 3.8	49.9 ± 1.3	51.4 ± 4.9
QY-7	18.2 ± 5.1	24.1 ± 1.9	18.8 ± 2.6	25.3 ± 2.3
QY-8	3.4 ± 0.6	21.2 ± 1.7	11.8 ± 4.8	11.4 ± 2.1

The data are presented as the mean ± SEM ($n = 3$). Incubation time: 24 h.

Fig. 4A showed that Clip-71 and its derived peptides initially exhibited the rapid inhibition of both A20 suspended cancer cells and 4T1 adherent cancer cells, and then reached the highest inhibitory efficiency at 24 h. Consistent with the IC_{50} data, compared with other peptides except QY-8, the derived peptides QY-4 and QY-7 exhibited stronger inhibition rates at 24 h. Nevertheless, since the IC_{50} values of Clip-71 and other derived peptides except QY-8 were greater than 5 μmol/L against A20 cells and greater than 15 μmol/L against 4T1 cells, their highest inhibition rates were unable to exceed 50% throughout the test. Besides, it should be pointed out that the anticancer efficiencies of Clip-71 and its derived peptides except QY-8 exhibited a significant downward trend from 24 to 72 h, with the inhibition rates remaining below 20% and 5% after 48 and 72 h incubations, respectively. Specifically, peptide QY-2, which contains both C-terminal hydrazide modification and N-terminal acetylation, could not improve the anticancer durability of Clip-71 at the *in vitro* cellular level.

In contrast, unlike the L-type derived peptides, which showed significantly reduced inhibition rates from 24 to 72 h, the D-type peptide QY-8 maintained durable anticancer effects against both A20 suspended cancer cells and 4T1 adherent cancer cells throughout the assay. Especially, QY-8 was found to exhibit potent anticancer activity up to 72 h, with the inhibition rate up to 90% and 70% against A20 and 4T1 cancer cells, respectively. Collectively, the time-kill curve assay suggested that the N-terminal acetylation and PEGylation, as well as C-terminal hydrazidation could not significantly improve the anticancer durability of Clip-71. Strikingly, D-type amino acid substitutions not only significantly enhanced the anticancer efficacy of Clip-71, but also effectively prolonged the duration of the anticancer effect.

2.4. *Serum stability of Clip-71 derived peptides*

Previous studies have reported that anticancer peptides, especially the L-type linear peptides are easily degraded by various proteolytic enzymes, and suffer from short half-lives in human serum or tumor microenvironment[6,99]. Moreover, the clinical applications of multiple anticancer peptides are limited due to their poor stabilities and short half-lives[30,100]. The cytotoxicity assay and time-kill curve assay indicated that D-type amino acid substitutions could significantly improve the anticancer potency and prolong the anticancer durability of Clip-71, which should be attributed to the high proteolytic stability of derived peptides. Therefore, in order to detect the proteolytic stability of Clip-71 and its derived peptides, we performed serum stability experiments *in vitro*. The *in vitro* stability tests were carried out in 10% human serum, with the incubation time up to 72 h[23,24]. The analytical RP-HPLC and ESI-MS were jointly applied to monitor the integrity of peptides

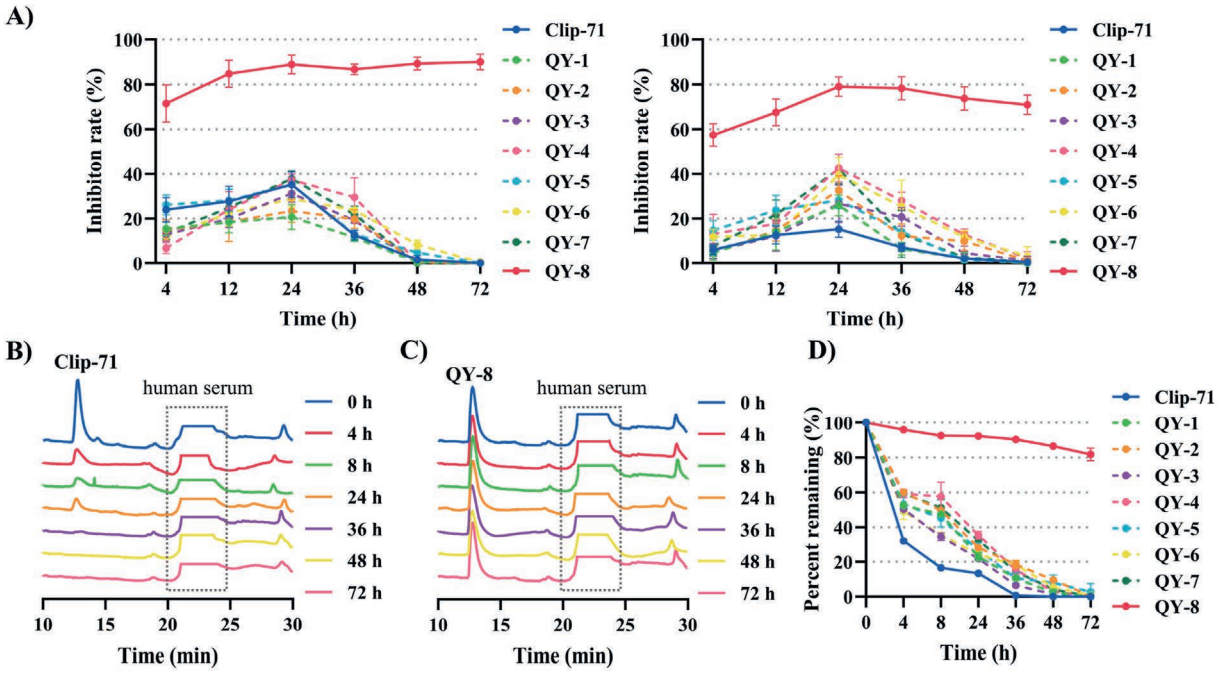

Figure 4 The time-kill curve assays and serum stabilities of Clip-71 derived peptides. (A) The A20 (left) and 4T1 (right) cells were treated with 5 and 15 μmol/L of Clip-71 derived peptides, respectively. Data are presented as mean ± SD (n = 3). (B, C) Analytical RP-HPLC spectra of the hydrolysis of Clip-71 (B) and QY-8 (C) by human serum (10%, *v*/*v*). (D) Human serum stability of Clip-71 and derived peptides (100 μmol/L tested concentration for each peptide, monitored by the analytical RP-HPLC and ESI-MS). Data are presented as mean ± SD (n = 3).

(Fig. 4B−D). The serum stability tests indicated that the integrity of Clip-71 rapidly decreased with the extension of incubation time. The content of full-length Clip-71 was calculated to be 32% at 4 h, and the content of Clip-71 dropped to below 5% after 36 h of incubation, indicating that the half-life of Clip-71 was less than 4 h.

Meanwhile, for QY-1 bearing C-terminal hydrazidation, 52%, 23% and 10% of full length QY-1 could be detected after 4, 24 and 36 h incubations, respectively. In addition, the attachment of AEEA to the N-terminal of QY-1 could not improve the stability (peptide QY-3). For QY-2 containing C-terminal hydrazidation and N-terminal acetylation, 60%, 28% and 18% of full length QY-2 were detected at 4, 24 and 36 h, respectively. The difference between QY-1 and QY-2 indicated that the simultaneous C-terminal hydrazidation and N-terminal acetylation could improve the stability, and the effect was superior to C-terminal hydrazidation alone. Meanwhile, 15%, 11%, 18% and 14% of full length QY-4, QY-5, QY-6, and QY-7 could be detected after 36 h incubation. These data indicated that N-terminal modifications such as PEGylation (QY-4, QY-5, QY-6) and alkylation (QY-7) could enhance the proteolytic stability. Nevertheless, it should be pointed out that except for QY-8, all Clip-71 derived peptides gradually lost integrity after 4 h incubation, with the integrity below 20% at 36 h and below 5% at 72 h.

Strikingly, unlike the L-type peptides (QY-1−QY-7), all of which rapidly lost integrities with the extension of incubation time, the D-type peptide QY-8 remained rather stable throughout the tests. Especially, only 18% degradation of QY-8 was detected even after 72 h incubation. Collectively, compared with C-terminal hydrazidation and N-terminal modifications (acetylation, PEGylation, and alkylation), the D-type amino acid substitutions could more significantly improve the stability of peptide. Different from L-type Clip-71 derived peptides, the D-type peptide possessed promising resistance to enzymatic degradation, which effectively prolonged the duration of anticancer effects. Nevertheless, although time-kill curve assay and serum stability experiment indicated that QY-8 possessed high proteolytic stability and sustained anticancer efficiency, further experiments are required to investigate the *in vivo* stability of QY-8.

2.5. Anticancer action of Clip-71 and QY-8 at the subcellular level

Although the Clip-71 based agent has entered clinical trials, to the best of our knowledge, little effort has been devoted to investigating the anticancer action of Clip-71. Besides, understanding the subcellular mechanism of Clip-71 will facilitate the development of Clip-71 based anticancer agents. The cytotoxicity tests, the time-kill curve assay and serum stability tests indicated that D-type peptide represented by QY-8 possessed significantly improved anticancer activity and durable anticancer efficiency, as well as strikingly high proteolytic stability. Therefore, to investigate the anticancer action of Clip-71 and its derived peptides, the prototype Clip-71 and D-type peptide QY-8 were selected and investigated for the membranolytic effect and subcellular localization. Especially, to monitor the subcellular localization, the representative fluorescent group 7-DCCA was attached to the N-terminal of Clip-71 and QY-8, affording 7-DCCA-AEEA-Clip-71 (QY-9) and 7-DCCA-AEEA-QY-8 (QY-10), respectively.

2.5.1. MD simulation of QY-8 binding to the cell membrane of cancer cells

Previous studies have shown that there are several widely accepted models to explain the mechanism by which oncolytic peptides

bind to cell membranes[43,101]. Inspired by previous studies, 100 ns molecular dynamics simulations were performed to explore the way D-type peptide QY-8 interacts with cancer cell membranes (Fig. 5A). The structure of Clip-71 was predicted using AlphaFold3[102]. Subsequently, the L-type Clip-71 was inverted into a D-type peptide, peptide QY-8, using the LtoD.py script from the finDr website[103]. Peptide QY-8 was positioned at a distance of 40 Å from the surface of POPC cell membranes[104]. A 100 ns molecular dynamics simulation was initiated to observe the interaction of oncolytic peptide QY-8 with the cell membrane. In comparison to the initial state, QY-8 demonstrated greater adhesion to the cell membrane surface at an inclined angle in 30 and 60 ns simulations (Fig. 5A), whereas by 100 ns, QY-8 exhibited tight attachment to the cell membrane surface in a nearly pendulous orientation, resulting in the bending of the monolayer towards the peptide side of the cell membrane. Consequently, we hypothesize that D-type peptide QY-8 may disrupt the cell membrane at an angle perpendicular to the cell membrane, thereby facilitating its entry into the cytoplasm. However, it should be noted that further experimentation is necessary to verify the membranolytic effect of D-type peptide QY-8.

2.5.2. *Membranolytic effect of Clip-71 and QY-8*

Various studies have reported that oncolytic peptides could destroy the integrity of cancer cell membranes, which contributed to the rapid anticancer effects of oncolytic peptides[7,105,106]. To study the cell membrane disrupting potency of prototype Clip-71 and D-type peptide QY-8, the membrane integrity assay was conducted on the 4T1 adherent cancer cells. After the treatment of negative control DMSO, Clip-71, or QY-8, PI/Hoechst 33258 costaining was conducted. The cancer cells with intact cell membranes, which were stained by the Hoechst 33258, emitted blue fluorescence. With the rupture of tumor cell membrane, PI will enter cells and the cancer cells then emitted red fluorescence. As depicted in Fig. 5B and C, for the DMSO group, the percentage of PI positive cancer cells was less than 5% throughout the tests, suggesting that most cancer cells possessed intact cell membranes within 30 min.

On the contrary, 30 min treatment of Clip-71 or QY-8 induced an obvious increase in red fluorescence, indicating the rapid membrane disrupting potency of Clip-71 and QY-8. 4.7% and 10.8% of whole cells stained by PI were detected within 10 min for Clip-71 and QY-8 respectively. As the time extended to 30 min, the membranolytic effects significantly increased, and 7.6% and 18.9% of whole cells stained by PI were detected for Clip-71 and QY-8 respectively. Besides, the mitochondrial membrane potential analysis was also conducted, suggesting that Clip-71 and QY-8 did not obviously destroy the mitochondrial membrane (Supporting Information Fig. S25). Collectively, the membrane integrity assay indicated that both Clip-71 and QY-8 possess rapid membranolytic activity, which could subsequently induce cancer cell death in a relatively short period of time. Of note, it was first found that, in terms of the speed and degree of membranolytic effects, the D-type peptide QY-8 exhibited more potent disruption potency on the cancer cell membranes than that of Clip-71.

2.5.3. *Subcellular localization of QY-9 and QY-10*

To investigate subcellular localization of Clip-71 and QY-8, the live-cell imaging experiment was conducted on 4T1 cancer cells. To monitor the subcellular localization, 7-DCCA labeled Clip-71 (QY-9) and 7-DCCA labeled QY-8 (QY-10) were utilized to perform live-cell imaging assay on 4T1 cancer cells. The *in vitro* cytostatic assay indicated that N-terminal attachment of

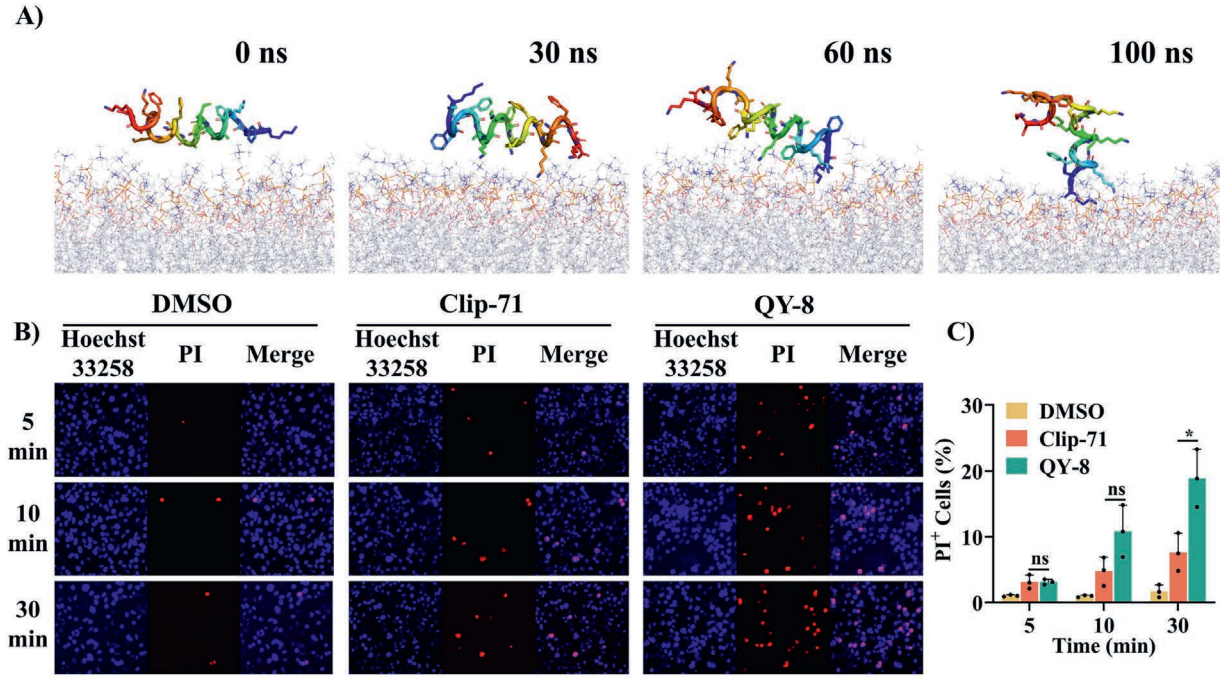

Figure 5 Molecular dynamics simulations and membranolytic effect of QY-8. (A) Presenting the binding processes of QY-8 with POPC lipids at different times. (B) PI/Hoechst 33258 costaining of 4T1 cancer cells (objective magnification, 10 ×). The 4T1 cancer cells were treated with DMSO, 15 μmol/L Clip-71 or 15 μmol/L QY-8. (C) Quantification of the PI-positive cells using ImageJ. Data are presented as mean ± SD ($n = 3$). One-way ANOVA was applied for multiple comparisons. *$P < 0.05$, ns: not significant.

fluorescent group 7-DCCA did not alter the activity of Clip-71 (IC_{50}: 75.3 μmol/L for QY-9 *versus* 74.6 μmol/L for Clip-71) or QY-8 (IC_{50}: 14.1 μmol/L for QY-10 versus 11.8 μmol/L for QY-8) against 4T1 cells (Table 3, Supporting Information Table S1 and Fig. S28). The nucleus of cancer cells was stained green by SYBR Green I, while QY-9 and QY-10 emitted blue fluorescence. As shown in Fig. 6A, within 5 min administration of QY-9 or QY-10, obvious blue fluorescence could be detected. Meanwhile, with the extension of incubation time, Blue/Green ratios gradually increased, indicating that Clip-71 and QY-8 could progressively and efficiently enter the cancer cells. Besides, QY-9 and QY-10 were found to cluster into a hollow circle, while positioning around the nucleus, indicating that Clip-71 and QY-8 could rapidly penetrate the cell membrane and accumulate in the cytoplasm.

In addition, to evaluate the interference of fluorescent probe 7-DCCA on the penetrating and localization of Clip-71 and QY-8, the noncovalent combination of free 7-DCCA and Clip-71, or the noncovalent combination of free 7-DCCA and QY-8 was applied for live-cell imaging. As shown in Fig. 6A and B, very weak blue fluorescence could be detected from 5 to 30 min, and the blue/green ratios remained below 0.2 throughout the experiment. These phenomena indicated that free 7-DCCA could not obviously enter the cancer cells or label the 4T1 cancer cells. Collectively, the subcellular localization experiment indicated that both Clip-71 and QY-8 could rapidly penetrate the cell membrane, enter cancer cells and aggregate in the cytoplasm. Of note, in terms of the speed and degree of cell penetration efficiency, no statistical difference was detected between Clip-71 and QY-8.

2.6. *Inhibition of tumor growth by Clip-71 and QY-8 in mice*

The above study indicated that D-type peptide represented by QY-8 possessed improved anticancer activity and durable anticancer efficiency, high proteolytic stability, as well as improved membranolytic effect. To evaluate the *in vivo* anticancer potential of Clip-71 derived peptides, QY-8 was selected and applied for tumor growth and survival experiments utilizing the solid tumor models (4T1 tumors-bearing mice) (Fig. 7A). Normal saline and Clip-71 were applied as negative and positive controls, respectively.

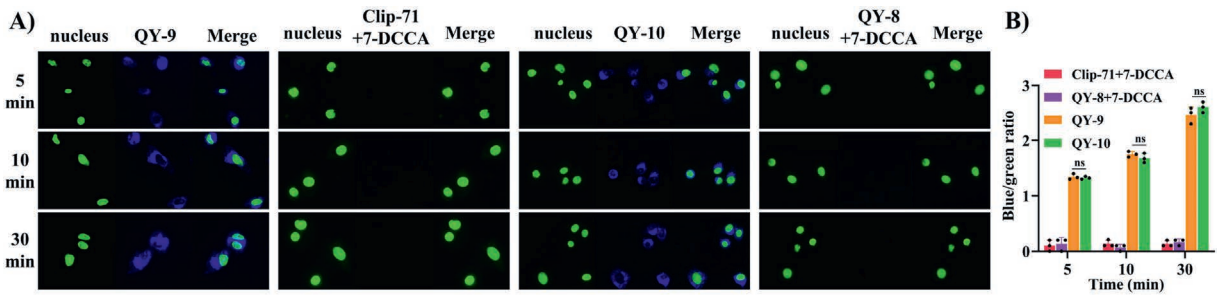

Figure 6 Subcellular localization of QY-9 and QY-10. (A) Fluorescence images of 4T1 cells treated with 15 μmol/L QY-9, 15 μmol/L QY-10, 15 μmol/L Clip-71 plus 15 μmol/L free 7-DCCA, or 15 μmol/L QY-8 plus 15 μmol/L free 7-DCCA at different time points. Cells were labeled with the nuclear probe SYBR Green I. (B) The quantification of the fluorescence intensity of (A) was conducted utilizing the ImageJ software. Data are presented as mean ± SEM ($n = 3$). One-way ANOVA was applied for multiple comparisons. ns: not significant.

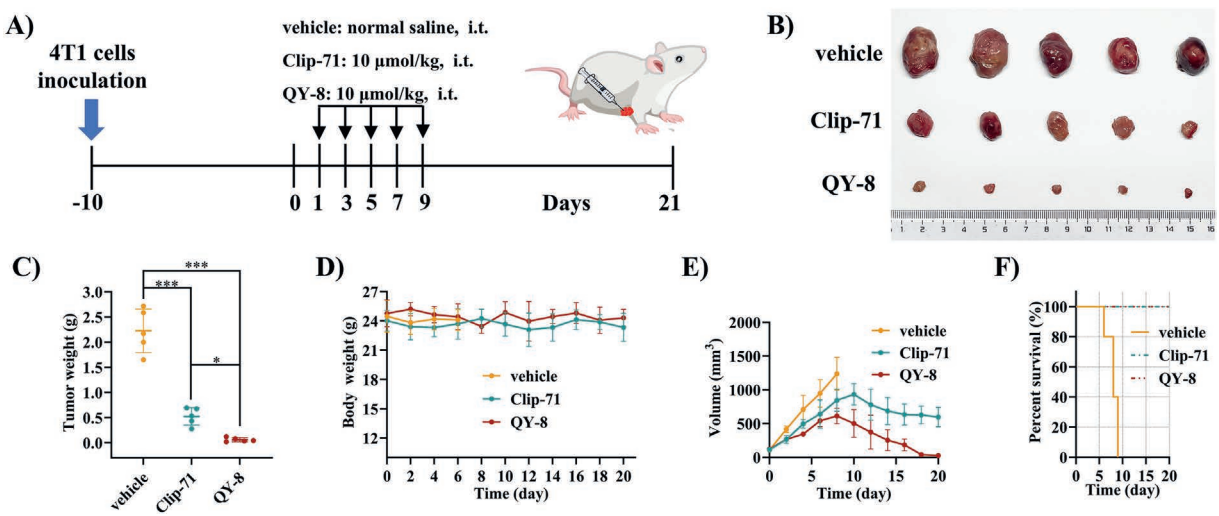

Figure 7 Tumor growth inhibition by Clip-71 and QY-8 in 4T1 tumor-bearing mice. (A) Schematic illustration of the timeline for the treatment of normal saline, Clip-71 or QY-8. (B) Images of 4T1 tumors excised from mice. (C) Weights of 4T1 tumors. Data are presented as mean ± SD ($n = 3$). (D) Body weights of mice in different experimental groups. Data are presented as mean ± SD ($n = 3$). (E) Tumor growth kinetics of different groups. Data are presented as mean ± SEM ($n = 3$). (F) Survival analysis of the 4T1 tumor-bearing mice. All P value were determined by multiple comparisons after one-way ANOVA. $^{*}P < 0.05$, $^{***}P < 0.001$.

According to animal ethical guidelines, mice were euthanized when the tumor volume exceeded 2000 mm^3 or if bleeding ulcers developed, and euthanasia was performed through cervical dislocation.

As shown in Fig. 7F, the tumor growth of the normal saline-treated mice was not suppressed, and all mice were euthanized within 9 days in accordance with animal ethical guidelines. Compared to the vehicle group, the intratumoral administration of either Clip-71 or QY-8 exhibited significant cancer growth inhibition in terms of tumor volume and weight (Fig. 7B−F). Notably, QY-8 exhibited a more potent tumoricidal effect than Clip-71, which was consistent with the higher cytotoxic effect of QY-8 in the *in vitro* cytotoxicity assay. Especially, the stripped tumors treated with QY-8 were obviously smaller than those in the Clip-71 treated groups, further suggesting the potent tumoricidal activity of QY-8 (Fig. 7B and C).

Compared with saline-treated mice which were euthanized within 9 days in accordance with animal ethical guidelines, Fig. 7F indicated that the administration of Clip-71 and QY-8 significantly lengthened the survival time, and the mice survived for more than 21 days. The survival analysis of mice in different groups further verified that Clip-71 and QY-8 possess favorable anticancer activity and could effectively extend the survival of tumor-bearing mice. In addition, the mice treated in the Clip-71 and QY-8 groups maintained stable body weight and normal physical condition throughout the *in vivo* therapy (Fig. 7D), suggesting that the administration of D-type peptide QY-8 did not cause serious *in vivo* toxicity at the dose tested. Collectively, the *in vivo* anticancer experiment indicated that QY-8 possessed superior *in vivo* anticancer activity to Clip-71, which may serve as a potential candidate for further optimizations.

2.7. Design and synthesis of TATE-oncolytic peptide based PPCs

The above stability and anticancer experiments indicated that the D-type peptide QY-8 exhibited improved proteolytic stability, more durable anticancer efficiency, as well as significantly higher *in vitro* and *in vivo* anticancer activities. Nevertheless, like most oncolytic peptides, including those in clinical trials, QY-8 still exhibited moderate selectivity toward cancer cells and was thus administered through intratumoral injection in the *in vivo* anticancer experiments. Recently, peptide−drug conjugates (PDCs) are gaining increasing recognition as a new strategy for targeted drug delivery possessing improved efficacy and reduced side effects for anticancer therapy[17,19,74,107-109]. To improve the therapeutic efficiency and reduce the undesired toxicity to normal tissues of chemotherapeutic agents, PDCs have been designed by conjugating chemotherapeutic agents with tumor-targeting peptides[74]. These tumor-targeting peptides could selectively bind to the membrane proteins/cell surface receptors uniquely expressed or overexpressed in cancer cells (*e.g.*, SSTR2, EGFR, GnRH-R, integrin receptors), which could increase the cancer penetration and selectivity of chemotherapeutic agents[17]. Especially, SSTR2 holds great potential for the development of PDCs, and multiple SSTR2-targeting PDCs have been approved or entered clinical trials[17,110,111]. Inspired by the PDC strategy, we intended to develop novel peptide−peptide conjugates (PPCs), which were designed through the hybridization of tumor-targeting peptides and oncolytic peptides.

To improve the tumor-specific targeting of oncolytic peptides, the PPCs were created by linking tumor-targeting peptide to oncolytic peptides. As both *in vitro* and *in vivo* studies suggested that D-type peptide QY-8 may be a promising anticancer candidate for further optimization, we selected QY-8 as the warhead for PPCs. The SSTR2 (Somatostatin Receptor 2) targeting peptide Tyr^3-octreotate (TATE) has been considered as a promising tumor-homing peptide and has been widely applied in the design of PDCs[78,112]. TATE is a cyclic octapeptide and possesses extremely high affinity with SSTR2 (Fig. 8A). Notably, SSTR2, which is frequently overexpressed on the surface of multiple tumors, serves as a promising therapeutic target, enabling tumor imaging and targeted treatment in cancers with high SSTR2 expression[111,113-117]. Especially, ^{177}Lu-DOTA-TATE (Lutathera), which uses TATE as the targeting peptide, is the first approved PDC and is primarily applied to treat pancreatic, gastrointestinal, and neuroendocrine tumors[17,110].

Although multiple PDCs based therapeutic agents have entered clinical or preclinical evaluations, little effort has been devoted to developing PPCs composed of tumor-targeting peptides and anticancer peptides. Meanwhile, to the best of our knowledge, the anticancer effects of TATE-oncolytic peptide based PPCs have not been explored. Therefore, in order to improve the anticancer effect of oncolytic peptides and enhance their targeting toward tumor cells, Clip-71 and QY-8 were conjugated to tumor-targeting peptide TATE *via* amide bonds, generating the PPCs QY-12 and QY-13, respectively (Fig. 8A and Figs. S15 and S16). The hydrophilic AEEA group was utilized as the linker connecting the TATE and oncolytic peptides (Fig. 8A and Fig. S2). The binding ability of TATE-oncolytic peptide based PPCs to SSTR2 receptor, *in vitro* serum stability, hemolysis effects, *in vivo* and *in vitro* anticancer activity, intracellular uptake, and preliminary anticancer mechanism were systematically investigated.

The TATE-oncolytic peptide based PPCs are composed of three parts: the lytic peptide sequence, the SSTR2 binding sequence and the linker AEEA (Fig. 8A and B). The DIC/Oxyma based condensation system was utilized for the efficient manual synthesis of hybrid peptides at 50 °C (Fig. 8D−F and Fig. S16), and the results demonstrated the compatibility of Wang resin with DIC/Oxyma based Fmoc-SPPS. Fmoc-Cys(Acm)-OH was used for the coupling of two cysteine residues, which facilitates the solid-phase disulfide bond formation (Fig. 8C). The TATE moiety was first attached to the resin by the above-mentioned coupling strategy. Subsequently, after the coupling of AEEA to D-type Phe, the oncolytic peptide moiety was attached to TATE moiety. After the coupling of all amino acid residues, $Tl(TFA)_3$ was added to remove the Acm protecting groups and simultaneously construct the disulfide bonds during the SPPS (Fig. 8C)[118-121]. Especially, utilizing the protocols including the peptide cleavage, peptide purification, and lyophilization as the synthesis of oncolytic peptides, the target peptides QY-12 and QY-13 were obtained with good RP-HPLC purity (42% and 49%, respectively, based on peak area ratios, Figs. S15 and S16) for crude peptide, and the isolated yield above 15% for both peptides.

Furthermore, Tris(2-carboxyethyl)phosphine hydrochloride (TCEP) has been shown to be a highly effective reducing agent that could selectively reduce disulfide bonds[114,122]. The purified QY-12 and QY-13 were mixed with freshly prepared TCEP solution, and then subjected to the RP-HPLC and ESI-MS analysis. The TCEP based reduction experiment further confirmed the correct construction of disulfide bonds in QY-12 and QY-13 (Figs. S15 and S16). To accelerate the coupling efficiency, the DIC/Oxyma-based condensation system was used for the efficient manual synthesis of PPCs. To further verify the robustness of the

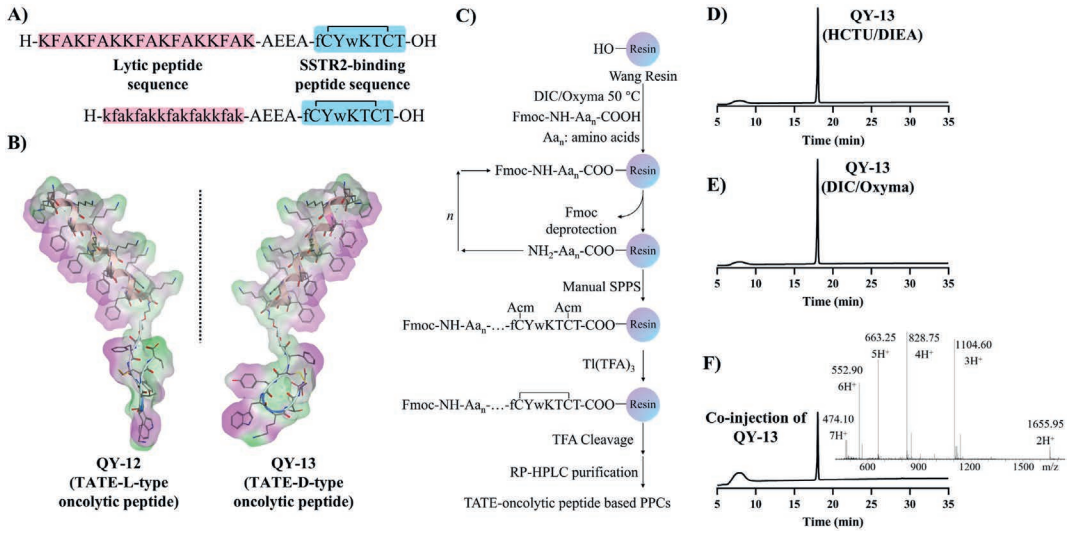

Figure 8 Synthesis and identification of TATE-Oncolytic peptides. (A) The amino acid sequence of TATE-Oncolytic peptide based PPCs (up QY-12, down QY-13), consisting of the SSTR2-binding peptide fragment and the lytic peptide fragment. (B) Calculated secondary structure model of QY-12 and QY-13 (generated by the MOE 2014. 0901). (C) The synthetic route of TATE-oncolytic peptide based PPCs. (D) The RP-HPLC spectra of QY-13 synthesized by the HCTU/DIEA condensation system at 28 °C. (E) The RP-HPLC spectra of QY-13 synthesized by the DIC/Oxyma condensation system at 50 °C. (F) RP-HPLC and ESI-MS spectra of coinjections of QY-13 prepared by two condensation systems. RP-HPLC condition: a linear gradient of 20%−60% buffer B in buffer A over 30 min (10%−20% for 2 min, then 20%−60% for 30 min) on an Agilent C18 column. The ESI-MS of QY-13 gave the observed mass of 3311.01 (calculated 3311.07 Da, average isotopes).

DIC/Oxyma based condensation system, the QY-13 prepared by the HCTU/DIEA based condensation system at 28 °C or the DIC/Oxyma based condensation system at 50 °C was analyzed by the analytical RP-HPLC and ESI-MS (Fig. 8 and Fig. S16). For the coinjections of QY-13 synthesized by different methods, only one main peak was detected by the analytical RP-HPLC and ESI-MS analysis (Fig. 8F). Moreover, for the coinjections of purified QY-12 (composed of TATE and Clip-71 moieties) and QY-13 (composed of TATE and QY-8 moieties), only one peak was detected by the analytical RP-HPLC analysis (Fig. S17). These data proved the robustness of DIC/Oxyma condensation system, which features with low rate of racemization during peptide synthesis at 50 °C. Collectively, by utilizing of DIC/Oxyma based manual SPPS, the cost-effective and efficient method was established for the preparation of TATE-oncolytic peptide based PPCs, which will provide valuable references for the synthesis of other TATE-containing hybrid peptides.

2.8. SSTR2 expression in different cancer cell lines

Somatostatin receptor 2 (SSTR2) is highly expressed in many solid tumor cells, which could be targeted for selective delivery of cytotoxic or radiotherapeutic warheads to the tumor tissue[16,74,123,124]. PDC strategies that specifically bind SSTR2 receptor have been widely used in the diagnosis and treatment of cancer[111,125]. According to previous literature, the SSTR2-high expressing cancer cell lines (HepG2, 4T1, and MCF-7), and SSTR2-low expressing cancer cell lines (PANC-1 and PC-3) were selectively applied for anticancer evaluation of SSTR2-targeting PPCs[126-130]. To investigate the differences in SSTR2 protein expression between different cancer cell lines, the western blotting was conducted. As illustrated in Fig. 9A and B, consistent with previous studies[126-129], SSTR2 was highly expressed in HepG2, 4T1, and MCF-7 cancer cell lines, while lowly expressed in

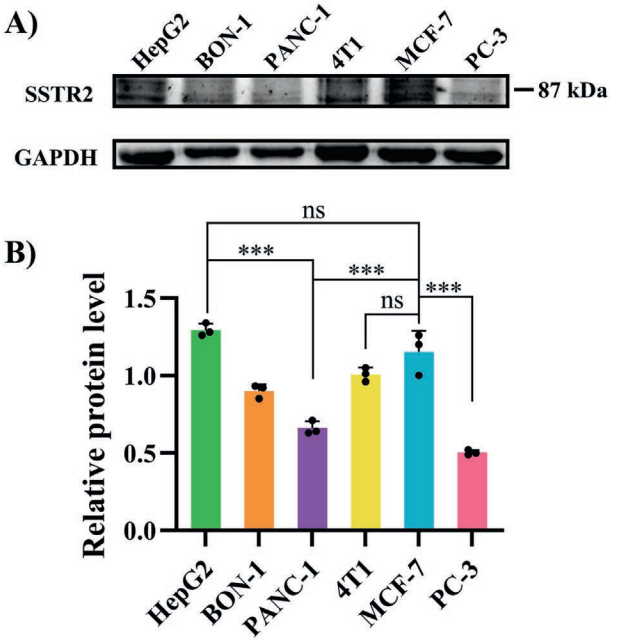

Figure 9 The SSTR2 expression in various cancer cells. (A) The levels of SSTR2 were measured using Western blotting assay in six cancer cells. (B) Quantification of SSTR2 using ImageJ. Data are presented as mean ± SEM ($n = 3$). P values were determined by multiple comparisons after one-way ANOVA. ***$P < 0.001$, ns: not significant.

PANC-1 and PC-3 cancer cells. These results further verified that SSTR2 has the potential to be applied in targeted cancer therapy. According to the results of western blotting, HepG2, 4T1, and MCF-7 cell lines (high SSTR2 expression) and PANC-1 and PC-

3 cell lines (low SSTR2 expression) were selected and applied for the subsequent cytostatic experiments.

2.9. *The interaction between TATE-oncolytic peptide based PPCs and SSTR2*

In order to verify the binding of PPC QY-13 with SSTR2, the Amber software was utilized to perform 50 ns of molecular dynamics simulations on the QY-13-SSTR2 complex[131]. As demonstrated in Fig. 10A, the TATE sequence, which functions as the primary binding site of QY-13, exhibits a profound penetration into the pocket of SSTR2. AEEA fulfills a role as a linker, effectively separating the TATE sequence from the lytic peptide sequence. Additionally, it has been observed to form hydrogen bond interactions with certain amino acids (Fig. 10B).

As illustrated in Supporting Information Fig. S26A, the TATE sequence demonstrates a low root mean square fluctuation (RMSF) value (0−5 Å)[132], while lytic peptide sequence exhibits high flexibility due to the absence of spatial constraints. The root mean square deviation (RMSD) can be used to measure the stability of QY-13-SSTR2 complex[133,134]. Specifically, QY-13 demonstrated stable RMSD values during the 50 ns simulation (Fig. S26B). It is noteworthy that the lytic peptide sequence demonstrates increased flexibility, and the complex-c (SSTR2-QY-13 after removal of the lytic peptide sequence) and ligand-c (QY-13 after removal of the lytic peptide sequence) regions, exhibit lower RMSD values (Fig. 10C). This further substantiates the stability of the core region. Furthermore, Molecular Mechanics Generalized Born/Surface Area (MMGB/SA) binding free energy was calculated of QY-13 and SSTR2 receptors[135,136]. As demonstrated in Fig. 10D, the TATE sequence contributed to the majority of the binding free energy. In summary, the computer simulation indicated that PPC QY-13 exhibits a robust binding to the SSTR2 receptor.

2.10. *Western blotting results of pull-down fraction*

To further investigate the effect of oncolytic peptides and AEEA linker on the interaction between TATE and SSTR2, the pull-down experiments were conducted (Fig. 10E) [137-139]. To achieve the pull-down assay, peptides QY-14, QY-15, and QY-16 were designed and synthesized by conjugating Biotin to the N-terminus of TATE, QY-8, and QY-13, respectively (Table 2, Fig. S18−S20). The pull-down experiments were analyzed by western blotting using anti-SSTR2 specific antibodies. The results showed that QY-16 had an affinity for SSTR2 that was equivalent to 0.8 times that of QY-14 at the same concentration, whereas both the Biotin and QY-15 groups did not show detectable protein bands of SSTR2 (Fig. 10F). These results indicated that the SSTR2 protein could be captured by TATE, but not by Biotin or oncolytic peptide.

Using the concentration of 25 μmol/L QY-14 or QY-16, the relative SSTR2 binding in the QY-16 group was slightly lower than that in the QY-14 group, suggesting that conjugation with the oncolytic peptide QY-8 may reduce TATE's affinity for SSTR2.

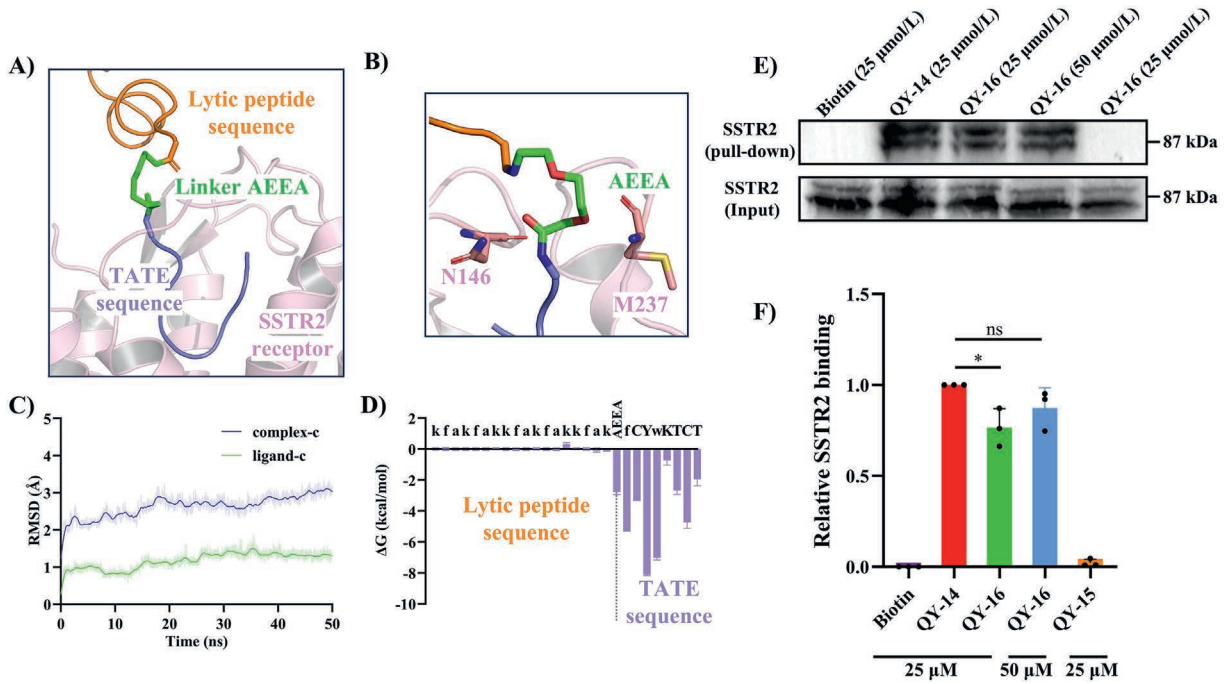

Figure 10 Evaluation of the affinity of peptide QY-13 with SSTR2. (A) Binding mode of QY-13 at the SSTR2 (pink cartoons) obtained through over 50 ns MD simulations. (B) Binding model of AEEA of QY-13 at the SSTR2 receptor. (C) Root mean square deviation (RMSD) of the backbone of the complex-c and ligand-c in MD trajectories. (D) Bar statistics of total binding free energies (shown as ΔG) of each amino acids of QY-13 toward SSTR2. ΔG was calculated and shown as the mean ± SEM. (E) Validation of QY-16-SSTR2 binding by Western blotting. MCF-7 cell lysates were incubated with Biotin (25 μmol/L), QY-14 (25 μmol/L), QY-16 (25 μmol/L), QY-16 (50 μmol/L), or QY-15 (25 μmol/L) at 4 °C overnight. The lysates were used for streptavidin pull down assays, and the precipitates were separated by SDS-PAGE, followed by western blotting analysis. Input: 5% of cell lysate. (F) Quantitative analysis of the relative binding of different treatment agents to SSTR2. Signal intensities of pull-downed samples were normalized relative to those of input. Data are presented as mean ± SD ($n = 3$). All P values were determined by multiple comparisons after one-way ANOVA. *$P < 0.05$, ns: not significant.

Meanwhile, 50 μmol/L QY-16 exhibited comparable SSTR2 binding ability as that of 25 μmol/L QY-14, suggesting that the conjugation of oncolytic peptide and AEEA linker may not significantly impair the binding between TATE and SSTR2. Moreover, these observations align with the results of molecular dynamics simulations, verifying the high binding affinity between TATE and SSTR2 (Fig. 10A). Nevertheless, it should be pointed out that more detailed assays such as surface plasmon resonance (SPR) are required to investigate the binding affinity between hybrid peptides and SSTR2[23,24,140]. Collectively, the pull-down assays confirmed that the binding affinity of TATE toward SSTR2 could be retained after conjugation with oncolytic peptides, and the TATE-oncolytic peptide QY-13 still possessed specific binding affinity toward SSTR2.

2.11. In vitro cytostatic effects of TATE-oncolytic peptides based PPCs

To evaluate the *in vitro* cytotoxic effects of TATE-oncolytic peptide based PPCs, the *in vitro* anti-proliferation effects were investigated against SSTR2 high-expressed cancer cell lines MCF-7, HepG2, and 4T1, SSTR2 low-expressed cancer cell lines PANC-1 and PC-3, and the normal cell line MRC-5 (Table 4 and Supporting Information Fig. S27). As shown in Table 4, consistent with reported results, the SSTR2-specific binding peptide TATE exhibited a weak anti-proliferation effect against both cancer and normal cell lines, with the IC_{50} values above 100 μmol/L throughout the experiments[114-116]. Meanwhile, Clip-71 exhibited moderate cytotoxicity ($IC_{50} > 50$ μmol/L) against MCF-7, 4T1, PANC-1, and PC-3 cells, while QY-8 showed improved cytotoxic effects with IC_{50} values ranging from about 10 to 50 μmol/L. Nevertheless, it was found that HepG2 cells exhibited resistance to Clip-71 and QY-8, with IC_{50} above 100 μmol/L for both oncolytic peptides. Consistent with the cytostatic observations in Table 3, these data further verified that D-type amino acid substitutions could improve the *in vitro* anticancer efficacy of Clip-71.

Compared with free Clip-71, the TATE-oncolytic peptide based PPCs QY-12 and QY-13 exhibited improved anti-proliferation effects against all five cancer cell lines. Especially, QY-12 and QY-13 could effectively inhibit the proliferation of HepG2 cells which were resistant to both Clip-71 and QY-8. Compared with Clip-71, QY-12 exhibited at least 3.1-fold increase in killing effect against the SSTR2 high-expressed cancer cell lines (MCF-7, HepG2, and 4T1). On the contrary, for the SSTR2 low-expressed cancer cell lines (PANC-1 and PC-3), QY-12 exhibited about 1.3-fold increase compared with Clip-71. Of note, compared with Clip-71, QY-13 exhibited more than 10-fold increase in killing effects against the SSTR2 high-expressed cell lines (MCF-7, HepG2, and 4T1), while only about 2-fold increase against SSTR2 low-expressed cell lines (PANC-1 and PC-3). Besides, the SI^b values were applied to characterize the differential cytotoxicity of peptides against cancer cells with high and low expression of SSTR2. The SI^b value of QY-8 was 1.9, while that of QY-13 was calculated to be 6.5, which suggested that QY-13 exhibited stronger killing activity against SSTR2-high expressing cancer cells. The different anti-proliferation effects between SSTR2 high- and low-expressed cancer cell lines may be attributed to the fact that TATE in QY-12 and QY-13 interacted with surface receptor SSTR2, which then improves the membrane interaction and disruption efficiency of oncolytic peptide.

The selectivity indexes SI^a (IC_{50} normal cells/IC_{50} cancer cells) have been widely applied to preliminarily analyze the selective anti-proliferation effects of oncolytic peptides[141]. Especially, MRC-5 has been widely utilized as the normal cells to compare the selectivity of oncolytic peptides[28,30,142]. Therefore, to investigate the selectivity of TATE-oncolytic peptide based PPCs, the SI^a values (SI^a = IC_{50} MRC-5/IC_{50} MCF-7) were determined by calculating the ratios between the IC_{50} values of normal MRC-5 cells and IC_{50} values of SSTR2 high-expressed MCF-7 cells. The parent Clip-71 and D-type peptide QY-8 exhibited weak selectivity against MCF-7, with SI^a values of 1.0 and 1.6, respectively (Table 4). On the contrary, QY-12 and QY-13 possessed improved selectivity, with SI^a values of 2.3 and 5.0, respectively, which were higher than those of Clip-71 and QY-8. Promisingly, the IC_{50} values of QY-13 for MCF-7, HepG2 and 4T1 cancer cell lines ranged from 5.3 to 9.3 μmol/L, while the IC_{50} value was 26.5 μmol/L against the normal cell MRC-5, suggesting the robust selectivity of QY-13 for SSTR2 high-expressed cancer cells. Collectively, the SI^a values indicated that the conjugation of tumor targeting peptide TATE may improve the selectivity of oncolytic peptides. Moreover, QY-13, which contains the D-type oncolytic peptide QY-8, exhibited superior selectivity for cancer cells in comparison to QY-12 containing L-type oncolytic peptide Clip-71.

Compared with free Clip-71 or free QY-8, the TATE-QY-8 based PPC (QY-13) exhibited significantly improved activity and selectivity against cancer cells. To investigate whether covalent ligation of TATE is necessary for these improvements, the different combinations (noncovalent application) of free TATE and free QY-8 were applied to test their cytotoxic effects against

Table 4 IC_{50} values (μmol/L) of TATE-Oncolytic peptides based PPCs.

Combined agents	Agent	SSTR2 high expression			SSTR2 low expression		MRC-5	SI^a	SI^b
		MCF-7	HepG2	4T1	PANC-1	PC-3			
−	Clip-71	53.9 ± 2.1	>100	74.6 ± 5.6	59.6 ± 5.6	51.7 ± 1.3	54.5 ± 2.6	1.0	1.1
−	QY-8	23.0 ± 0.8	>100	11.8 ± 4.8	42.7 ± 3.8	26.8 ± 2.0	36.8 ± 3.1	1.6	1.9
−	QY-12	17.2 ± 2.4	22.4 ± 4.6	11.7 ± 1.8	41.0 ± 2.4	40.2 ± 2.9	39.0 ± 4.3	2.3	2.4
−	QY-13	5.3 ± 0.6	9.3 ± 2.1	5.6 ± 0.4	34.2 ± 1.7	23.3 ± 3.6	26.5 ± 1.9	5.0	6.5
−	TATE	>100	>100	>100	>100	>100	>100	−	−
10 μmol/L TATE	QY-8	25.3 ± 2.5	−	−	−	−	−	−	−
10 μmol/L QY-8	TATE	>100	−	−	−	−	−	−	−
TATE: QY-8 = 1:1 (molar ratio)		23.2 ± 1.3	−	−	−	−	−	−	−

The data are presented as the mean ± SEM (n = 3). SI^a = IC_{50}(MRC-5)/IC_{50}(MCF-7). SI^b = IC_{50}(PANC-1)/IC_{50}(MCF-7). Incubation time: 24 h
− Not applicable.

SSTR2 high-expressed MCF-7 cells. Table 4 and Supporting Information Fig. S28 indicated that regardless of the mixed proportions of TATE and QY-8, all three types of noncovalent administrations did not improve the *in vitro* anticancer activity of QY-8. Meanwhile, most of the combination index (CI) values were above 1, suggesting that the noncovalent administration did not produce obvious synergistic effects of anticancer activity or selectivity (Supporting Information Table S2)[143,144]. The above data illustrated that covalent ligation is necessary for improving the anticancer activity and selectivity of oncolytic peptides. Collectively, the conjugation of TATE moieties to oncolytic peptides may improve the anticancer potential of oncolytic peptides, and the obtained TATE-D-type oncolytic peptide based PPC (QY-13) exhibited significantly improved activity and selectivity against SSTR2 high-expressed cancer cells. Nevertheless, it should be noted that further detections such as the affinity assays are required to investigate the detailed role of TATE in TATE-oncolytic peptide based PPC.

2.12. In vitro cytostatic effects of QY-13 against drug-resistant cancer cell lines

Besides the evaluation of conventional *in vitro* cytostatic effects, this study also studied the *in vitro* activity of QY-13 against drug-resistant cancer cell lines, and compared its synergistic effect with traditional chemotherapeutic drugs doxorubicin (DOX) and cisplatin (DDP). The doxorubicin-resistant MCF-7/ADR cell line and cisplatin-resistant MDA-MB-231/DDP cell line were selected and tested following established methods[145]. As shown in Table 5 and Supporting Information Fig. S29, compared with wild-type cell lines, the killing activity of DOX against MCF-7/ADR cells decreased by 30.5-fold, and that of cisplatin against MDA-MB-231/DDP cells decreased by 7.3-fold. Consistent with previous reports[146-148], these results confirm that the selected cancer cell lines possessed stable drug resistance. Meanwhile, the *in vitro* killing activity of QY-13 against the above-mentioned drug-resistant cancer cell lines was evaluated. It was found that QY-13 exhibited comparable inhibitory activity against both wild type and drug-resistant cancer cell lines, indicating its potent *in vitro* cytotoxic effect on clinically drug-resistant cancer cells (Table 5).

Previous studies indicated that oncolytic peptides may reverse tumor chemoresistance and enhance drug sensitivity[6,149]. Thus, we investigated whether QY-13 at different concentrations could enhance the sensitivity of drug-resistant cancer cells to chemotherapy drugs DOX and DDP. The reversal fold (RF) was used to evaluate the resistance-reversing efficacy of QY-13, with RF $>$ 1 indicating enhanced drug sensitivity[150,151]. As shown in Table 5, QY-13 at 2 and 4 μmol/L significantly increased the sensitivity of MCF-7/ADR cells to DOX, with RF values of 1.56 and 4.77, respectively. In MDA-MB-231/DDP cells, QY-13 also exerted a comparable effect by enhancing the sensitivity of drug-resistant cells to cisplatin, with RF values of 1.59 and 5.23. Collectively, these results indicated that QY-13 not only exerted potent *in vitro* killing activity against drug-resistant cancer cells, but also enhanced the sensitivity of drug-resistant cancer cells to chemotherapy drugs.

2.13. Time-kill curve assay for TATE-Oncolytic peptide based PPCs

The above serum stability test and time-kill curve assay for Clip-71-derived peptides showed that the prototype peptide Clip-71 may be rapidly degraded by various protease, resulting in low stability and short anticancer durability, while D-type oncolytic peptides represented by QY-8 showed excellent proteolytic stability and durable anticancer efficiency. Since the TATE moiety may be degraded at the cellular level, to investigate the anticancer durability of TATE-oncolytic peptide based PPCs (QY-12 and QY-13), the time-kill curve assay was conducted. The SSTR2-high expressing cancer cell lines 4T1 and MCF-7 were selected and applied for the time-kill curve assay. As the *in vitro* cytostatic experiments indicated that the IC_{50} values for QY-8, QY-12, QY-13 against the MCF-7 and 4T1 cancer cells ranged from about 5 to 20 μmol/L, the intermediate concentration (10 μmol/L) was applied for the time-kill curve assay. 10 μmol/L of each peptide was co-incubated with MCF-7 or 4T1 cells at 37 °C for 4, 12, 24, 36, 48, and 72 h, respectively. The viabilities of 4T1 and MCF-7 cells at different time points were evaluated by MTT test.

It was found that 10 μmol/L treatment of Clip-71 exhibited weak inhibition against both MCF-7 and 4T1 cancer cells with the inhibition rates below 20% from 0 to 72 h, which was consistent with the high IC_{50} values of Clip-71 (Fig. 11A). On the contrary, QY-12 could more efficiently inhibit cancer cell proliferation against both MCF-7 and 4T1 cells, indicating that the conjugation of TATE could improve the anticancer efficiency of Clip-71. Nevertheless, with time prolonged, the antiproliferative effects of QY-12 gradually reduced, with the inhibition rates of 18% and 30% against MCF-7 and 4T1 cells respectively at 72 h, which may be attributed to the degradation of QY-12. Besides, consistent with the high *in vitro* IC_{50} values, the 10 μmol/L treatment of QY-8 exhibited moderate inhibition against 4T1 and MCF-7 from 4 to 72 h.

Notably, the QY-13, which was obtained through the hybridization of TATE and D-type oncolytic peptide QY-8, could induce rapid inhibition of cancer cells with 4 h, with the inhibition rates of 70% and 60% for 4T1 and MCF-7, respectively. With time prolonged, the antiproliferative effects of QY-13 gradually increased, with inhibition rates above 80% against 4T1 and MCF-

Table 5 Effect of QY-13 on IC_{50} values (μmol/L) of free DOX or free Cisplatin in resistant cell lines MCF-7 and MDA-MB-231.

Combined agents	agent	MCF-7	MCF-7/ADR	MDA-MB-231	MDA-MB-231/DDP	RF
−	QY-13	4.9 ± 0.8	5.4 ± 0.7	11.4 ± 3.1	12.3 ± 1.4	−
0 μmol/L QY-13	DOX	1.5 ± 3.1	45.8 ± 1.2	−	−	−
0 μmol/L QY-13	DDP	−	−	8.0 ± 1.2	58.6 ± 3.2	−
2 μmol/L QY-13	DOX		29.4 ± 2.2		−	1.56
4 μmol/L QY-13	DOX		9.6 ± 5.6		−	4.77
5 μmol/L QY-13	DDP		−		36.8 ± 2.1	1.59
10 μmol/L QY-13	DDP		−		11.2 ± 1.8	5.23

The data are presented as the mean ± SEM (n = 3). Incubation time: 48 h − Not applicable.

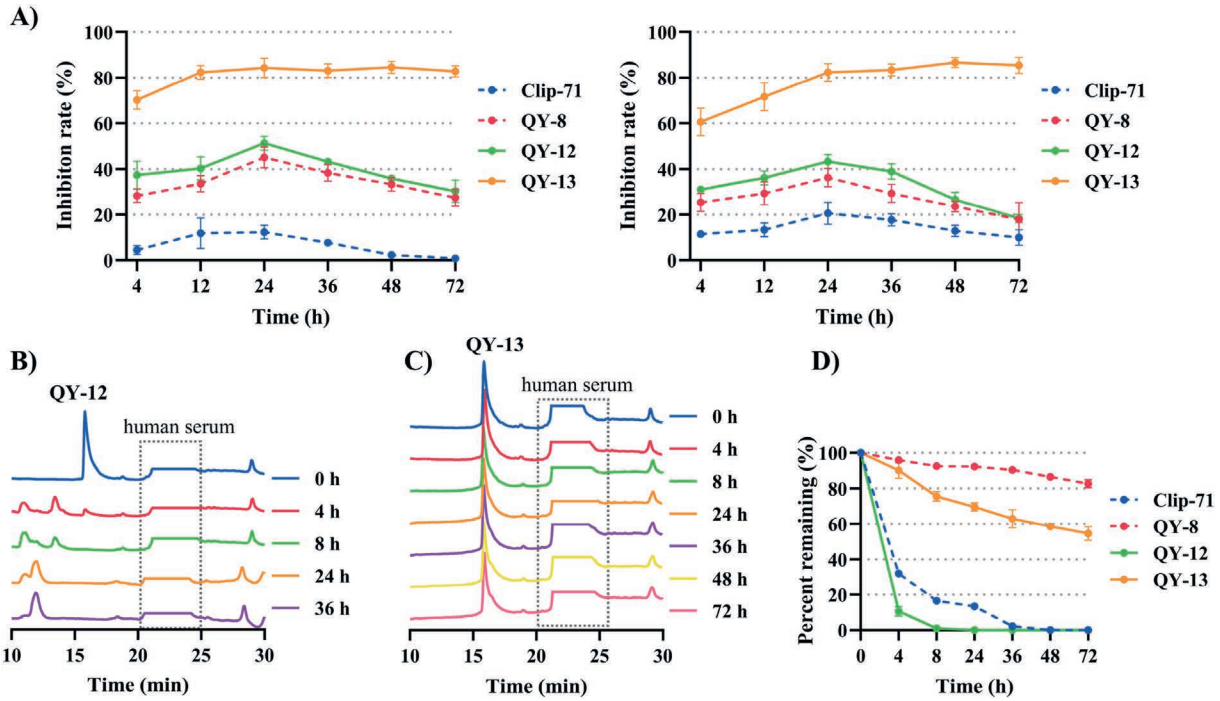

Figure 11 The time-kill curve assays and serum stabilities of TATE-Oncolytic peptide based PPCs. (A) Inhibition rate of peptides (10 μmol/L) against 4T1 (left) and MCF-7 (right) at the given treatment time. Data are presented as mean ± SEM ($n = 3$). (B, C) Analytical RP-HPLC spectra of the hydrolysis of QY-12 (B) and QY-13 (C) by human serum (10%, *v*/*v*). (D) Human serum stability of Clip-71, QY-8, QY-12 and QY-13 (100 μmol/L tested concentration for each peptide, monitored by the analytical RP-HPLC and ESI-MS). Data are presented as mean ± SD ($n = 3$).

7 at 24 h. Strikingly, different from the Clip-71, QY-8, and QY-12, all of which exhibited moderate inhibition efficiency or gradually lost anticancer ability from 24 to 72 h, QY-13 showed outstanding antiproliferative effects throughout the experiments, remaining inhibition rates above 80% at 72 h. Collectively, the time-kill curve assay indicated that PPC QY-13 possessed potent and durable anticancer effects until 72 h. Moreover, the conjugation of TATE could significantly improve the anticancer potency and durability of Clip-71-derived peptides.

2.14. *Serum stability of TATE-Oncolytic peptide based PPCs*

In order to evaluate the protease stability of the TATE-oncolytic peptides based PPCs (QY-12 and QY-13), the *in vitro* stability tests were conducted in 10% human serum at 37 °C. The analytical RP-HPLC and ESI-MS were used to monitor the integrity of peptides (Clip-71, QY-8, QY-12 and QY-13) from 0 to 72 h (Fig. 11B−D). Serum stability tests showed that Clip-71 was almost completely digested within 36 h, while QY-12 was nearly completely degraded within 8 h. The half-life of Clip-71 was calculated to be about 2.5 h, while the half-life of QY-12 was only about 1.2 h. As expected, the short half-lives of Clip-71 and QY-12 indicated that L-type oncolytic peptide sequence could be rapidly digested. Moreover, compared with Clip-71, QY-12 was more easily degraded, which may be attributed to the degradation of TATE moiety. Especially, TATE contains the disulfide bond and lysine (K) residue, both of which tend to be degraded in the serum environments.

Notably, unlike the L-type peptides Clip-71 and QY-12, it was found that the TATE-D-type oncolytic peptide based PPC QY-13 was relatively stable and exhibited resistance to human serum *in vitro* (Fig. 11C). Different from the rapid degradation of Clip-71 and QY-12, only 25% and 31% degradations of QY-13 were detected at 8 and 24 h, respectively. After 72 h incubation, 55% of full-length QY-13 could still be detected (Fig. 11D). Nevertheless, it should be pointed out that compared with the D-type oncolytic peptide QY-8 that was highly stable throughout experiments, QY-13 exhibited reduced proteolytic stability, which may be attributed to the degradation of TATE moiety. Collectively, the conjugation of TATE may reduce the stability of oncolytic peptides, and thus PPC QY-13 exhibited lower stability than the D-type oncolytic peptide QY-8. Previous studies have shown that disulfide bonds may be unstable in serum[152-154]. The LC−MS analysis was employed to monitor the stability of QY-13 in the serum, which indicated that the new HPLC peak 13* may be the disulfide bond-cleaved form of QY-13 (Supporting Information Fig. S30). Combined with the retention time and molecular weight of QY-13 co-incubated with TCEP, it is speculated that the disulfide bonds of QY-13 may be cleaved in serum (Fig. S30). Nevertheless, compared with the prototype Clip-71 and L-type oncolytic peptide based PPC QY-12, the D-type oncolytic peptide based PPC QY-13 possessed significantly higher protease stability and satisfactory integrity even after 72 h incubations in human serum.

2.15. *Anti-migration effect of Clip-71 and QY-13*

The overexpression of SSTR2 is associated with cancer cell migration, which is considered as one of the main causes of death for cancer patients[155-157]. To evaluate the anti-migration effect of Clip-71 and QY-13, the scratch healing assay was conducted on

the SSTR2-high expressing MCF-7 cancer cells. As expected, compared with the DMSO-treated group, the migration of the MCF-7 cells was more significantly hampered by Clip-71 and QY-13 (Fig. 12A). Especially, QY-13, which exhibited potent *in vitro* cytostatic effects, exhibited the strongest anti-migration ability on MCF-7 cells throughout the tests. Of note, 200 nmol/L of QY-13 (13% and 29% of relative mobility at 12 and 24 h respectively) exhibited stronger anti-migration effects than even 2 μmol/L of Clip-71 treated groups (36% and 54% of relative mobility at 12 and 24 h respectively) (Fig. 12A and B).

With the concentration increasing from 200 to 400 nmol/L, the migrations of cancer cells were more efficiently inhibited by QY-13, with 5% and 16% of relative mobility at 12 and 24 h, respectively. In contrast, there was no significant difference in the anti-migration ability between Clip-71 and TATE plus QY-8 treated groups, indicating that the non-covalent administration of TATE and QY-8 did not improve the anti-migration efficiency. Collectively, the wound healing tests suggested that conjugating oncolytic peptide with tumor-targeting peptide TATE could significantly enhance the anti-migration effect of oncolytic peptides on SSTR2 high-expressed cancer cells, which should be attributed to TATE-mediated binding to SSTR2.

2.16. Anticancer mechanism of TATE-Oncolytic peptide based PPCs

To enhance the anticancer potency and selectivity of oncolytic peptide, the novel tumor-targeting peptide and oncolytic peptide based conjugates (PPCs) were developed. The above cytostatic effect tests, time-kill curve and anti-migration assay indicated that QY-13, obtained by the conjugation of TATE and D-type oncolytic peptide QY-8, possessed durable anticancer effects against cancer cell lines within 72 h. Just like QY-8, QY-13 could effectively prolong the action time and overcome the stability problem of L-type oncolytic peptide Clip-71. More importantly, compared with QY-8, QY-13 exhibited significantly improved anticancer selectivity and higher activity against SSTR2 high-expressed cancer cells. Subsequently, the preliminary anticancer mechanism of the QY-13 was investigated for the membranolytic effect and cellular uptake assays.

2.16.1. Membranolytic effects of Clip-71, QY-8 and QY-13

Our above membranolytic effect assay showed that oncolytic peptides Clip-71 and QY-8 could disrupt cancer cell membranes, which induces the rapid death of cancer cells. Compared with D-type oncolytic peptide QY-8, the IC_{50} data indicated that the TATE-QY-8 based PPC (QY-13) exhibited significantly improved activity and selectivity against SSTR2 high-expressed cancer cells. To investigate the cell membrane disrupting effect of QY-13, the membrane integrity assay was performed against SSTR2 high-expressed cancer cell line MCF-7 and SSTR2 low-expressed cancer cell line PANC-1. After the treatment of negative control DMSO, Clip-71, QY-8, QY-8 plus TATE, or QY-13, the PI/Hoechst 33258 costaining was conducted. Subsequently, with the loss of cell membrane integrity, the cancer cells will gradually emit red fluorescence.

As depicted in Fig. 13A and C, the treatment of DMSO did not induce obvious red fluorescence within 90 min, and fewer than 5% of whole MCF-7 cells were stained by PI throughout the test. On the contrary, after treatment with 10 μmol/L Clip-71 or QY-8, cancer cells emitting red fluorescence were gradually increased from 10 min to 90 min. Meanwhile, 25% and 64% of MCF-7 cancer cells stained by PI were observed for Clip-71 and QY-8 respectively at 90 min. These data indicated that both oncolytic peptides possessed membranolytic effect. Moreover, the D-type oncolytic peptide QY-8 possesses the stronger membrane-lytic efficiency than the prototype Clip-71, which was consistent with the potent *in vitro* anticancer activity of QY-8 (Table 3). In addition, there was no obvious differences in PI positive cancer cells between the QY-8 plus TATE and QY-8 treated groups, indicating that the non-covalent combinations of QY-8 and TATE did not enhance the membranolytic ability of QY-8.

Strikingly, compared with Clip-71, QY-8, or QY-8 plus TATE treated groups, PPC QY-13 exhibited the most rapid and potent membranolytic effect against MCF-7 cancer cells. As depicted in Fig. 13A and C, 30 min treatment of 10 μmol/L QY-13 induced obvious red fluorescence in MCF-7 cells, which was significantly higher than all other groups. Moreover, the red fluorescence increased over time and 83% of whole MCF-7 cells were stained by PI at 90 min for the QY-13 treated group, indicating that the membrane integrity of most MCF-7 cells was changed by QY-13.

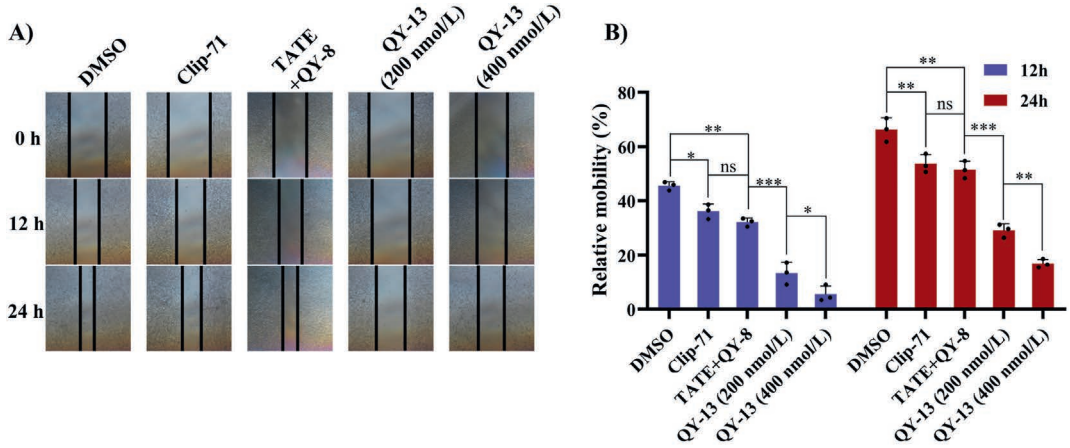

Figure 12 Anti-migration effects of Clip-71 and QY13 against MCF-7 cells. (A) Images of cell migration at 0, 12, and 24 h (objective magnification × 10). The MCF-7 cancer cells were treated with DMSO, 2 μmol/L Clip-71, 2 μmol/L QY-8 plus 2 μmol/L TATE, 200 nmol/L QY-13 and 400 nmol/L QY-13. (B) Quantification of the relative mobility. $*P < 0.05$, $**P < 0.01$, $***P < 0.001$, ns: not significant. Data are presented as mean ± SD ($n = 3$).

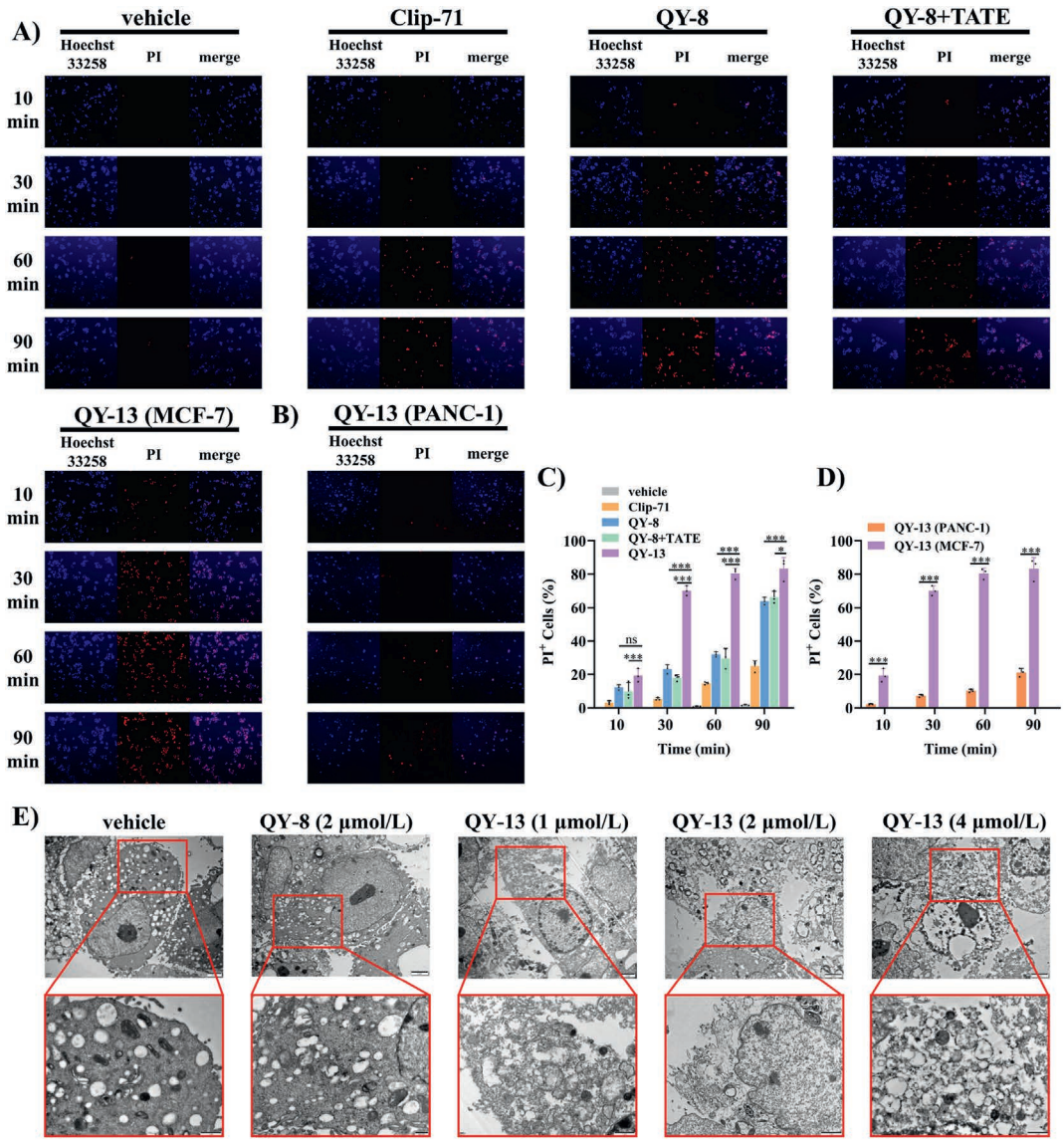

Figure 13 Membranolytic effect of TATE-oncolytic peptide based PPCs. (A−B) PI/Hoechst 33258 costaining of MCF-7 (A) and PANC-1 (B) cancer cells (objective magnification, 10 ×). The MCF-7 cancer cells were treated with DMSO, 10 μmol/L Clip-71, 10 μmol/L QY-8, 10 μmol/L QY-8 plus 10 μmol/L TATE, or 10 μmol/L QY-13. The PANC-1 cancer cells were treated with 10 μmol/L QY-13. (C−D) Quantification of PI-positive cells in MCF-7 (C) and PANC-1 (D) cells using ImageJ. Data are presented as mean ± SD ($n = 3$). One-way ANOVA was applied for multiple comparisons. *$P < 0.05$, ***$P < 0.001$, ns: not significant. (E) MCF-7 cells were treated with DMSO, 2 μmol/L QY-8, 1 μmol/L QY-13, 2 μmol/L QY-13 and 4 μmol/L QY-13 for 12 h followed by transmission electron microscopy observations.

On the contrary, for the SSTR2 low-expressed PANC-1 cancer cells, the treatment of 10 μmol/L QY-13 did not induce obvious red fluorescence, where fewer than 25% of whole PANC-1 cells were stained by PI within 90 min (Fig. 13B and D, Supporting Information Fig. S31). Consistent with the moderate cytotoxicity ($IC_{50} > 30$ μmol/L), QY-13 did not exhibit potent membranolytic effects against the PANC-1 cells. Collectively, QY-13 possessed the rapid and potent and membranolytic activity against SSTR2 high-expressed MCF-7 cancer cells, which may be one of the reasons for the increased *in vitro* anticancer activity of QY-13 against SSTR2 high-expressed cancer cells. Of note, compared with QY-8 or QY-8 plus TATE treated group, QY-13 exhibited significantly improved membrane-disrupting effects, which may be attributed to the interaction between TATE in QY-13 and SSTR2 protein.

2.16.2. The morphological changes of MCF-7 cancer cells treated with QY-8 or QY-13

The morphological changes of MCF-7 cancer cells treated with QY-8 or QY-13 were observed by transmission electron microscopy (TEM, Fig. 13E)[158]. After being treated with 2 μmol/L of QY-8 for 12 h, no significant morphological changes were observed in MCF-7 cells. In contrast, 1 μmol/L treatment of QY-13 caused the fragmentation of cell membrane, while the treated cell nucleus appeared intact. QY-13 at a concentration of 2 μmol/L triggered the moderate cell membrane rupture. Especially, QY-13 at a concentration of 4 μmol/L significantly caused the rupture of cell membrane and the leakage of nuclear components. The morphological changes in MCF-7 cancer cells indicated that QY-13 could dose-dependently disrupt the integrity of cancer cell membrane, while further triggering the leakage of nuclear

components. Meanwhile, the analysis of mitochondrial membrane potential indicated that Clip-71 and QY-8 did not change the mitochondrial membrane potential, suggesting that Clip-71 and QY-8 did not obviously destroy the mitochondrial membrane of cancer cells (Fig. S25). Still, it should be pointed out that more accurate experiments are needed to investigate the specific mechanism of QY-13 inducing the rupture of cell membrane and the leakage of nuclear component.

2.16.3. The cellular uptake of QY-13

The above membranolytic assay showed that the membranolytic ability of QY-13 was significantly higher than those of Clip-71 and QY-8. Moreover, QY-13 exhibited stronger membranolytic effects against cancer cells with high expression of SSTR2 than those with low expression of SSTR2. To investigate the potential reasons why QY-13 possessed potent membranolytic effect against the SSTR2-high expressed cancer cells, the cellular uptake and subcellular localization of QY-13 were explored by the live-cell imaging experiment. To monitor the uptake and subcellular localization of QY-13 in MCF-7 and PANC-1 cell lines, the typical fluorescent group 7-DCCA was attached to the N-terminal of QY-13, affording the fluorescent probe QY-17 (Supporting Information Fig. S21). The cytostatic assay indicated that the attachment of fluorescent group 7-DCCA did not attenuate the activity of QY-17 (Table 4 and Table S1). As shown in Fig. 14, the nucleus of cancer cells was stained green by SYBR Green I, while QY-10 (composed of 7-DCCA and D-type oncolytic peptide QY-8), QY-17 (composed of 7-DCCA and QY-13) or free 7-DCCA emitted blue fluorescence.

For the SSTR2-high expressed MCF-7 cells, obvious blue fluorescence could be detected after 15 min administration of QY-17 (Fig. 14A). With the extension of incubation time, the blue fluorescence gradually increased, and the ratio of blue to green fluorescence intensity reached about 3.2 at 90 min for the QY-17 treated group (Fig. 14C). Especially, compared with the QY-10 treated group, stronger blue fluorescence in the QY-17 treated group could be detected throughout the experiment (Fig. 14C). Moreover, for the noncovalent combination of 7-DCCA and QY-13, weak blue fluorescence was detected for MCF-7 cells, with the ratios of blue to green fluorescence intensity below 0.05 within 90 min (Fig. 14C). The absence of blue fluorescence suggested that free 7-DCCA could not label or enter cancer cells, and free QY-13 could not help 7-DCCA enter cancer cells within a short treatment time. Collectively, these data indicated that the attachment of TATE could significantly facilitate the cellular uptake of oncolytic peptide into cancer cells, which contributed to the improved *in vitro* anticancer potency of QY-13.

To further verify that the binding of TATE and SSTR2 promotes cellular uptake of QY-13, MCF-7 cells were first incubated with TATE and then treated with QY-17 for 15−90 min. Of note, pre-incubation of TATE significantly reduced the intensity of blue fluorescence, with an obvious decrease in the ratios of blue to green fluorescence intensity within 15−90 min (Fig. 14A and C). The reduction of blue fluorescence indicated that pre-incubation of TATE impaired the cellular uptake of QY-17. Moreover, the

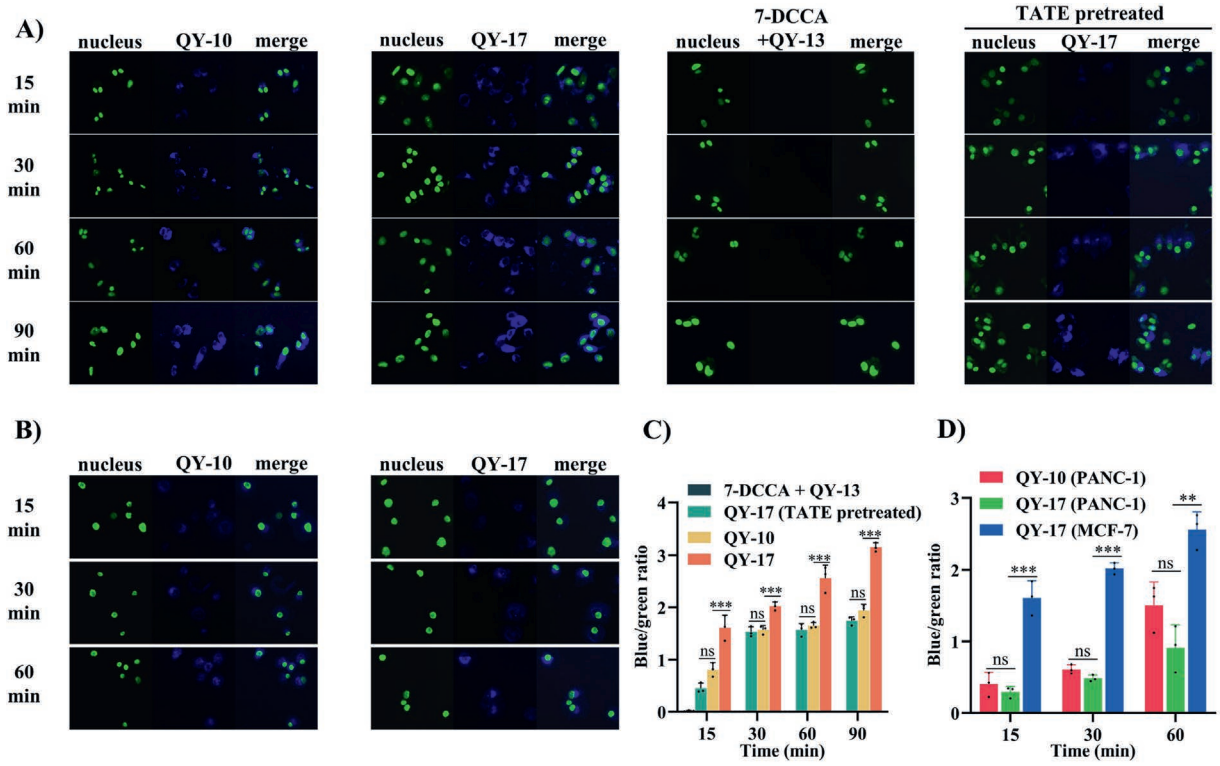

Figure 14 The cellular uptake of TATE-Oncolytic peptide based PPCs. (A) Fluorescence imaging of MCF-7 cells treated with QY-10, QY-17, QY-13 plus 7-DCCA, and QY-17 (MCF-7 cells preincubated with TATE). (B) Fluorescence imaging of PANC-1 cells treated with QY-10 and QY-17. (C, D) Quantification of fluorescence intensity of TATE-oncolytic peptide based PPCs on MCF-7 (C) and PANC-1 (D) cells using imageJ. Data are presented as mean ± SD ($n = 3$). One-way ANOVA was applied for multiple comparisons. $^{**}P < 0.01$, $^{***}P < 0.001$, ns: not significant.

cellular uptake of QY-13 was also investigated in the SSTR2-low expressed PANC-1 cells (Fig. 14B). The moderate blue fluorescence was detected in PANC-1 cells treated with either QY-10 or QY-17 within 60 min (Fig. 14D). Especially, there were no significant differences in blue fluorescence intensity between PANC-1 cells treated with either QY-10 or QY-17 group, both group of which exhibited much lower blue fluorescence intensity than the MCF-7 group treated with QY-17. Taken together, QY-13 exhibited significantly higher cellular uptake ability than other oncolytic peptides, which helped the improved anticancer activity of QY-13 toward SSTR2-high expressed cancer cells. Moreover, the interaction between TATE and SSTR2 may facilitate the binding and cellular uptake of QY-13 in entering SSTR2-high expressed cancer cells.

2.17. *Hemolytic activity of TATE-oncolytic peptide based PPCs*

Previous studies have reported that the administration of oncolytic peptides may induce the lysis of red blood cells and the clinical application of oncolytic peptides may be hindered by their severe hemolysis[31,159]. To investigate the hemolysis effect and preliminarily evaluate the safety of Clip-71, Clip-71-derived peptides, and TATE-oncolytic peptide based PPCs, the hemolysis assay was performed using the whole fresh mouse blood. The test concentrations of Clip-71, QY-8, QY-12, and QY-13 were 0.5 × IC_{50}, 1 × IC_{50}, 2 × IC_{50}, 4 × IC_{50}, 8 × IC_{50}, and 16 × IC_{50}. Triton X-100 and PBS (1 ×) treated groups were used as positive and negative controls, respectively. Overall, Fig. 15 indicated that all tested peptides caused the dose-dependent hemolysis at concentrations ranging from 0.5 × IC_{50} to 16 × IC_{50}. Like other oncolytic peptides, the prototype peptide Clip-71 exhibited severe hemolytic effects, with the hemolysis rates above 9%, 12%, and 18% at the concentrations of 1 × IC_{50}, 2 × IC_{50}, and 4 × IC_{50} respectively. At a peptide concentration of 8 × IC_{50}, the hemolysis rate of Clip-71 increased dramatically to 31%.

Interestingly, QY-8, which was obtained through L-type to D-type amino acid substitutions, exhibited weak hemolytic effects, with the hemolysis rates below 15% at all tested concentrations. In addition, even at a maximum concentration of 16 × IC_{50}, only 13% of erythrocytes were destroyed by QY-8, indicating that L-type to D-type amino acid substitutions may attenuate the undesired hemolytic activity. Meanwhile, the QY-12 and QY-13 showed low hemolytic effects, destroying only 15% and 10% of erythrocytes even at the concentration of 8 × IC_{50}. Especially, the hemolysis effect of hybrid peptide QY-13 was comparable to that of QY-8 at 0.5 to 8 × IC_{50} concentrations, suggesting that the conjugation of tumor-targeting peptide TATE did not improve the hemolysis effects.

It is worth mentioning that at working concentrations (1 × IC_{50}, about 5 μmol/L), only 3% of erythrocytes were destroyed by QY-13. Collectively, the hemolytic activity assay suggested that L-type to D-type amino acid substitutions could attenuate the undesired hemolytic effects of oncolytic peptides. Especially, the TATE-D-type oncolytic peptide based PPC QY-13 showed low hemolytic effects at its working concentrations. Nevertheless, it should be pointed out that *in vitro* hemolysis assay is not sufficient data, further explorations are required to investigate the detailed toxicity of Clip-71 and QY-13 against normal human cells. Meanwhile, the hematoxylin-eosin (H&E) staining, which is used to preliminarily explore the toxicity of peptides on normal mouse tissues, will be discussed below.

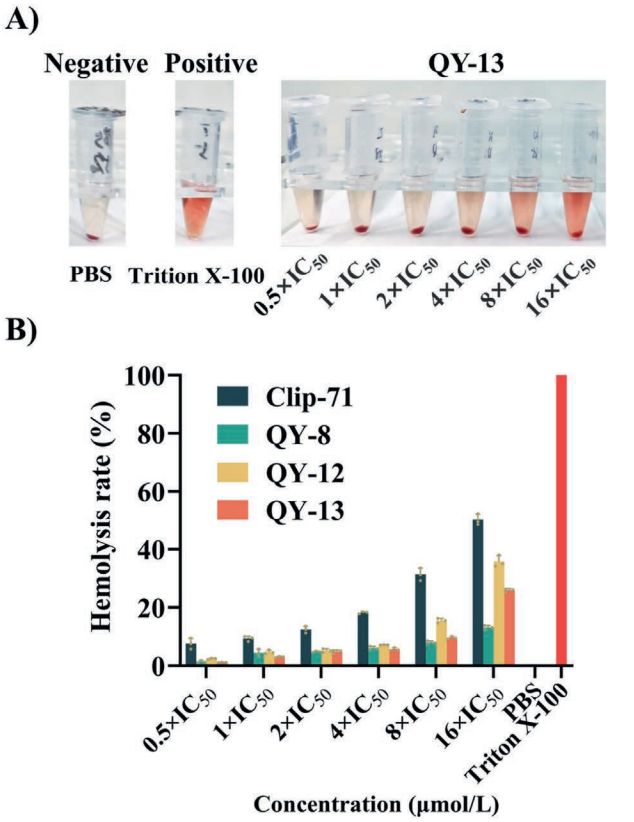

Figure 15 Hemolysis effects of Clip-71, QY-8, QY-12 and QY-13. (A) Images of hemolysis experiments with PBS, TritionX-100 and different concentrations of QY-13. (B) Hemolysis rates of Clip-71, QY-8, QY-12 and QY-13. Data are presented as mean ± SEM (n = 3). Red blood cells treated with 2% Trition X-100 were used as positive controls, and those treated with PBS were used as negative control.

2.18. *QY-13 significantly inhibited cancer growth in mice*

To further investigate the *in vivo* anticancer activity of the QY-13 composed of TATE and D-type oncolytic peptides, the tumor growth and survival experiments were conducted in the 4T1-Luc tumor-bearing mouse model (Fig. 16A). The 4T1-luc cells were injected into the armpits of Balb/c mice (n = 5 mice/group), and the growth of cancer tissue was monitored by the bioluminescence imaging (BLI Imaging) using *in vivo* imaging system (IVIS) for up to 16 days (Fig. 16A and B)[160,161]. The vehicle (normal saline), QY-8 (10 μmol/kg), QY-13 (5 μmol/kg), or QY-13 (10 μmol/kg) were given through intraperitoneal injection once every two days respectively, for seven consecutive administrations. The survival of mice and tumor volume were monitored daily. According to animal ethical guidelines, the euthanasia was performed through cervical dislocation when the tumor volume exceeded 2000 mm^3 or bleeding ulcers developed.

The bioluminescence signals of total tumor cells were quantified using LivingImage 4.4 (PerkinElmer, USA) (Fig. 16 B and C). In the saline-treated group, the luminescence intensity reached to 3.8 × 10^8 p/s on Day 16, while that of the QY-8-treated group was 2.55 × 10^8 p/s, indicating that QY-8 exhibited moderate antiproliferative activity (Fig. 16B and C). In the QY-13-treated groups of 5 μmol/kg and 10 μmol/kg, the luminescence signals

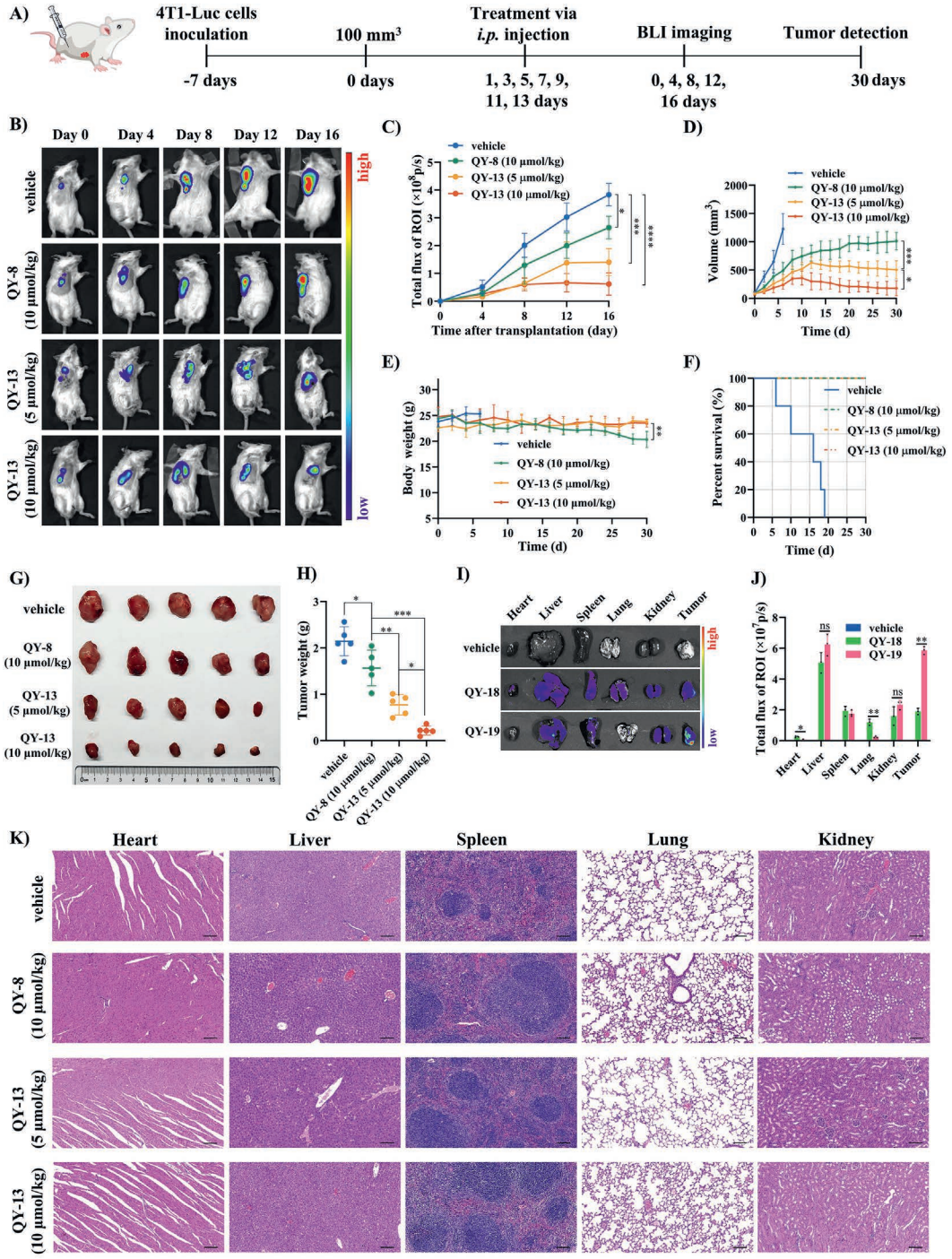

Figure 16 Cancer growth inhibition by QY-8 and QY-13 in 4T1-Luc tumor-bearing mice. (A) Schematic illustration of timeline for the *in vivo* anticancer experiment in Balb/c mice bearing 4T1-Luc tumors. (B) *In vivo* bioluminescence images (BLI) of mice on Days 0, 4, 8, 12 and 16. (C) Tumor growth curves as determined by quantification analysis of the *in vivo* bioluminescence signal. Data are presented as mean ± SD ($n = 3$). (D) Tumor volume kinetics. Data are presented as mean ± SEM ($n = 3$). (E) Body weights of the different groups. Data are presented as mean ± SD ($n = 3$). (F) Survival analysis of the 4T1-Luc tumor-bearing mice. (G) Images of the excised 4T1-Luc tumors. (H) Weights of the 4T1-Luc tumors. mean ± SD. (I) *Ex vivo* fluorescent images of different organs and tumors. (J) quantification fluorescence intensity of different organs and tumors. Data are presented as mean ± SD ($n = 3$). (K) Representative hematoxylin−eosin (H&E) staining of the heart, liver, spleen, lung and kidney excised from the mice. All P values were determined by multiple comparisons after one-way ANOVA. $^{*}P < 0.05$, $^{**}P < 0.01$, $^{***}P < 0.001$, $^{****}P < 0.0001$, ns: not significant.

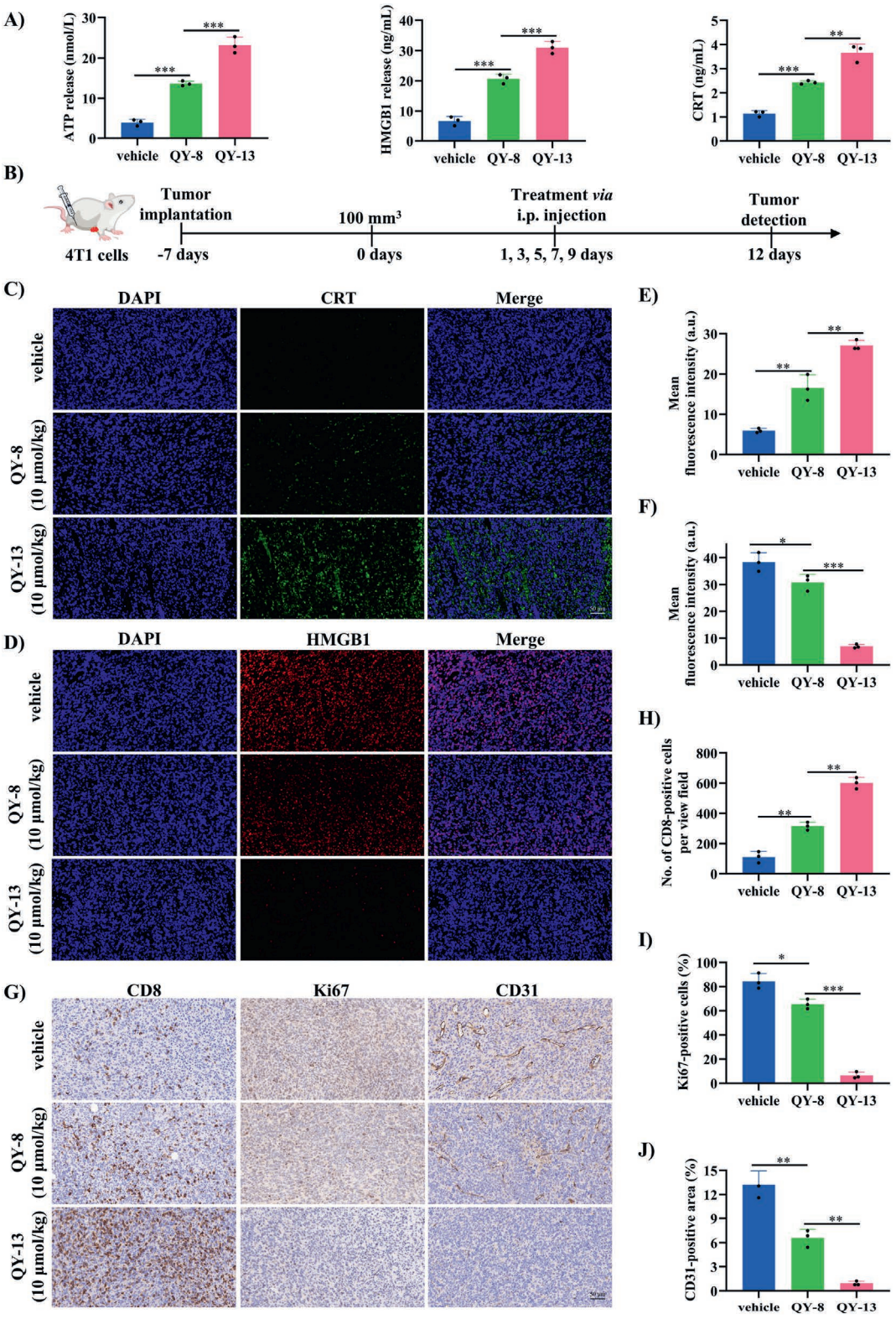

Figure 17 *In vitro* and *in vivo* ICD-eliciting·and immunity-activating·effects of QY-8 and QY-13. (A) Quantification analysis of ATP, HMGB1, and CRT release in MCF-7 cells. MCF-7 cells were treated with DMSO, 6 μmol/L QY-8, or 6 μmol/L QY-13 for 12 h. Amounts of released ATP determined by a chemiluminescent ATP determination kit. Amounts of released HMGB1 and CRT determined by HMGB-1 ELISA kit and CRT ELISA kit, respectively. (B) Schematic illustration of timeline for the immunotherapy experiment in Balb/c mice bearing 4T1 tumors. (C, D) Representative immunofluorescence images of CRT and HMGB1 of tumors after different treatments. Scale bar: 50 μm. CRT: green fluorescence. HMGB1: red fluorescence. (E, F) Quantitative fluorescence analysis of CRT (E) and HMGB1 (F). (G) Immunohistochemical detection of CD8, Ki67, and CD31 in 4T1 tumor sections. Scale bar: 50 μm. (H−J) Quantification of CD8 (H), Ki67 (I), and CD31 (J) expression in 4T1 tumor sections. Data are presented as mean ± SD ($n = 3$). All P values were determined by multiple comparisons after one-way ANOVA. *$P < 0.05$, **$P < 0.01$, ***$P < 0.001$.

were 1.41×10^8 p/s and 0.61×10^8 p/s on Day 16 respectively, which are 1.8 and 4.2-fold reduction in luminescence intensity compared to QY-8-treated group. The real time fluorescence monitoring showed that the QY-13 exhibited outstanding *in vivo* anti-proliferative activity, which is significantly higher than of QY-8.

Except the luminescence intensity, the tumor volume also indicated the tumor growth of the saline-treated mice was not suppressed, and QY-8 exhibited weak cancer growth inhibition (Fig. 16D). Besides, the stripped cancers treated with QY-13 were obviously smaller than those in the QY-8 and vehicle groups (Fig. 17G and H). Although the intratumoral administration of QY-8 induced the potent *in vivo* anticancer activity, intraperitoneal injection of QY-8 only induced weak anticancer potency, which may be contributed to its moderate selectivity toward cancer cells. Strikingly, from the perspectives of *in vivo* bioluminescence imaging, tumor volume and tumor weight, both 5 and 10 μmol/kg administration of QY-13 exhibited potent anticancer potencies, which was significantly higher than that of QY-8 (Fig. 16B−E, G and H).

In the survival experiments (Fig. 16F), the average survival time of normal saline-injected mice was 16 days (6 to 19 days) and all mice died within 19 days. In contrast, all other mice treated with either QY-8 (10 μmol/kg), QY-13 (5 μmol/kg), or QY-13 (10 μmol/kg) survived for more than 30 days (Fig. 16F). The administration of QY-8 caused body weight loss and muscle wasting in mice during the experiment (Fig. 16E). Still, no significant weight loss or hair loss was detected during the experiment for both the QY-13 (5 μmol/kg) and QY-13 (10 μmol/kg)-treated groups, suggesting that mice may be well tolerated at the peptide-administered dose.

To track the *in vivo* distribution of QY-13, the tumor-specific accumulation assay was conducted. Rhodamine B is a commonly used fluorophore in the *in vivo* distribution studies of peptide[162]. Thus, Rhodamine B was conjugated to the N-terminal of QY-8 and QY-13, affording the fluorescent probes QY-18 and QY-19 for *in vivo* imaging experiments (Figs. S22 and S23). Mice were inoculated with 4T1 cells to establish tumor-bearing models. When the tumor volume reached approximately 200−300 mm^3, a single dose of QY-18 (10 μmol/kg) or QY-19 (10 μmol/kg) was administered *via* intraperitoneal injection. 24 h later, the mice were euthanized, and fluorescence imaging of their organs was performed.

As shown in Fig. 16I and J, the fluorescent signal was not detected in the saline control group. In contrast, fluorescent signals were observed in all organs of mice in the QY-18 group, indicating that QY-18 could distribute to major organs 24 h after injection. Different from QY-18, the fluorescence in the QY-19 group was localized to the liver, spleen, kidneys, and tumor tissues of mice. Compared with QY-18, the distribution of QY-19 was obviously reduced in the heart and lungs. Especially, QY-19 was found to aggregate at the tumor site, with fluorescence intensity significantly higher than that of QY-18. QY-19 is composed of TATE, oncolytic peptide QY-8, and fluorophore rhodamine B. It is speculated that the TATE moiety, which targets SSTR2, could enhance the accumulation of QY-19 at the tumor site. Collectively, the tumor-specific accumulation assay demonstrated that QY-13 exhibited specific targeting to tumor tissues and effectively minimized non-specific distribution of the oncolytic peptide.

To further investigate whether QY-8 and QY-13 caused damage to major organs, histological analysis of organ sections (heart, liver, spleen, lung, and kidney) was performed by hematoxylin-eosin (H&E) staining (Fig. 16K)[134,163]. As shown in Fig. 16K, no significant histological damage was observed in the QY-8 and QY-13 treatment groups. Nevertheless, it should be pointed out that further *in vivo* toxicity studies should be conducted to explore the safety and selectivity of QY-13. Collectively, the *in vivo* anticancer experiments indicated that intraperitoneal injection of D-type oncolytic peptide QY-8 could not efficiently inhibit the proliferation of tumor cells, which induced moderate anticancer effects and weight loss in mice. Promisingly, from the perspectives of bioluminescence imaging, tumor volume and tumor weight, as well as survival time, the intraperitoneal injection of QY-13 exhibited excellent *in vivo* anticancer potentials, which was consistent with the potent *in vitro* cytostatic effects of QY-13. Furthermore, it is anticipated that the conjugation of TATE could significantly enhance the *in vitro* and *in vivo* anticancer capacity, as well as the anticancer selectivity of D-type oncolytic peptides.

2.19. In vitro and in vivo ICD-eliciting and immunity-activating effects of QY-13

Previous studies have demonstrated that oncolytic peptides could disrupt cancer cell membranes or induce membrane destabilization, followed by the release of DAMPs and tumor antigens, thereby inducing immunogenic cell death (ICD) and robust anti-tumor immune responses[7,29]. Our initial mechanism research indicated that QY-13 exhibited potent cancer cell membrane lysis activity, leading to rapid death of cancer cells (Fig. 13). To evaluate whether QY-13 could induce ICD in cancer cells, we detected the release of three DAMP molecules, ATP, High mobility group protein B1 (HMGB1), and calreticulin (CRT). When ICD occurs in cancer cells, ATP, HMGB1, and CRT, which act as signals for immune recognition, are transferred from the intracellular space to the extracellular space. As shown in Fig. 17A, QY-8 treatment group increased the release of ATP, HMGB1, and CRT by approximately 3.5, 3.1, and 2.1 times respectively higher than the control group, indicating the ability of QY-8 to induce DAMPs release. It is worth noting that compared with QY-8, QY-13 released significantly higher levels of ATP, HMGB1, and CRT, which were 1.7, 1.5, and 1.5 times higher than QY-8, respectively. The analysis and quantification of DAMPs release indicated that both QY-8 and QY-13 could induce ICD in tumor cells, and QY-13 exhibited more potent ICD-eliciting effects.

To further evaluate the induction of ICD in cancer cells by QY-8 and QY-13 *in vivo*, we established tumor-bearing models and analyzed the levels of DAMP agents in tumor tissues (Fig. 17B). The mice received five intraperitoneal injections of QY-8 or QY-13, after which tumor tissues were collected for immunofluorescence analysis of HMGB1 and CRT expression. During ICD, CRT was translocated from the perinuclear endoplasmic reticulum to the cell surface, while HMGB1 is released from the nucleus to the extracellular space[164]. As shown in Fig. 17C, weak green fluorescence of CRT was observed surrounding the nucleus in the QY-8 treated group. Notably, significantly more intense green fluorescence was detected in the extranuclear region after QY-13 treatment. Furthermore, compared with the control group, the red fluorescence signal of HMGB1 within the nucleus was diminished in QY-8 treated cells, and only very faint red fluorescence was observed in the QY-13 group (Fig. 17D). These results demonstrated that QY-8 and QY-13 could significantly enhance the exposure of CRT (Fig. 17C and E) and promoted the

release of HMGB1 (Fig. 17D and F), with QY-13 exhibiting the stronger ICD-inducing potency than QY-8. The immunofluorescence assay in the tumor-bearing models further confirmed that QY-13 could effectively induce ICD *in vivo* and may be further applied in immunotherapy.

In addition to quantifying DAMP and monitoring ICD at both *in vitro* and *in vivo* levels, the immune-activating effects of QY-8 and QY-13 were further investigated in the tumor-bearing models. The infiltration of $CD8^+$ T cell, expression of vascular endothelial marker CD31, and cell proliferation marker Ki67 in tumor tissues were analyzed by immunohistochemical (IHC) staining (Fig. 17G). $CD8^+$ T cells play a crucial role in tumor immunity[165]. Once activated, $CD8^+$ T cells could directly kill tumor cells[166]. The tumor tissues of QY-8 and QY-13 treatment groups showed enhanced $CD8^+$ T cell infiltration, with QY-13 exerting a stronger effect than QY-8 (Fig. 17G and H). In addition, the IHC assay of the vascular endothelial marker CD31 and the cell proliferation marker Ki67 revealed that QY-13 treatment significantly reduced the expression levels of Ki67 (Fig. 17G and I) and CD31 (Fig. 17G and J) compared to the control group, suggesting its effective inhibition of tumor angiogenesis and cancer cell proliferation. Meanwhile, the immunity-activating effects of QY-13 were higher than those of QY-8, indicating that the conjugation of TATE could enhance the immunity-activating ability of oncolytic peptides. Collectively, Fig. 17 indicated that QY-13 could activate the body's antitumor immune response through pathways including ICD-eliciting and $CD8^+$ T cell infiltration recruitment. Moreover, QY-13 exhibited potent ability to inhibit tumor proliferation and angiogenesis *in vivo*. Strikingly, these data indicated that QY-13 could induce ICD in cancer cells and subsequent immunity-activating effects, forming a synergistic therapeutic effect of "direct tumor cell killing followed by tumor immunity activation".

3. Conclusions

Recently, oncolytic peptides have emerged as increasingly attractive candidates for anticancer therapy due to their novel skeletons and unique mechanism of action. Especially, the unique anticancer mechanism of oncolytic peptides, which involve the direct membranolytic potency and synergistic oncolytic-immunotherapy effect, could not only overcome cancer heterogeneity, but also reduces the risk of acquired resistance. Nevertheless, although multiple oncolytic peptides have entered clinical trials, conventional oncolytic peptides often suffer from three major limitations: (1) poor proteolytic stability and moderate anticancer durability, (2) limited efficacy against solid tumors[167], and (3) moderate anticancer selectivity due to the nonspecific biodistribution. In our efforts to improve the anticancer potential of oncolytic peptides, the stability, potency and selectivity guided optimization were conducted on the first in class oncolytic peptide Clip-71. The robust and efficient synthetic strategy, *in vitro* and *in vivo* anticancer activity, as well as the mechanism of action were systematically investigated for obtained peptides.

In order to improve the proteolytic stability and anticancer durability, anticancer efficiency, as well as the anticancer selectivity, two rounds of optimization were conducted on the representative oncolytic peptide Clip-71. The DIC/Oxyma based condensation system was established, which could achieve the accelerated manual synthesis of Clip-71-derived peptides. Through the N-/C-terminal modifications and mirror image strategy, the first round of stability- and potency-guided optimization was conducted, affording ten Clip-71-derived peptides. The proteolytic stability and time-kill kinetics assays indicated that D-type peptides represented by QY-8 possessed high enzymatic stability and sustained anticancer effects, which was significantly superior to other Clip-71-derived peptides. The CD spectrum of QY-8 was basically the mirror image form of Clip-71, indicating that the D-amino acid substitutions did not impair the amphipathic structure of Clip-71. The mechanism explorations indicated that QY-8 exhibited significantly enhanced membranolytic effect compared to Clip-71, which may contribute to the improved anticancer efficacy of QY-8. Strikingly, it was found that QY-8 possessed outstanding *in vitro* and *in vivo* anticancer activity, which may serve as a potential candidate for further optimizations.

Through the first round of stability- and potency-guided optimization, the D-type peptide QY-8 was found to possess high proteolytic stability and sustained anticancer durability, as well as superior *in vitro* and *in vivo* anticancer activity to Clip-71. Nevertheless, like most oncolytic peptides, QY-8 still suffers from moderate anticancer selectivity and was thus administrated through intratumoral injection in the *in vivo* anticancer experiments. In order to improve the therapeutic efficiency and reduce the undesired toxicity of chemotherapeutic agents, the peptide–drug conjugates (PDCs) have been designed, which possess increased cancer penetration and selectivity. Inspired by the PDCs strategy, we turned our attention to developing the tumor-targeting peptide and oncolytic peptide based conjugates (PPCs). To the best of our knowledge, although multiple PDCs based therapeutic agents have entered clinical or preclinical evaluations, little effort has been devoted to developing PPCs composed of tumor-targeting peptide and oncolytic peptides.

In order to enhance the anticancer selectivity and overcome the administration limitation of D-type oncolytic QY-8, the second round of selectivity-guided and PPCs-strategy based optimization was conducted. Utilizing the tumor-homing peptide TATE and D-type oncolytic peptide QY-8, the novel PPC QY-13 was designed and efficiently synthesized by the DIC/Oxyma-based manual SPPS. Molecular dynamics simulations and pull-down assays demonstrated that the conjugation of oncolytic peptide did not impair the SSTR-2 targeting efficiency of TATE. Especially, the TATE-QY-8 based PPC QY-13 still possessed comparable binding efficiency toward SSTR2 to that of TATE. The *in vitro* cytotoxicity assays demonstrated that TATE conjugation significantly enhanced the anticancer potency of Clip-71-derived oncolytic peptides against SSTR2-high cancer cells. Of noted, compared with Clip-71, QY-13 exhibited more than 10-fold increase in killing effects against the SSTR2 high-expressed cancer cell lines. Besides, this study also investigated the *in vitro* activity of QY-13 in drug-resistant cell lines and compared its synergistic effects with those of doxorubicin (DOX) and cisplatin. Especially, it was found that QY-13 not only exerts potent cytotoxicity against drug-resistant cancer cells but also exhibits dual effects of enhancing drug sensitivity and reversing drug resistance. Moreover, the time-kill curve assay and serum stability assay indicated that QY-13 possessed potent and durable anticancer effects, as well as satisfactory proteolytic stability even up to 72 h incubation.

The wound healing tests indicated that the conjugation of tumor-targeting peptide TATE could significantly enhance the anti-migration effect of oncolytic peptides against SSTR2 high-expressed cancer cells, suggesting the potential anti-metastatic properties of QY-13. The membranolytic assays showed that QY-

13 exhibited rapid and potent membrane lysis activity against SSTR2 high-expressed cancer cells, and its activity was significantly higher than that of D-type oncolytic peptide QY-8. Moreover, the morphological changes of cancer cells and cell imaging experiment indicated that, compared with D-type oncolytic peptide QY-8, QY-13 could more effectively destroy and penetrate the cell membrane of SSTR2 high-expressed cancer cells. Importantly, all these data indicated that the enhanced anti-migration effect, stronger and selective membranolytic effect, as well as the higher membrane penetration efficiency of QY-13 should be attributed to the interaction between TATE moiety in QY-13 and membrane protein SSTR2.

It should be pointed out that although the intratumoral administration of QY-8 induced the potent *in vivo* anticancer activity, the intraperitoneal injection of QY-8 could not efficiently inhibit the proliferation of tumor cells, which induced moderate anticancer effects and weight loss in mice. The weak anticancer potency of QY-8 may be attributed to its moderate selectivity toward cancer cells and nonspecific distribution. Strikingly, consistent with a series of *in vitro* experiments, the attachment of TATE could significantly enhance the *in vivo* anticancer potential of oncolytic peptides. From the perspectives of bioluminescence imaging, tumor volume and weight, as well as survival time of mice, the intraperitoneal injection of QY-13 exhibited significantly higher anticancer activity than that of D-type oncolytic peptide QY-8. Moreover, the hemolysis assay suggested that the conjugation of tumor-targeting peptide TATE did not improve the hemolysis of oncolytic peptides and QY-13 exhibited low hemolysis rates (<5%) at its IC_{50} concentration. To further investigate whether QY-13 caused damage to major organs of mice, organ sections were observed by H&E staining and no obvious toxicity was observed by the histological analysis.

In the tumor-specific accumulation assay, compared with QY-18, QY-19 showed reduced distribution in the heart and lungs, with enhanced accumulation at the tumor site more. The tumor-specific accumulation assay demonstrated that QY-13 exhibited specific targeting to tumor tissues and effectively minimized nonspecific distribution of the oncolytic peptide. Immunotherapy experiments demonstrated that QY-13 significantly enhance the release of DAMP and induce ICD. Furthermore, in 4T1 tumor-bearing mouse models, QY-13 promotes $CD8^+$ T cell infiltration, inhibits tumor angiogenesis, and suppresses tumor cell proliferation. The immunotherapy experiments indicated that QY-13 could activate the body's antitumor immune response through mechanisms including ICD induction and $CD8^+$ T cell recruitment, thereby exerting a dual effect of directly killing cancer cells and subsequently activating antitumor immunity.

In summary, the novel tumor-targeting peptide and D-type oncolytic peptide based conjugates were developed through the stability-, potency-, and selectivity guided optimization of Clip-71. Especially, through two rounds of optimization, we successfully addressed the key limitations of Clip-71, including its poor proteolytic stability and moderate anticancer durability, limited efficacy against solid tumors, as well as the moderate anticancer selectivity and nonspecific distribution. Strikingly, the novel PPC QY-13, obtained through the conjugation of TATE to D-type oncolytic peptide QY-8, exhibited excellent anticancer potentials in both *in vitro* and *in vivo* experiments, as well as superior biosafety and tumor targeting potency. The immunotherapy explorations indicated that QY-13 could elicit ICD and enhance $CD8^+$ T cell recruitment, thereby exerting a synergistic therapeutic effect of "direct tumor cell killing followed by antitumor immunity activation". Due to its high proteolytic stability, sustained anticancer effects, increased anticancer selectivity, as well as ICD-eliciting and immunity-activating effects, QY-13 may serve as the emerging anticancer candidate for further optimizations. Collectively, our study not only established promising strategies to improve the anticancer potential of oncolytic peptides but also provided references for the future development of tumor-targeting peptide and oncolytic peptide based PPC for oncolytic-immunotherapy.

4. Experimental

4.1. Synthesis of Clip-71 derived and TATE-oncolytic peptide based PPCs

All peptides were synthesized in an air-bath constant-temperature shaker using the 9-fluorentlme-thyloxycarbonyl (Fmoc)-based solid phase peptide synthesis (SPPS)[70,153,168-175]. The chemical structures of reagents for peptide synthesis are provided in Supporting Information Fig. S1. Briefly, the DIC/Oxyma system was used to couple amino acids. First, Rink Amide MBHA Resin (0.05 mmol, 1 eq., Tianjin Nankai Hecheng Technology) was added into the peptide synthesis vessel. After a standard washing procedure (DMF twice, DCM twice, DMF once, DCM once, DMF twice), the resin was swollen in a DMF/DCM = 3:1 (*v*/*v*) solution for 2.5 h. The Fmoc protecting group was removed twice with 20% piperidine in DMF (3 min, 5 min) at 50 °C. Following another standard washing step, a mixture of Fmoc-amino acid (3 eq.), DIC (6 eq.), and Oxyma (3 eq.) in DMF was activated at 28 °C for 5 min and then added to the vessel for coupling at 50 °C. Typically, two rounds of condensation (15 min for the first, 20 min for the second) were sufficient for most amino acids. The Fmoc group was subsequently removed again with 20% piperidine in DMF (3 min, then 5 min) at 50 °C. Meanwhile, QY-8 and QY-13 were also synthesized using the traditional HCTU/DIEA system at 28 °C.

After all amino acid residues were coupled, the peptides were cleaved and deprotected using a TFA cleavage cocktail (TFA/phenol/H_2O/TIPS, 88:5:5:2, *v*/*v*/*v*/*v*) for 2 h at 28 °C. The crude products were concentrated under nitrogen flow, precipitated with precooled anhydrous ether, and the crude peptide was obtained by centrifugation (three times). The crude peptide was then dissolved in the CH_3CN/H_2O solvents (containing 0.1% TFA, *v*/*v*). Finally, the crude peptide was purified by semipreparative RP-HPLC (Shimadzu Prominence, LC-20A) and lyophilized for 48 h to collect the target solid peptide. The purity of the target peptide was analyzed by RP-HPLC, and its molecular weight was verified by ESI-MS (Thermo Scientific, LTQ Orbitrap XL) (Fig. S3−S23). Of noted, all obtained peptides were >95% pure by analytical RP-HPLC.

4.1.1. Synthesis of Clip-71 derived peptides

Rink Amide MBHA resin was applied for the synthesis of Clip-71, QY-4 to QY-10 and QY-18. AEEA, 7-DCCA, MOEOEA, MOEOEOEA, Acp, NH_2-PEG_1-CH_2 and Rhodamine B were coupled using the HATU/HOAt/DIEA system at 28 °C (Fig. S2). For QY-7, after removal of the N-terminal Fmoc protecting group, a mixture of Fmoc-Acp-OH (2 eq.), HATU (1.8 eq.), HOAt (2 eq.), and DIEA (4 eq.) in DMF was mixed and coupled twice at 28 °C (30, 45 min).

2-Chlorotrityl-$NHNH_2$ resin was synthesized by the previous method[76,95,169,176]. First, 2-chlorotrityl chloride resin was treated with 5% NH_2NH_2 in DMF solution (30 min, 40 min), and subsequently capped with 5% methanol in DMF for 10 min. All amino acids were then coupled to generate QY-1 and QY-3. After removal of the N-terminal Fmoc protecting group, QY-2 was obtained by acetylating the peptide QY-1 with a mixture of acetic anhydride/DIEA/DMF (1:1:8, *v*/*v*/*v*) at 28 °C (5 min for the first time, 10 min for the second time).

4.1.2. Synthesis of TATE-oncolytic peptide based PPCs

The TATE-oncolytic peptide based PPCs were synthesized by Wang resin. The resin (0.05 mmol, 1 eq., Tianjin Nankai Hecheng Technology) was added to the peptide synthesis vessel and swollen in DMF/DCM = 3:1 (*v*/*v*) solution for 2.5 h. For the initial coupling of the first amino acid, Fmoc-Thr(*t*Bu)-OH (3 eq., GL Biochem) was activated with DIC (6 eq.), Oxyma (3 eq.), and DMAP (0.4 eq.) in DMF at 28 °C for 5 min, then added to the resin for double coupling at 28 °C (6, 10 h). Following Fmoc deprotection at 28 °C (5, 10 min), Fmoc-Cys(Acm)-OH was coupled twice using the HCTU/DIEA system (30, 40 min) at 28 °C. After subsequent Fmoc removal at 28 °C (5, 10 min), Fmoc-Thr(*t*Bu)-OH was coupled using the HCTU/DIEA system, with remaining amino acids in the sequence coupled using the DIC/Oxyma system at 50 °C.

After all the amino acids had been coupled, the peptide was treated with a solution of thallium(III) trifluoroacetate (64 mg) in DMF/anisole (2.5 mL/0.125 mL) that had been pre-chilled in an ice bath for 10 min[119-121], then reacted at 28 °C for 2 h. Final cleavage was performed using TFA/H_2O/TIPS (95:2.5:2.5, *v*/*v*/*v*) at 28 °C for 2 h to yield the crude peptide.

4.2. The circular dichroism (CD) analysis

The secondary structures of Clip-71-derived and TATE-Oncolytic peptides were determined by circular dichroism (Jasco-J-1500, Japan). A 1 mm quartz cuvette was used to detect the secondary structures of Clip-71-derived peptides and TATE-oncolytic peptide based PPCs in highly purified nitrogen at room temperature. The concentration of Clip-71 derived peptides and PPCs was 1 mg/mL. The instrument parameters were set as follows, wavelength scanning range 200−260 nm, bandwidth 1 nm, scanning speed 100 nm/min, and repeated scanning three times. Data were analyzed using the JASCO standard analysis procedure.

4.3. Cell culture

The cell lines were purchased from the National Infrastructure of Cell Line Resource (NICR) with the exception of the DOX-resistant breast cancer cell line (MCF-7/ADR), which was purchased from American Type Culture Collection (ATCC). Cancer cells were grown in the appropriate growth media (RPMI-1640 for A20, MCF-7/ADR, and Daudi cell lines; MEM for MCF-7 cell line; Ham's F-12K for PC-3; DMEM for 4T1, PANC-1, A549, HepG2, MDA-MB-231, and MRC-5) containing 10% fetal bovine serum (FBS, PAN-Biotech). All cell lines were kept in a humidified atmosphere at 37 °C, 5% CO_2.

The DDP-resistant human TNBC cell line MDA-MB-231/DDP was obtained by stimulating MDA-MB-231 cell lines with different DDP concentrations, following a previously described protocol[145]. MDA-MB-231/DDP cell line was cultured in the medium with DDP (1.5 μg/mL) in the atmosphere of 5% CO_2 at 37 °C.

4.4. In vitro cytotoxicity assay

Cell Counting Kit-8 (CCK-8, TargetMol, USA) was used to detect the inhibitory effect of Clip-71-derived peptides and TATE-oncolytic peptide based PPCs on the suspension cells[177]. Peptides were dissolved in DMSO to form 30 mmol/L stock solutions. Cancer cells were inoculated in 96-well plates at a density of 10,000 cells per well, and cultured overnight. The stock solutions of Clip-71-derived peptides and TATE-oncolytic peptide based PPCs were diluted in FBS-free media to prepare working solutions with concentrations gradients of 100, 50, 25, 12.5, 6.25, 3.125 μmol/L or 100, 25, 6.25, 1.56, 0.39, 0.10 μmol/L. The cancer cells were incubated with different concentrations of peptides for 24 h, and then 15 μL CCK-8 solution was added to each well and incubated at 37 °C for 4 h. Finally, the optical density (OD) of each well at 450 nm was detected by the microplate reader (Tecan).

The MTT experiment was used to detect Clip-71-derived peptides and TATE-oncolytic peptide based PPCs inhibition of adherent cells[158,178]. Cells were seeded in 96-well plates at a density of 10,000 cells per well and adhered overnight. The stock solutions of Clip-71-derived peptides and TATE-oncolytic peptide based PPCs were diluted in FBS-free media to prepare working solutions with concentrations gradients of 100, 50, 25, 12.5, 6.25, 3.125 μmol/L or 100, 25, 6.25, 1.56, 0.39, 0.10 μmol/L. After incubation for 24 h, 15 μL of 5 mg/mL MTT was added to each well and cultured in the incubator for 4 h. The supernatant was removed, then 150 μL DMSO was added to each well and placed in the incubator for 1 h. Finally, the OD at 492 nm of each well was detected by the microplate reader (Tecan). The cytostatic rate was calculated according to Eq. (1):

$$\text{Cytostatic rate } (\%) = [(OD_{\text{control}} - OD_{\text{sample}})/ (OD_{\text{control}} - OD_{\text{blank}})] \times 100 \quad (1)$$

All assays were carried out in triplicate. The IC_{50} values were calculated by IBM SPSS Statistics 22 software. IC_{50} values are presented as mean ± SEM. Combination index (CI) values were determined by CompuSyn software.

4.5. Time-kill curve assay

To evaluate the anticancer effect of Clip-71 derived peptides and TATE-Oncolytic peptide based PPCs in each time period, the time-kill curve assay against MCF-7, 4T1, and A20 cancer cells was carried out. First, MCF-7, 4T1, and A20 cells were seeded in 96-well plates at a density of 10,000 cells/well, respectively, and incubated at 37 °C overnight. Then, cancer cells and peptide working solutions were incubated at 37 °C for 4, 12, 24, 36, 48, and 72 h. The final concentrations of the peptide working solutions were set according to the IC_{50} value of QY-8 or QY-13 on different cells, respectively: 1) the final concentrations of Clip-71 derived peptides were 15 μmol/L against 4T1 cell and 5 μmol/L against A20 cell. 2) the final concentrations of TATE-Oncolytic peptide based PPCs were 10 μmol/L against 4T1 cells and MCF-7 cells. Finally, the CCK-8 test was performed against A20 cell, and MTT test was carried out against MCF-7 and 4T1

cells at each time point. All experiments were repeated three times.

4.6. Hemolytic activity assay

Fresh mouse erythrocytes were used to assess the hemolytic activity of Clip-71, QY-8, QY-12, and QY-13. Blood was collected in anticoagulated tubes and centrifuged at the speed of 1000 rpm for 10 min. The red blood cells were washed three times and then suspended in PBS. A specific volume of peptide was combined with an equal volume of erythrocyte suspension. Thereafter, the hemolytic activity of parent peptide Clip-71, QY-8, QY-12, and QY-13 on mouse red blood cells was determined at the concentrations of 0.5 × IC_{50} (against 4T1 cell line), 1 × IC_{50}, 2 × IC_{50}, 4 × IC_{50}, 8 × IC_{50}, and 16 × IC_{50}, respectively, with the 2% Triton X-100 as positive control and 1 × PBS as negative control. The mixture was incubated at 37 °C for 4 h, and then centrifuged at 1000 rpm for 5 min. The absorbance of the supernatant in the 96-well plate was measured at 450 nm. Each peptide experiment was repeated three times. The hemolytic percentage was calculated according to Eq. (2):

$$\text{Hemolysis (\%)} = [(A_{\text{sample}} - A_{\text{negative}})/ (A_{\text{positive}} - A_{\text{negative}})] \times 100 \quad (2)$$

4.7. Investigation of the anticancer action of Clip-71 derived peptides and TATE-oncolytic peptides

4.7.1. Intracellular localization

To ascertain the subcellular localization of Clip-71 and QY-8, the fluorescent probes QY-9 and QY-10 were designed and synthesized. Firstly, MTT and CCK-8 tests were used to evaluate the effects of 7-DCCA modification on Clip-71 and QY-8 activity. 4T1 cells were seeded onto six-well plates at a density of 50,000 cells per well and allowed to adhere overnight. Subsequently, 4T1 cells were subjected to a 30-min treatment with SYBR Green I (Solarbio) for the labeling of nucleus. The cells were incubated with 15 μmol/L QY-9, 15 μmol/L QY-10, 15 μmol/L Clip-71 plus 15 μmol/L 7-DCCA, or 15 μmol/L QY-8 plus 15 μmol/L 7-DCCA for different times. After incubation, the medium was discarded and the cells were washed three times with PBS buffer (1 ×). Finally, the cells were observed using a fluorescence microscope (Nikon, Eclipse Ti-S).

4.7.2. Membranolytic activity assay

To investigate the cell membrane disrupting effect of different peptides, propidium iodide (PI) staining was employed to assess the integrity of the cell membrane. PI possesses a potent binding ability with DNA but cannot pass through normal cell membranes. PI only binds to DNA in cells with damaged membranes, emitting red fluorescence. Hoechst 33258 was applied to stain the nucleus of all cells, while PI was applied to stain the nucleus of those cells that had lost cell membrane integrity. The 4T1 or MCF-7 cells were seeded onto 12-well plates and allowed to adhere overnight. Thereafter, the medium was discarded, and 4T1 or MCF-7 cells were cultured with 10 μg/mL Hoechst 33258, 2 μg/mL PI, and different peptides. After three washes with PBS (1 ×), the cells were examined by fluorescence microscopy (Nikon, Eclipse Ti-S).

4.7.3. Assessment of mitochondrial membrane potential

The disruption of mitochondrial membrane potential (MMP) induced by QY-8 was investigated using the fluorescent dye JC-10 mitochondrial probe kit (Solarbio). 4T1 cells were seeded in six-well plates and allowed to adhere overnight. The 4T1 cells were treated with 15 μmol/L Clip-71 or 15 μmol/L QY-8 for different times. Subsequently, the medium was replaced with 500 μL of DMEM containing 200 nmol/L JC-10. After 30 min of incubation, the cells were washed three times and examined by fluorescence microscopy (Nikon, Eclipse Ti-S).

4.7.4. Cellular uptake

To evaluate the cellular uptake of QY-13 in SSTR2-high and SSTR2-low expressing cells, we first synthesized the fluorescent probe QY-17. Subsequently, the MTT and CCK-8 assays were employed to assess the impact of coumarin modification on the activity of QY-13. The MCF-7 or PANC-1 cells were seeded in six-well plates at a density of 50,000 cells per well and allowed to adhere overnight. Cells were treated with SYBR Green I for 30 min to label the nucleus. Then, cells were incubated with 10 μmol/L QY-17 or 10 μmol/L QY-10 for different periods of time. In addition, to investigate whether QY-13 cellular uptake was mediated through SSTR2 binding, cells were preincubated with 100 μmol/L TATE for 24 h. The medium was then replaced with 10 μmol/L QY-17, followed by incubation at 37 °C for different times. Finally, cancer cells were washed three times, and then examined by fluorescence microscopy (Nikon, Eclipse Ti-S).

4.8. Stability assays

Human serum was used to test the stability of the Clip-71-derived peptides and TATE-oncolytic peptide based PPCs in serum. The peptides were dissolved in PBS, and then mixed with 10% serum in equal volume to obtain working solutions with a final concentration of 100 μmol/L, and incubated at 37 °C. Thereafter, the working solutions were sampled at 0, 4, 8, 24, 36, 48 and 72 h, and immediately added with 50 μL acetonitrile and 250 μL distilled water (both containing 0.1% TFA). Samples were centrifuged at 12,000 rpm for 5 min at 4 °C and analyzed by RP-HPLC and ESI-MS.

4.9. Molecular dynamics simulation

Initially, PyMOL was utilized to modify the octreotate structure from the PDB database (PDB ID: 7XAU), followed by ChemDraw 3D for linker structure design[179]. The three-dimensional structure of oncolytic peptide was predicted using AlphaFold3[102], and the LtoD.py script from finDr website was implemented to convert L-type oncolytic peptide to its D-type counterpart[103]. Subsequently, the GAFF force field in Amber was applied to generate force field parameters for the linker. The complete system was constructed using LEaP in AMBER22[131], where the ff19SB force field was assigned to proteins and peptides, while GAFF was specifically applied to the linker region. The complexes were solvated in a truncated regular octahedron TIP3P water box with a 10 Å size distance in AMBER22. System neutrality was achieved through the addition of sodium ions, followed by energy optimization. The initial optimization involved constraining the solute with a harmonic force (elastic constant: 10 kcal/(mol·Å^2)), employing 3000 steps of steepest descent method and 3000 steps of conjugate gradient method. A subsequent optimization round

was performed without position restrictions. For system equilibration, the temperature was gradually increased from 50 to 300 K over 100 ps in the NVT ensemble, with a 5 kcal/(mol·Å^2) harmonic force applied to restrain solute positions. Finally, molecular dynamics (MD) simulations were conducted in the NPT ensemble, with position constraints systematically removed during the process.

We employed CHARMM-GUI (http://www.charmm-gui.org) to construct a POPC lipid bilayer membrane with dimensions of 125 × 125 × 129 Å[104]. The D-type oncolytic peptide was positioned 40 Å above the membrane surface. The system was subsequently solvated with TIP3P water molecules, and sodium ions (Na^+) were added to achieve electrical neutrality, maintaining an overall ion concentration of 0.15 mol/L through CHARMM-GUI's automated parameterization. Following system preparation, molecular dynamics simulations were performed using the previously described parameters.

4.10. Binding energy calculations using MMGB/SA

Molecular mechanics generalized Born surface area (MMGB/SA) were applied to calculate the binding affinities of octreotate against receptor[135]. The energies were averaged on the 5 frames extracted from the 50 ns MD simulations. The parameters are as previously reported[180]. Briefly, the internal dielectric and external dielectric constants were set to 2.0 and 80.0, respectively. A probe radius of 1.4 Å, a grid spacing of 0.5 Å and ionic strength 0.1 mol/L were set up for the calculations.

4.11. Western blotting assay

The Western blotting assay was conducted as described previously[181-183]. HepG2, BON-1, PANC-1, 4T1, MCF-7, and PC-3 cells were lysed by RIPA lysis buffer with phosphatase and protease inhibitor cocktails. After centrifugation at 13,200 rpm for 15 min, the supernatant was obtained. Thereafter, a BCA Protein Assay Reagent Kit was used to determine the protein concentration. Total proteins were separated by 10% SDS-PAGE and electrotransferred to polyvinylidene fluoride membranes. After the block, the membrane was incubated with antibody against GAPDH (1:3000, Absin) or SSTR2 monoclonal antibody (1:1000, ABclonal) at 4 °C overnight. Then, the corresponding secondary antibody (1:5000, Absin) was added and incubated at room temperature for 1 h. The antigen−antibody complex was detected with enhanced chemiluminescence (ECL) reagent. ImageJ was used for the quantification of proteins.

4.12. Pull-down experiments

In order to conduct the pull-down analysis of the TATE-oncolytic peptide based PPCs, MCF-7 whole cell extracts were prepared using RIPA lysis buffer (Solabio), with protease inhibitors (MedChemExpress) included. Subsequent to the centrifugation of the cell extracts at 12,000 rpm for a duration of 15 min, the supernatant was collected. Subsequently, the supernatant was divided into five groups, and 25 μmol/L Biotin, 25 μmol/L QY-14, 25 μmol/L QY-15, 25 μmol/L QY-16 or 50 μmol/L QY-16 were added to each group respectively. The mixture was then subjected to a co-incubation process at a temperature of 4 °C for a duration of 12 h. Subsequently, the mixtures of protein and peptides were subjected to incubation with streptavidin magnetic beads (MedChemExpress) for a duration of 3 h at a temperature of 4 °C. The beads were washed three times with RIPA buffer, after which the binding proteins were eluted with 1 × SDS loading buffer. The samples were isolated through the application of 10% SDS-PAGE, and the binding proteins were subsequently detected using the SSTR2 antibody as previously described. Western blotting images were captured using the Mini chemiluminescence imaging and analysis system (Beijing Sage Creation Science) and quantified by Image J software.

4.13. Cell migration assay

MCF-7 cells (2 × 10^5 cells/well) were seeded into a 6-well plate. When the cells were nearly 90% confluent, two parallel lines were drawn along the bottom of the culture plate with a 1 mL pipette tip, and each well was washed three times with PBS. Then, the cells were treated with FBS-free media containing different concentrations of peptides (2 μmol/L Clip-71, 2 μmol/L QY-8 plus 2 μmol/L TATE, 200 nmol/L QY-13 or 400 nmol/L QY-13). The cells were imaged at 0, 12, and 24 h by the microscopy (Nikon, Eclipse Ti-S) and quantified with ImageJ software, respectively.

4.14. Transmission electron microscopy

Ultrastructural studies were performed on MCF-7 cells treated with 2 μmol/L QY-8 and 1, 2, or 4 μmol/L QY-13 for 12 h. The treated cells were collected with a spatula and centrifuged at 1000 rpm for 3 min. Then, the cells were added with 1 mL 2.5% glutaraldehyde, centrifuged again at 1000 rpm for 10 min, and fixed overnight at 4 °C. Dehydration was performed with a graded ethanol series. The slices were examined and pictures were taken using a transmission electron microscope (Hitachi, HT7800) after embedding and ultrathin sectioning (Leica UC7).

4.15. In vivo anticancer experiments

The experimental protocol was approved by the Medical Ethics Committee of Qingdao University. The six- to eight- week-old male Balb/c mice were procured from GemPharmatech Co., Ltd. (Nanjing, China). 10^7 4T1 or 4T1-Luc cells were subcutaneously transplanted into the right axilla of Balb/c mice to establish tumor xenografts. Tumor volume was detected by vernier caliper, and tumor volume was calculated as Eq. (3):

$$V = 0.5 \times \text{Length} \times \text{Width}^2 \quad (3)$$

When the tumor volume reached about 100 mm^3, mice were randomly divided into three or four groups (5 mice in each group). In the three groups of mice, normal saline, 10 μmol/kg Clip-71 or 10 μmol/kg QY-8 were injected intratumorally every 2 days for a total of 5 times. Moreover, the four groups of mice were intraperitoneally injected with normal saline, 10 μmol/kg QY-8, 5 μmol/kg QY-13 or 10 μmol/kg QY-13, respectively. The frequency of administration was once every two days for a total of 7 injections. Mice were euthanized when the tumor volume exceeded 2000 mm^3 or at the termination of the experiment, and the tumors were stripped and weighed.

Besides, for axillary tumor xenografts established with 4T1-Luc cells, the *in vivo* imaging system was used to visualize the

growth status of tumors. The mice were anesthetized at predetermined time points and injected with D-luciferin potassium salt. Subsequently, the fluorescence signals were recorded using a Master *in vivo* imaging system. Images were acquired and analyzed by Living Image 4.0 software. At the end of the experiment, the major organs were stripped and H&E staining was used for routine histological analysis.

4.16. Ex vivo fluorescence imaging

To investigate the biodistribution of QY-13, the fluorescent probes QY-18 and QY-19 were designed and synthesized, and 4T1 tumor-bearing mouse model was established. When the tumor volume reached approximately 200−300 mm^3, the mice were randomized into three groups and received intraperitoneal injections of saline, 10 μmol/kg QY-18, or 10 μmol/kg QY-19. After 24 h, the organs and tumors were collected and imaged using the *in vivo* imaging system (AniView600, BioLight, Guangzhou, China).

4.17. In vitro and in vivo ICD response assessment

MCF-7 cells were seeded in 12-well plates and cultured for 24 h until reaching 70%−80% confluency. Culture media containing different formulations (DMSO, 6 μmol/L QY-8, 6 μmol/L QY-13) were added to the wells. After 12 h of treatment, the culture supernatants were collected for the detection of released HMGB-1 (HMGB-1 ELISA kit, J&L Biological), ATP (chemiluminescence ATP assay kit, Servicebio) and CRT (CRT ELISA kit, J&L Biological).

To evaluate the ICD response induced by QY-13 in mice, tumor tissues were harvested and sectioned after different treatments. The levels of HMGB-1 and CRT in tumor sections were detected by immunofluorescence staining.

4.18. Immunohistochemistry

4T1 tumor-bearing mice were intraperitoneally administered normal saline, 10 μmol/kg QY-8, or 10 μmol/kg QY-13 every two days, respectively. After five injections, the mice were euthanized, and the tumors were carefully excised and fixed with 4% PFA. Samples were embedded in paraffin and cut into 6 μm thick slices. Tissue sections were dewaxed, rehydrated, and then underwent heat-induced epitope retrieval. Following blocking with BSA, the sections were incubated overnight at 4 °C with anti-CD8 (1:400, GB13429, Servicebio), anti-Ki67 (1:500, GB111141, Servicebio), or anti-CD31 (1:100, GB13063, Servicebio). After several washes, the sections were treated with corresponding secondary antibodies (1:200, GB23303 or GB23204, Servicebio). DAB (Servicebio) was used as a substrate, and hematoxylin was used as a counterstain. Finally, images were acquired using a panoramic scanner and analyzed with Image-Pro Plus 6.0 software.

Acknowledgments

We are grateful to Prof. Lei Liu in Department of Chemistry, Tsinghua University for both valuable support and constructive advice on the manuscript. This study was supported by the National Natural Science Foundation of China (Grant No. 22177058), the Taishan Scholar Program of Shandong Province (Grant No. tsqn202312168, China), and the Natural Science Foundation of Shandong Province (Grant No. ZR2024YQ061, China).

Author contributions

Yunkun Qi conceived and designed the experiments. Qianyao Yu and Jingfang Yao carried out the experiments and wrote the manuscript. Ming Meng, Zixuan Zhang, Chengjian Pang, Zhihao Zhang, Qing Liu, and Xinqi Chen participated part of the experiments. Yunkun Qi, Rilei Yu and Kewei Wang wrote and revised the manuscript. All of the authors have read and approved the final manuscript.

Conflicts of interest

The authors have no conflicts of interest to declare.

Appendix A. Supporting information

Supporting information to this article can be found online at https://doi.org/10.1016/j.apsb.2026.01.006.

References

1. Siegel RL, Kratzer TB, Giaquinto AN, Sung H, Jemal A. Cancer statistics, 2025. *CA-Cancer J Clin* 2025;**75**:10−45.
2. Anderson RL, Balasas T, Callaghan J, Coombes RC, Evans J, Hall JA, et al. A framework for the development of effective anti-metastatic agents. *Nat Rev Clin Oncol* 2019;**16**:185−204.
3. Ma QX, Xu QQ, Zhao JJ, Zhang WW, Wang Q, Fang J, et al. Coupling HDAC4 with transcriptional factor MEF2D abrogates SPRY4-mediated suppression of ERK activation and elicits hepatocellular carcinoma drug resistance. *Cancer Lett* 2021;**520**:243−54.
4. Shan P, Ye T, Tang Y, Song H, Wang C, Zhu K, et al. First total synthesis, antitumor evaluation and target identification of mornaphthoate E: a new tubulin inhibitor template acting on PI3K/Akt signaling pathway. *Acta Pharm Sin B* 2024;**14**:2177−93.
5. Lim Z-F, Ma PC. Emerging insights of tumor heterogeneity and drug resistance mechanisms in lung cancer targeted therapy. *J Hematol Oncol* 2019;**12**:134.
6. Luan X, Wu Y, Shen YW, Zhang H, Zhou YD, Chen HZ, et al. Cytotoxic and antitumor peptides as novel chemotherapeutics. *Nat Prod Rep* 2021;**38**:7−17.
7. Vitale I, Yamazaki T, Wennerberg E, Sveinbjornsson B, Rekdal O, Demaria S, et al. Targeting cancer heterogeneity with immune responses driven by oncolytic peptides. *Trends Cancer* 2021;**7**:557−72.
8. Anand U, Dey A, Chandel AKS, Sanyal R, Mishra A, Pandey DK, et al. Cancer chemotherapy and beyond: current status, drug candidates, associated risks and progress in targeted therapeutics. *Genes Dis* 2023;**10**:1367−401.
9. Liu H, Shen W, Liu W, Yang Z, Yin D, Xiao C. From oncolytic peptides to oncolytic polymers: a new paradigm for oncotherapy. *Bioact Mater* 2024;**31**:206−30.
10. Hamley IW. Small bioactive peptides for biomaterials fesign and therapeutics. *Chem Rev* 2017;**117**:14015−41.
11. Muttenthaler M, King GE, Adams DJ, Alewood PE. Trends in peptide drug discovery. *Nat Rev Drug Discov* 2021;**20**:309−25.
12. Vadevoo SMP, Gurung S, Lee H-S, Gunassekaran GR, Lee S-M, Yoon J-W, et al. Peptides as multifunctional players in cancer therapy. *Exp Mol Med* 2023;**55**:1099−109.
13. Chiangjong W, Chutipongtanate S, Hongeng S. Anticancer peptide: physicochemical property, functional aspect and trend in clinical application. *Int J Oncol* 2020;**57**:678−96 (Review).
14. Alas M, Saghaeidehkordi A, Kaur K. Peptide-drug conjugates with different linkers for cancer therapy. *J Med Chem* 2021;**64**:216−32.
15. Al Musaimi O. Peptide therapeutics: unveiling the potential against cancer-A journey through 1989. *Cancers* 2024;**16**:1032.

16. Cooper BM, Iegre J, O' Donovan DH, Halvarsson MO, Spring DR. Peptides as a platform for targeted therapeutics for cancer: peptide–drug conjugates (PDCs). *Chem Soc Rev* 2021;**50**:1480–94.
17. Fu C, Yu L, Miao Y, Liu X, Yu Z, Wei M. Peptide–drug conjugates (PDCs): a novel trend of research and development on targeted therapy, hype or hope?. *Acta Pharm Sin B* 2023;**13**:498–516.
18. Rizvi SFA, Zhang H, Fang Q. Engineering peptide drug therapeutics through chemical conjugation and implication in clinics. *Med Res Rev* 2024;**44**:2420–71.
19. He H, Deng X, Wang Z, Chen J. Recent progress in the development of peptide–drug conjugates (PDCs) for cancer therapy. *Eur J Med Chem* 2025;**284**:117204.
20. Yu Q, Meng M, Yao J, Du S, Qi Y. Two step synthesis of octreotide-doxorubicin conjugates based on disulfide bond linker. *Acta Chim Sinica* 2025;**83**:341–53.
21. Du Q, Huang YH, Wang CK, Kaas Q, Craik DJ. Mutagenesis of bracelet cyclotidehyen D reveals functionally and structurally critical residues for membrane binding and cytotoxicity. *J Biol Chem* 2022; **298**:101822.
22. Zhang P, Luo W, Zhang Z, Lv M, Sang L, Wen Y, et al. A lipid-sensitive spider peptide toxin exhibits selective anti-leukemia efficacy through multimodal mechanisms. *Adv Sci* 2024;**11**:2404937.
23. Chang HN, Liu BY, Qi YK, Zhou Y, Chen YP, Pan KM, et al. Blocking of the PD-1/PD-L1 interaction by a D-peptide antagonist for cancer immunotherapy. *Angew Chem Int Ed* 2015;**54**:11760–4.
24. Zhou X, Zuo C, Li W, Shi W, Zhou X, Wang H, et al. A novel D-peptide identified by mirror-image phage display blocks TIGIT/PVR for cancer immunotherapy. *Angew Chem Int Ed* 2020; **59**:15114–8.
25. Niu X, Wu M, Li G, Zhou X, Cao W, Zhai W, et al. Identification and optimization of peptide inhibitors to block VISTA/PSGL-1 interaction for cancer immunotherapy. *Acta Pharm Sin B* 2023;**13**:4511–22.
26. Qi YK, Zheng JS, Liu L. Mirror-image protein and peptide drug discovery through mirror-image phage display. *Chem* 2024;**10**: 2390–407.
27. Qian Y, Sun Y, Shi P, Zhou X, Zhang Q, Dong Q, et al. Development of LAG-3/FGL1 blocking peptide and combination with radiotherapy for cancer immunotherapy. *Acta Pharm Sin B* 2024;**14**:1150–65.
28. Haug BE, Camilio KA, Eliassen LT, Stensen W, Svendsen JS, Berg K, et al. Discovery of a 9-mer cationic peptide (LTX-315) as a potential first in class oncolytic peptide. *J Med Chem* 2016;**59**: 2918–27.
29. Tang T, Huang X, Zhang G, Liang T. Oncolytic immunotherapy: multiple mechanisms of oncolytic peptides to confer anticancer immunity. *J Immunother Cancer* 2022;**10**:e005065.
30. Fu XY, Yin H, Chen XT, Yao JF, Ma YN, Song M, et al. Three rounds of stability-guided optimization and systematical evaluation of oncolytic peptide LTX-315. *J Med Chem* 2024;**67**:3885–908.
31. Liu Q, Jia SX, Chi QN, Jin L, Chen XQ, Li J, et al. Efficient synthesis, stability-guided optimization and anticancer evaluation of bee venom peptide melittin. *Bioorg Chem* 2025;**159**:108344.
32. Phuong HBT, Nguyen BL, Huang L, Nguyen TOO, Le ND, Kim B, et al. Developing potent and selective anticancer therapy through chemical approaches and the combination of cationic amphipathic oncolytic peptides. *J Med Chem* 2025;**68**:11875–93.
33. Yao J, Zhang L, Hu L, Guo B, Hu X, Borjigin U, et al. Tumorigenic potential is restored during differentiation in fusion-reprogrammed cancer cells. *Cell Death Dis* 2016;**7**:e2314.
34. Galluzzi L, Guilbaud E, Schmidt D, Kroemer G, Marincola FM. Targeting immunogenic cell stress and death for cancer therapy. *Nat Rev Drug Discov* 2024;**23**:445–60.
35. Sveinbjornsson B, Camilio KA, Haug BE, Rekdal Ø. LTX-315: a first-in-class oncolytic peptide that reprograms the tumor microenvironment. *Future Med Chem* 2017;**9**:1339–44.
36. Curtis KK, Sarantopoulos J, Northfelt DW, Weiss GJ, Barnhart KM, Whisnant JK, et al. Novel LHRH-receptor-targeted cytolytic peptide, EP-100: first-in-human phase I study in patients with advanced LHRH-receptor-expressing solid tumors. *Cancer Chemother Pharmacol* 2014;**73**:931–41.
37. Mahlapuu M, Sidorowicz A, Mikosinski J, KrzyZanowski M, Orleanski J, Twardowska-Saucha K, et al. Evaluation of LL-37 in healing of hard-to-heal venous leg ulcers: a multicentric prospective randomized placebo-controlled clinical trial. *Wound Repair Regen* 2021;**29**:938–50.
38. Spicer J, Marabelle A, Baurain J-F, Jebsen NL, Jossang DE, Awada A, et al. Safety, antitumor activity, and T-cell responses in a dose-ranging phase I trial of the oncolytic peptide LTX-315 in patients with solid tumors. *Clin Cancer Res* 2021;**27**:2755–63.
39. Chen CH, Zan B, Ulmschneider JP, Wimley WC, Lu TK, Ulmschneider MB, et al. Development of membrane-active peptide therapeutics in oncology. *J Pept Sci* 2023;**29**:e3482.
40. Cichon T, Smolarczyk R, Matuszczak S, Barczyk M, Jarosz M, Szala S. D-K_6L_9 peptide combination with IL-12 inhibits the recurrence of tumors in mice. *Arch Immunol Ther Exp* 2014;**62**:341–51.
41. Kikuchi O, Ohashi S, Horibe T, Kohno M, Nakai Y, Miyamoto Si, et al. Novel EGFR-targeted strategy with hybrid peptide against oesophageal squamous cell carcinoma. *Sci Rep* 2016;**6**:22452.
42. Jannoo R, Xia Z, Row PE, Kanamarlapudi V. Targeting of the interleukin-13 receptor (IL-13R)α2 expressing prostate cancer by a novel hybrid lytic peptide. *Biomolecules* 2023;**13**:356.
43. Leuschner C, Hansel W. Membrane disrupting lytic peptides for cancer treatments. *Curr Pharm Des* 2004;**10**:2299–310.
44. Hansel W, Enright F, Leuschner C. Destruction of breast cancers and their metastases by lytic peptide conjugates *in vitro* and *in vivo*. *Mol Cell Endocrinol* 2007;**260**:183–9.
45. Ramezanzadeh M, Saeedi N, Mesbahfar E, Farrokh P, Salimi F, Rezaei A. Design and characterization of new antimicrobial peptides derived from aurein 1.2 with enhanced antibacterial activity. *Biochimie* 2021;**181**:42–51.
46. Jannoo R, Walker W, Kanamarlapudi V. Targeting and sensitization of breast cancer cells to killing with a novel interleukin-13 receptor α2-specific hybrid cytolytic peptide. *Cancers* 2023;**15**:2772.
47. Chelariu-Raicu A, Nick A, Urban R, Gordinier M, Leuschner C, Bavisotto L, et al. A multicenter open-label randomized phase II trial of paclitaxel plus EP-100, a novel LHRH receptor-targeted, membrane-disrupting peptide, versus paclitaxel alone for refractory or recurrent ovarian cancer. *Gynecol Oncol* 2021;**160**:418–26.
48. Lee SK, Han MS, Asokan S, Tung C-H. Effective gene silencing by multilayered siRNA-Coated gold nanoparticles. *Small* 2011;**7**: 364–70.
49. Li Y, Wu M, Fu Y, Xue J, Yuan F, Qu T, et al. Therapeutic stapled peptides: efficacy and molecular targets. *Pharmacol Res* 2024;**203**: 107137.
50. Xue J, Fu Y, Li H, Zhang T, Cong W, Hu H, et al. All-hydrocarbon stapling enables improvement of antimicrobial activity and proteolytic stability of peptide Figainin 2. *J Pept Sci* 2024;**30**:e3566.
51. Li F, Wu S, Chen N, Zhu J, Zhao X, Zhang P, et al. Fatty acid modification of the anticancer peptide LVTX-9 to enhance its cytotoxicity against malignant melanoma cells. *Toxins* 2021;**13**:867.
52. Wu Y, Lu D, Jiang Y, Jin J, Liu S, Chen L, et al. Stapled wasp venom-derived oncolytic peptides with side chains induce rapid membrane lysis and prolonged immune responses in melanoma. *J Med Chem* 2021;**64**:5802–15.
53. Zhao H, Qin X, Yang D, Jiang Y, Zheng W, Wang D, et al. The development of activatable lytic peptides for targeting triple negative breast cancer. *Cell Death Discov* 2017;**3**:17037.
54. Li Y, Xu N, Zhu W, Wang L, Liu B, Zhang J, et al. Nanoscale melittin@zeolitic imidazolate frameworks for enhanced anticancer activity and mechanism analysis. *ACS Appl Mater Interfaces* 2018; **10**:22974–84.
55. Zhang P, Jian C, Jian SD, Zhang QQ, Sun XL, Nie LQ, et al. Position effect of fatty acid modification on the cytotoxicity and antimetastasis potential of the cytotoxic peptide Lycosin-I. *J Med Chem* 2019; **62**:11108–18.

56. Zhang P, Ma J, Zhang Q, Jian S, Sun X, Liu B, et al. Monosaccharide analogues of anticancer peptide R-Lycosin-I: role of monosaccharide conjugation in complexation and the potential of lung cancer targeting and therapy. *J Med Chem* 2019;**62**:7857−73.
57. Liu J, Guo Z, Kordanovski M, Kaltbeitzel J, Zhang H, Cao Z, et al. Metal-organic frameworks as protective matrices for peptide therapeutics. *J Colloid Interface Sci* 2020;**576**:356−63.
58. Schnorenberg MR, Hawley KM, Thomas-Toth AT, Watkins EA, Tian Y, Ting JM, et al. Targeted polymersome delivery of a stapled peptide for drugging the tumor protein p53:BCL-2-family axis in diffuse large B-cell lymphoma. *ACS Nano* 2023;**17**:23374−90.
59. Chen XQ, Cui SS, Chen YZ, Wang CY, Liu Q, Qi YK, et al. Efficient delivery of oncolytic peptide LTX-315 by ZIF-8: pH-responsive release, improved stability, and reduced hemolysis. *Mol Pharm* 2025; **22**:1449−61.
60. Guo C, Gao F, Wu G, Li J, Sheng C, He S, et al. Precise HER2 protein degradation *via* peptide-conjugated photodynamic therapy for enhanced breast cancer immunotherapy. *Adv Sci* 2025;**12**:2410778.
61. Li X, Gohain N, Chen S, Li Y, Zhao X, Li B, et al. Design of ultrahigh-affinity and dual-specificity peptide antagonists of MDM2 and MDMX for P53 activation and tumor suppression. *Acta Pharm Sin B* 2021;**11**:2655−69.
62. Wu Y, Zou Y, Sun L, Garzino-Demo A, Hu H, Zhang W, et al. Peptide stapling with the retention of double native side-chains. *Chin Chem Lett* 2021;**32**:4045−8.
63. Chen B, Li Y, Bai H, Ji Y, Cong W, Hu H, et al. Unleashing the potential of natural biological peptide macropin: hydrocarbon stapling for effective breast cancer treatment. *Bioorg Chem* 2023;**140**: 106770.
64. Fu Y, Dou C, Gao X, Ji S, Zhao X, Xue J, et al. Design, synthesis, and biological evaluation of arginine *N*-glycosylation stapled peptides with potent antitumor activity i*n vivo*. *J Med Chem* 2025;**68**: 20435−48.
65. Li X, Ding Y, Xue J, Fu Y, Yan F, Song N, et al. Peptide double-stapling and arginine *N*-glycosylation triggered the development of therapeutic antimicrobial peptides capable of killing drug-resistant bacteria in mice. *J Med Chem* 2025;**68**:4511−26.
66. Wang N, Xu Z, Shen H, Cong W, Zhang S, Hu H, et al. Tyrosinase-catalyzed peptide stapling using *para*-amino phenylalanine and tyrosine anchoring residues. *Angew Chem Int Ed* 2025;**64**:e202420522.
67. Zhang H, Wei HM, Xue JH, Xia ZM, Zheng FH, Wan XC, et al. A ligase-based two-step approach for the generation of bicyclic peptides containing a benzylphenyl thioether framework. *Chembiochem* 2025;**26**:e202500240.
68. Li Z, Zhang B, Zuo C, Liu L. Studies on mirror-image proteins. *Chin J Org Chem* 2018;**38**:2412−9.
69. Zhang B, Zheng Y, Chu G, Deng X, Wang T, Shi W, et al. Backbone-installed split intein-assisted ligation for the chemical synthesis of mirror-image proteins. *Angew Chem Int Ed* 2023;**62**:e202306270.
70. Yang Z, Xiao Y, Shi Y, Liu L. Advances in the chemical synthesis of human proteoforms. *Sci China Life Sci* 2025;**68**:2515−49.
71. Zheng J, Liang J, Shi W, Li Y, Hu H, Tian C, et al. A mirror-image protein-based information barcoding and storage technology. *Sci Bull* 2021;**66**:1542−9.
72. Saha A, Suga H, Brik A. Combining chemical protein synthesis and random nonstandard peptides integrated discovery for modulating biological processes. *Accounts Chem Res* 2023;**56**:1953−65.
73. Xu H, Fu X, Bao Y, Zhu S, Xu Z, Song M, et al. D-type peptides based fluorescent probes for "turn on" sensing of heparin. *Bioorg Chem* 2024;**147**:107356.
74. Gong L, Zhao H, Liu Y, Wu H, Liu C, Chang S, et al. Research advances in peptide−drug conjugates. *Acta Pharm Sin B* 2023;**13**: 3659−77.
75. Chi QN, Jia SX, Yin H, Wang LE, Fu X, Ma YN, et al. Efficient synthesis and anticancer evaluation of spider toxin peptide LVTX-8-based analogues with enhanced stability. *Bioorg Chem* 2023;**134**: 106451.
76. Song M, Liu Q, Yao JF, Wang YT, Ma YN, Xu H, et al. Synthesis and structural optimization of oncolytic peptide LTX-315. *Bioorg Med Chem* 2024;**107**:117760.
77. Ding D, Xu S, da Silva-Junior EF, Liu X, Zhan P. Medicinal chemistry insights into antiviral peptidomimetics. *Drug Discov Today* 2023;**28**:103468.
78. Ma J, Wang X, Hu Y, Ma J, Ma Y, Chen H, et al. Recent advances in augmenting the therapeutic efficacy of peptide-drug conjugates. *J Med Chem* 2025;**68**:9037−56.
79. Liao H, Li X, Zhao L, Wang Y, Wang X, Wu Y, et al. A PROTAC peptide induces durable β-catenin degradation and suppresses Wnt-dependent intestinal cancer. *Cell Discov* 2020;**6**:35.
80. Markowska A, Markowski AR, Jarocka-Karpowicz I. The importance of 6-aminohexanoic acid as a hydrophobic, flexible structural element. *Int J Mol Sci* 2021;**22**:12122.
81. Pan M, Gao S, Zheng Y, Tan X, Lan H, Tan X, et al. Quasi-racemic X-ray structures of K27-linked ubiquitin chains prepared by total chemical synthesis. *J Am Chem Soc* 2016;**138**:7429−35.
82. Liang LJ, Wang Y, Hua X, Yuan R, Xia Q, Wang R, et al. Cell-permeable stimuli-responsive ubiquitin probe for time-resolved monitoring of substrate ubiquitination in live cells. *JACS Au* 2023; **3**:2873−82.
83. Subiros-Funosas R, Prohens R, Barbas R, El-Faham A, Albericio F. Oxyma: an efficient additive for peptide synthesis to replace the benzotriazole-based HOBt and HOAt with a lower risk of explosion. *Chem Eur J* 2009;**15**:9394−403.
84. Qu Q, Pan M, Gao S, Zheng Q, Yu Y, Su J, et al. A highly efficient synthesis of polyubiquitin chains. *Adv Sci* 2018;**5**:1800234.
85. Qu Q, Gao S, Wu F, Zhang M, Li Y, Zhang L, et al. Synthesis of disulfide surrogate peptides incorporating large-span surrogate bridges through a native-chemical-ligation-assisted diaminodiacid strategy. *Angew Chem Int Ed* 2020;**59**:6037−45.
86. Liang LJ, Chu GC, Qu Q, Zuo C, Mao J, Zheng Q, et al. Chemical synthesis of activity-based E2-ubiquitin probes for the structural analysis of E3 ligase-catalyzed transthiolation. *Angew Chem Int Ed* 2021;**60**:17171−7.
87. Zhang B, Deng Q, Zuo C, Yan B, Zuo C, Cao X, et al. Ligation of soluble but unreactive peptide segments in the chemical synthesis of haemophilus influenzae DNA ligase. *Angew Chem Int Ed* 2019;**58**: 12231−7.
88. Chen X, Wang J, Ma Y, Dong L, Jia S, Yin H, et al. DIC/Oxyma-based accelerated synthesis and oxidative folding studies of centipede toxin RhTx. *J Pept Sci* 2022;**28**:e3368.
89. Ma Y, Liu Yn, Wang J, Chen X, Yin H, Chi Q, et al. DIC/Oxyma based efficient synthesis and activity evaluation of spider peptide toxin GsMTx4. *Chin J Org Chem* 2022;**42**:498−506.
90. Yin H, Chen X, Fu X, Ma Y, Xu Y, Te Z, et al. Efficient chemical synthesis and oxidative folding studies of ccorpion toxin peptide WaTx. *Acta Chim Sinica* 2022;**80**:444−52.
91. Huang YC, Guan CJ, Tan XL, Chen CC, Guo QX, Li YM. Accelerated Fmoc solid-phase synthesis of peptides with aggregation-disrupting backbones. *Org Biomol Chem* 2015;**13**:1500−6.
92. Ni SH, Zhang HB, Huang WL, Zhou JP, Qian H. Solid phase synthesis of fatty acid modified glucagon-like peptide-1 (7−36) amide under thermal and controlled microwave irradiation. *Chin Chem Lett* 2010;**21**:27−30.
93. Zheng FH, Cui ZH, Wang YX, Zhu WJ, Wei HM, Xue JH, et al. Thiazolidine deprotection using an organic solvent extractable aldehyde scavenger for one-pot four-segment ligation. *Org Lett* 2024; **26**:7701−6.
94. Zuo C, Shi WW, Chen XX, Glatz M, Riedl B, Flamme I, et al. Chimeric protein probes for C5a receptors through fusion of the anaphylatoxin C5a core region with a small-molecule antagonist. *Sci China Chem* 2019;**62**:1371.
95. Ai HS, Chu GC, Gong QY, Tong ZB, Deng ZH, Liu X, et al. Chemical synthesis of post-translationally modified H2AX reveals redundancy in interplay between histone phosphorylation,

ubiquitination, and methylation on the binding of 53BP1 with nucleosomes. *J Am Chem Soc* 2022;**144**:18329.
96. Ai HS, Sun MS, Liu AJ, Sun ZX, Liu TT, Cao L, et al. H2B Lys34 ubiquitination induces nucleosome distortion to stimulate Dot1L activity. *Nat Chem Biol* 2022;**18**:972−80.
97. Serna N, Cano-Garrido O, Sanchez-Garcia L, Pesarrodona M, Unzueta U, Sanchez-Chardi A, et al. Engineering protein venoms as self-assembling CXCR4-targeted cytotoxic nanoparticles. *Part Part Syst Char* 2020;**37**:2000040.
98. Liu XL, Cao R, Wang S, Jia JL, Fei H. Amphipathicity determines different cytotoxic mechanisms of lysine- or arginine-rich cationic hydrophobic peptides in cancer cells. *J Med Chem* 2016;**59**: 5238−47.
99. Li X, Chen S, Zhang WD, Hu HG. Stapled helical peptides bearing different anchoring residues. *Chem Rev* 2020;**120**:10079−144.
100. Ma S, Pradeep S, Villar-Prados A, Wen Y, Bayraktar E, Mangala LS, et al. GnRH-R-targeted lytic peptide sensitizes BRCA wild-type ovarian cancer to PARP inhibition. *Mol Cancer Therapeut* 2019; **18**:969−79.
101. Chen N, Jiang C. Antimicrobial peptides: structure, mechanism, and modification. *Eur J Med Chem* 2023;**255**:115377.
102. Abramson J, Adler J, Dunger J, Evans R, Green T, Pritzel A, et al. Accurate structure prediction of biomolecular interactions with AlphaFold 3. *Nature* 2024;**630**:493.
103. Engel H, Guischard F, Krause F, Nandy J, Kaas P, Hoefflin N, et al. finDr: a web server for *in silico* D-peptide ligand identification. *Syn Syst Biotechno* 2021;**6**:402−13.
104. Lee J, Cheng X, Swails JM, Yeom MS, Eastman PK, Lemkul JA, et al. CHARMM-GUI input generator for NAMD, GROMACS, AMBER, OpenMM, and CHARMM/OpenMM simulations using the CHARMM36 additive force field. *J Chem Theor Comput* 2016;**12**: 405−13.
105. Lin L, Chi J, Yan Y, Luo R, Feng X, Zheng Y, et al. Membrane-disruptive peptides/peptidomimetics-based therapeutics: promising systems to combat bacteria and cancer in the drug-resistant era. *Acta Pharm Sin B* 2021;**11**:2609−44.
106. Tornesello AL, Borrelli A, Buonaguro L, Buonaguro FM, Tornesello ML. Antimicrobial peptides as anticancer agents: functional properties and biological activities. *Molecules* 2020;**25**:2850.
107. Li C, Lang J, Wang Y, Cheng Z, Zu M, Li F, et al. Self-assembly of CXCR4 antagonist peptide-docetaxel conjugates for breast tumor multi-organ metastasis inhibition. *Acta Pharm Sin B* 2023;**13**: 3849−61.
108. Dean TT, Jelu-Reyes J, Allen ALC, Moore TW. Peptide−drug conjugates: an emerging direction for the next generation of peptide therapeutics. *J Med Chem* 2024;**67**:1641−61.
109. Li YJ, Fang CB, Wang SS, Chen XQ, Li YT, Liu Q, et al. Design and synthesis of TH19P01-camptothecin based hybrid peptides inducing effective anticancer responses on sortilin positive cancer cells. *Bioorg Med Chem* 2024;**111**:117869.
110. Hennrich U, Kopka K. Lutathera®: the first FDA- and EMA-approved radiopharmaceutical for peptide receptor radionuclide therapy. *Pharmaceuticals* 2019;**12**:114.
111. White BH, Whalen K, Kriksciukaite K, Alargova R, Yeung TA, Bazinet P, et al. Discovery of an SSTR2-targeting maytansinoid conjugate (PEN-221) with potent activity *in vitro* and *in vivo*. *J Med Chem* 2019;**62**:2708−19.
112. Strosberg JR, Caplin ME, Kunz PL, Ruszniewski PB, Bodei L, Hendifar A, et al. ^{177}Lu-Dotatate plus long-acting octreotide versus high-dose long-acting octreotide in patients with midgut neuroendocrine tumours (NETTER-1): final overall survival and long-term safety results from an open-label, randomised, controlled, phase 3 trial. *Lancet Oncol* 2021;**22**:1752−63.
113. Gaviglio L, Gross A, Metzler-Nolte N, Ravera M. Synthesis and *in vitro* cytotoxicity of *cis,cis,trans*-diamminedichloridodisuccinatoplatinum (IV)−peptide bioconjugates. *Metallomics* 2012;**4**:260−6.
114. Lelle M, Kaloyanova S, Freidel C, Theodoropoulou M, Musheev M, Niehrs C, et al. Octreotide-mediated tumor-targeted drug delivery *via* a cleavable doxorubicin peptide conjugate. *Mol Pharm* 2015;**12**: 4290−300.
115. Ebaston TM, Rozoysky A, Zaporozhets A, Bazyleyich A, Tuchinsky H, Marks V, et al. Peptide-driven targeted drug-delivery system comprising turn-on near-infrared fluorescent xanthene-cyanine reporter for real-time monitoring of drug release. *ChemMedChem* 2019;**14**:1727−34.
116. Rozovsky A, Ebaston TM, Zaporozhets A, Bazylevich A, Tuchinsky H, Patsenker L, et al. Theranostic system for ratiometric fluorescence monitoring of peptide-guided targeted drug delivery. *RSC Adv* 2019;**9**:32656−64.
117. Deiser S, Fenzl S, Koenig V, Drexler M, Smith LM, George ME, et al. (SiFA)SeFe: a hydrophilic silicon-based fluoride acceptor enabling versatile peptidic radiohybrid tracers. *J Med Chem* 2024;**67**: 14077−94.
118. Sun J, Zhang Y, Huo S, Shen S. Construction of disulfide bonds in peptides *via* immobilized platinum (IV) complex oxidation. *Tetrahedron Lett* 2020;**61**:151496.
119. Kobayashi K, Taguchi A, Cui Y, Shida H, Muguruma K, Takayama K, et al. "On-resin" disulfide peptide synthesis with methyl 3-nitro-2-pyridinesulfenate. *Eur J Org Chem* 2021;**2021**:956−63.
120. Spears RJ, McMahon C, Chudasama V. Cysteine protecting groups: applications in peptide and protein science. *Chem Soc Rev* 2021;**50**: 11098−155.
121. Albert IL, Mercedes A, Fernando A. Amino acid-protecting groups. *Chem Rev* 2009;**109**:2455−504.
122. Qi Y, Chang H, Pan K, Tian C, Zheng J. Total chemical synthesis of the site-selective azide-labeled I66A HIV-1 protease. *Chem Commun* 2015;**51**:14632−5.
123. Elf AK, Johanson V, Marin I, Bergstrom A, Nilsson O, Svensson J, et al. Evaluation of SSTR2 expression in SI-NETs and relation to overall survival after PRRT. *Cancers* 2021;**13**:2035.
124. Heo Y, Yoon E, Jeon YE, Yun JH, Ishimoto N, Woo H, et al. Cryo-EM structure of the human somatostatin receptor 2 complex with its agonist somatostatin delineates the ligand-binding specificity. *eLife* 2022;**11**:e76823.
125. Eychenne R, Bouvry C, Bourgeois M, Loyer P, Benoist E, Lepareur N. Overview of radiolabeled somatostatin analogs for cancer imaging and therapy. *Molecules* 2020;**25**:4012.
126. He Y, Yuan XM, Lei P, Wu S, Xing W, Lan XL, et al. The anti-proliferative effects of somatostatin receptor subtype 2 in breast cancer cells. *Acta Pharmacol Sin* 2009;**30**:1053−9.
127. Heidari P, Kunawudhi A, Martinez-Quintanilla J, Szretter A, Shah K, Mahmood U. Somatostatin receptor type 2 as a radiotheranostic PET reporter gene for oncologic interventions. *Theranostics* 2018;**8**: 3380−91.
128. Zou Y, Tan HP, Zhao YF, Zhou Y, Cao L. Expression and selective activation of somatostatin receptor subtypes induces cell cycle arrest in cancer cells. *Oncol Lett* 2019;**17**:1723−31.
129. Gonzalez P, Debnath S, Chen Y-A, Hernandez E, Jha P, Dakanali M, et al. A theranostic small-molecule prodrug conjugate for neuroendocrine prostate cancer. *Pharmaceutics* 2023;**15**:481.
130. Dalezis P, Trafalis DT, Geromichalos GD, Pissimissis N, Panagiotopoulou D, Galaktidou G, et al. Adriamycin in combination with dexamethasone and octreotide lacks activity on the treatment of a 4T1 metastatic breast cancer model. *Anti Cancer Drugs* 2017;**28**: 489−502.
131. Case DA, Aktulga HM, Belfon K, Cerutti DS, Cisneros GA, Cruzeiro VWD, et al. The AmberTools. *J Chem Inf Model* 2023;**63**: 6183−91.
132. Krishnamani V, Lanyi JK. Molecular dynamics simulation of the unfolding of individual bacteriorhodopsin helices in sodium dodecyl sulfate micelles. *Biochemistry* 2012;**51**:1061−9.
133. Xu X, Liang J, Zhang Z, Jiang T, Yu R. Blockade of human 7 nicotinic acetylcholine receptor by -conotoxin imI dendrimer: insight from computational simulations. *Mar Drugs* 2019;**17**:303.
134. Zhang Y, Fan Y, Liu S, Guan Y, Wan J, Ren Q, et al. Development of peptide paratope mimics derived from the anti-ROR1 antibody and

long-acting peptide−drug conjugates for targeted cancer therapy. *J Med Chem* 2024;**67**:10967−85.
135. Wittayanarakul K, Hannongbua S, Feig M. Accurate prediction of protonation state as a prerequisite for reliable MM-PB(GB)SA binding free energy calculations of HIV-1 protease inhibitors. *J Comput Chem* 2008;**29**:673−85.
136. Liang J, Tae H-S, Xu X, Jiang T, Adams DJ, Yu R. Dimerization of α-conotoxins as a strategy to enhance the inhibition of the human $\alpha7$ and $\alpha9\alpha10$ nicotinic acetylcholine receptors. *J Med Chem* 2020;**63**: 2974−85.
137. Bhowmik A, Chakravarti S, Ghosh A, Shaw R, Bhandary S, Bhattacharyya S, et al. Anti-SSTR2 peptide based targeted delivery of potent PLGA encapsulated 3,3′-diindolylmethane nanoparticles through blood brain barrier prevents glioma progression. *Oncotarget* 2017;**8**:65339−58.
138. Zhang YN, Wan XC, Tang Y, Chen Y, Zheng FH, Cui ZH, et al. Employing unnatural promiscuity of sortase to construct peptide macrocycle libraries for ligand discovery. *Chem Sci* 2024;**15**:9649−56.
139. Xiao Y, He Z, Li W, Chen D, Niu X, Yang X, et al. A covalent peptide-based lysosome-targeting protein degradation platform for cancer immunotherapy. *Nat Commun* 2025;**16**:1388.
140. Liang YQ, Li SX, W XL, Zhang Y, Sun YN, Wang YQ, et al. A comparative study of the antitumor efficacy of peptide−doxorubicin conjugates with different linkers. *J Control Release* 2018;**275**: 129−41.
141. Eksteen JJ, Ausbacher D, Simon-Santamaria J, Stiberg T, Cavalcanti-Jacobsen C, Wushur I, et al. Iterative design and *in vivo* evaluation of an oncolytic antilymphoma peptide. *J Med Chem* 2017;**60**:146−56.
142. Song P, Zhao F, Li D, Qu J, Yao M, Su Y, et al. Synthesis of selective PAK4 inhibitors for lung metastasis of lung cancer and melanoma cells. *Acta Pharm Sin B* 2022;**12**:2905−22.
143. Ha SYY, Zhou Y, Fong WP, Ng DKP. Multifunctional molecular therapeutic agent for targeted and controlled dual chemo- and photodynamic therapy. *J Med Chem* 2020;**63**:8512−23.
144. Gao F, Wu Y, Wang R, Yao Y, Liu Y, Fan L, et al. Precise nano-system-based drug delivery and synergistic therapy against androgen receptorpositive triple-negative breast cancer. *Acta Pharm Sin B* 2024;**14**:2685−97.
145. Zhang Y, Wu J, Ye M, Wang B, Sheng J, Shi B, et al. ETS1 is associated with cisplatin resistance through IKKα/NF-κB pathway in cell line MDA-MB-231. *Cancer Cell Int* 2018;**18**:86.
146. Mi H, Wang X, Wang F, Li L, Zhu M, Wang N, et al. SNHG15 contributes to cisplatin resistance in breast cancer through sponging miR-381. *OncoTargets Ther* 2020;**13**:657−66.
147. Vojtek M, Martins CB, Ramos R, Duarte SG, Ferreira IMPLVO, de Carvalho ALMB, et al. Pd(II) and Pt(II) trinuclear chelates with spermidine: selective anticancer activity towards TNBC-sensitive and -resistant to cisplatin. *Pharmaceutics* 2023;**15**:1205.
148. Yang Z, Cai Y, Mao S, Wu Q, Zhu M, Cao X, et al. Discovery of 2,5-disubstituted furan derivatives featuring a benzamide motif for overcoming P-glycoprotein mediated multidrug resistance in MCF-7/ADR cell. *Eur J Med Chem* 2023;**257**:115462.
149. Luo X, Wu Y, Zhang X, Tang M, Ju F, Qin Z, et al. Peptide-based strategies for overcoming multidrug-resistance in cancer therapy. *Chin Chem Lett* 2025;**36**:109724.
150. Feng S, Zhou H, Wu D, Zheng D, Qu B, Liu R, et al. Nobiletin and its derivatives overcome multidrug resistance (MDR) in cancer: total synthesis and discovery of potent MDR reversal agents. *Acta Pharm Sin B* 2020;**10**:327−43.
151. Yang Z, Cai Y, Yang X, Li Y, Wu Q, Yu Y, et al. Novel benzo five-membered heterocycle derivatives as P-glycoprotein inhibitors: design, synthesis, molecular docking, and anti-multidrug resistance activity. *J Med Chem* 2023;**66**:5550−66.
152. Gori A, Gagni P, Rinaldi S. Disulfide bond mimetics: strategies and challenges. *Chem Eur J* 2017;**23**:14987−95.
153. Qi Y, Qu Q, Bierer D, Liu L. A diaminodiacid (DADA) strategy for the development of disulfide surrogate peptides. *Chem Asian J* 2020; **15**:2793−802.
154. Zhao R, Shi P, Chen JY, Sun SS, Chen JN, Cui JB, et al. Chemical synthesis and biological activity of peptides incorporating an ether bridge as a surrogate for a disulfide bond. *Chem Sci* 2020;**11**:7927−32.
155. Vitali E, Piccini S, Trivellin G, Smiroldo V, Lavezzi E, Zerbi A, et al. The impact of SST2 trafficking and signaling in the treatment of pancreatic neuroendocrine tumors. *Mol Cell Endocrinol* 2021;**527**: 111226.
156. Shen H, Zhang N, Kong X, Wang N, Hu HG, Cong W, et al. Benzyl stapled modification and anticancer activity of antimicrobial peptide A4K14-Citropin 1.1. *Bioorg Med Chem Lett* 2023;**96**:129499.
157. Yin H, Fu X, Gao H, Gao H, Ma Y, Chen X, et al. Hybrid peptide NTP-217 triggers ROS-mediated rapid necrosis in liver cancer cells by induction of mitochondrial leakage. *Front Oncol* 2023;**12**:1028600.
158. Yin H, Fu XY, Gao HY, Ma YN, Yao JF, Du SS, et al. Design, synthesis and anticancer evaluation of novel oncolytic peptide-chlorambucil conjugates. *Bioorg Chem* 2023;**138**:106674.
159. Lehto T, Vasconcelos L, Margus H, Figueroa R, Pooga M, Hallbrink M, et al. Saturated fatty acid analogues of cell-penetrating peptide PepFect14: role of fatty acid modification in complexation and delivery of splice-correcting oligonucleotides. *Bioconjug Chem* 2017;**28**:782−92.
160. Pulya S, Himaja A, Paul M, Adhikari N, Banerjee S, Routholla G, et al. Selective HDAC3 inhibitors with potent *in vivo* antitumor efficacy against triple-negative breast cancer. *J Med Chem* 2023;**66**: 12033−58.
161. Xu Y, Lv J, Liu Y, Du J, Luo C, Wang Y, et al. Coagulation-targeted TGF-β signaling pathway inhibitor nanomedicine for inhibiting the growth and lung metastasis of breast cancer. *Nano Lett* 2024;**25**:504−13.
162. Wang Y, Fan J, Meng XB, Shu QY, Wu YC, Chu GC, et al. Development of nucleus-targeted histone-tail-based photoaffinity probes to profile the epigenetic interactome in native cells. *Nat Commun* 2025; **16**:415.
163. Xiao D, Liu L, Xie F, Dong J, Wang Y, Xu X, et al. Azobenzene-based linker strategy for selective activation of antibody−drug conjugates. *Angew Chem Int Ed* 2024;**63**:e202310318.
164. Wang Z, Chen J, Hu J, Zhang H, Xu F, He W, et al. cGAS/STING axis mediates a topoisomerase II inhibitor induced tumor immunogenicity. *J Clin Investig* 2019;**129**:4850−62.
165. Garcia J, Daniels J, Lee YJ, Zhu IW, Cheng KT, Liu Q, et al. Naturally occurring T cell mutations enhance engineered T cell therapies. *Nature* 2024;**626**:626−34.
166. Sun K, Wei X, Han S, Sun Y, Xiao H, Wei D. Biotin receptor-targeting Pt^{IV} oxygen carrying prodrug amphiphile for alleviating tumor hypoxia induced immune chemotherapy suppression. *ACS Nano* 2025;**19**:13300−13.
167. Liu Q, Zhao H, Jiang Y, Wu M, Tian Y, Wang D, et al. Development of a lytic peptide derived from BH3-only proteins. *Cell Death Discov* 2016;**2**:16008.
168. Fang GM, Li YM, Shen F, Huang YC, Li JB, Lin Y, et al. Protein chemical synthesis by ligation of peptide hydrazides. *Angew Chem Int Ed* 2011;**50**:7645−9.
169. Fang GM, Wang JX, Liu L. Convergent chemical synthesis of proteins by ligation of peptide hydrazides. *Angew Chem Int Ed* 2012;**51**: 10347−50.
170. Zheng JS, Tang S, Qi YK, Wang ZP, Liu L. Chemical synthesis of proteins using peptide hydrazides as thioester surrogates. *Nat Protoc* 2013;**8**:2483−95.
171. Qi Y, Si Y, Du S, Liang J, Wang K, Zheng J. Recent advances in the chemical synthesis and semi-synthesis of poly-ubiquitin-based proteins and probes. *Sci China Chem* 2019;**62**:299−312.
172. Wang J, Dong L, Liu Y, Chen X, Ma Y, Yin H, et al. Efficient synthesis and oxidative folding studies of centipede toxin RhTx. *Chin J Org Chem* 2021;**41**:2800−9.
173. Ai H, Pan M, Liu L. Chemical synthesis of human proteoforms and application in biomedicine. *ACS Cent Sci* 2024;**10**:1442−59.
174. Dong S, Zheng J, Li Y, Wang H, Chen G, Chen Y, et al. Recent advances in chemical protein synthesis: method developments and biological applications. *Sci China Chem* 2024;**67**:1060−96.

175. Liu Y, Han D, Liu L. Temporary structural supports for chemical protein synthesis. *Angew Chem Int Ed* 2025;**64**:e202504405.
176. Huang YC, Fang GM, Liu L. Chemical synthesis of proteins using hydrazide intermediates. *Natl Sci Rev* 2016;**3**:107−16.
177. Ma Q, Jiang H, Ma L, Zhao G, Xu Q, Guo D, et al. The moonlighting function of glycolytic enzyme enolase-1 promotes choline phospholipid metabolism and tumor cell proliferation. *Proc Natl Acad Sci U S A* 2023;**120**:e2209435120.
178. Yin H, Chen XT, Chi QN, Ma YN, Fu XY, Du SS, et al. The hybrid oncolytic peptide NTP-385 potently inhibits adherent cancer cells by targeting the nucleus. *Acta Pharmacol Sin* 2023;**44**:201−10.
179. Bo Q, Yang F, Li Y, Meng X, Zhang H, Zhou Y, et al. Structural insights into the activation of somatostatin receptor 2 by cyclic SST analogues. *Cell Discov* 2022;**8**:47.
180. Yu R, Craik DJ, Kaas Q. Blockade of neuronal α7-nAChR by α-Conotoxin imI explained by computational scanning and energy calculations. *PLoS Comput Biol* 2011;**7**:e1002011.
181. Cong W, Shen H, Liao X, Zheng M, Kong X, Wang Z, et al. Discovery of an orally effective double-stapled peptide for reducing ovariectomy-induced bone loss in mice. *Acta Pharm Sin B* 2023;**13**:3770−81.
182. Wang D, Deng B, Cheng L, Li J, Zhang J, Zhang X, et al. A novel and low-toxic peptide DR3penA alleviates pulmonary fibrosis by regulating the MAPK/miR-23b-5p/AQP5 signaling axis. *Acta Pharm Sin B* 2023;**13**:722−38.
183. Deng X, Mai R, Zhang C, Yu D, Ren Y, Li G, et al. Discovery of novel cell-penetrating and tumor-targeting peptide−drug conjugate (PDC) for programmable delivery of paclitaxel and cancer treatment. *Eur J Med Chem* 2021;**213**:113050.